ESTIMATING THE EFFICIENCY OF CROSS-SHELF TRANSPORT OF TERRESTRIALLY DERIVED MATERIALS IN RIVER PLUMES

by

Jonathan George Izett

Submitted in partial fulfillment of the requirements
for the degree of Master of Science

at

Dalhousie University
Halifax, Nova Scotia
August 2016

TABLE OF CONTENTS

List of Tables . . . . . **iv**

List of Figures . . . . . **v**

Abstract . . . . . **viii**

List of Abbreviations and Symbols Used . . . . . **ix**

Acknowledgements . . . . . **xi**

Chapter 1 Introduction **1**

Chapter 2 Methods and Model **7**

2.1 Factors that Influence Cross-Shelf Transport in River Plumes 7

2.2 The Idealized River Plume Model 10
2.2.1 Wind and Tidal Forcing 13

2.3 Metrics Used to Assess the Simulated Plumes 14
2.3.1 The S_P Number 14
2.3.2 Export Efficiency 15

2.4 Global River Data 16

Chapter 3 Physical Controls on Cross-Shelf Transport **21**

3.1 Results of the Idealized Model Experiments 21
3.1.1 The Influence of Latitude and Discharge 21
3.1.2 Influence of Tide and Wind Forcing 30

3.2 Describing River Plumes with Simple Metrics 36
3.2.1 Cross-Shelf Export as a Function of the S_P Number 36
3.2.2 Other Plume Properties 41

3.3 Obtaining a Global Estimate of Open Ocean Export 46
3.3.1 Freshwater Export 46
3.3.2 Nutrient Export 49

Chapter 4 Discussion **58**

4.1 The Idealized Model Experiments 58
4.1.1 The Influence of Different Factors on Plume Transport 59
4.1.2 Describing River Plume Export with Simple Metrics 62

4.2 Estimates of River Plume Export 64
4.2.1 Estimating Nutrient Removal 64
4.2.2 Budgets of Fresh Water and Nutrients 67

Chapter 5 Conclusions **74**

Bibliography **76**

Appendix A Supplementary Figures for Chapter 3 . . . . . **83**

Appendix B Tables of Global Riverine Export of Fresh Water and Nutrients 92

Appendix C Calculation Steps for Estimating Export **99**

LIST OF TABLES

1.1	CMIP5 model overview	4
2.1	Overview of the idealized model experiements	12
2.2	Overview of the world's largest rivers by discharge	18
3.1	S_P regression coefficients	39
3.2	Comparison of local, regional, and global freshwater and nutrient budgets with previously published values	57
B.1	Global freshwater export estimates in 10° latitude bands	92
B.2	Global DIN export estimates in 10° latitude bands	93
B.3	Global DON export estimates in 10° latitude bands	94
B.4	Global DIP export estimates in 10° latitude bands	95
B.5	Global DOP export estimates in 10° latitude bands	96
B.6	Global DOC export estimates in 10° latitude bands	97
B.7	Global DSi export estimates in 10° latitude bands	98

LIST OF FIGURES

1.1 Images of real plumes 2

1.2 Schematic of coastal ocean budget sources and sinks 3

2.1 An idealized river plume in the northern hemisphere. 8

2.2 The idealized model domain 11

2.3 Examples of idealized wind and tide forcing 13

2.4 Rivers in the GlobalNEWS model 17

2.5 Columbia River bathymetry 19

2.6 GloabalNEWS DIN 19

2.7 Gloabal river discharge and shelf width 20

3.1 Surface salinity contours of simulated pumes after 20 days 22

3.2 Offshore distance of plume detachment after 20 days 23

3.3 Bottom salinity contours of simulated plumes after 20 days 24

3.4 Time series of cross-shelf freshwater transport 25

3.5 Development of bulge instabilities 26

3.6 Simulated freshwater export efficiency and retention without any forcing from wind or tides 27

3.7 Sensitivity of unforced transport to changes in the domain 29

3.8 Simulated plumes under different forcing conditions 31

3.9 Simulated freshwater export efficiency and retention with tidal forcing 32

3.10 Simulated freshwater export efficiency and retention with alongshore-dominant wind forcing 34

3.11 Simulated freshwater export efficiency and retention with cross-shelf dominant wind forcing 35

3.12 Cross-shelf export efficiency as a function of the S_P number for the unforced simulations 37

3.13 Cross-shelf export efficiency as a function of the S_P number for the alongshore-dominant wind forced simulations 38

3.14 Cross-shelf export predicted by the range of S_P coeffients 40

3.15 Alongshore freshwater export as a function of $R_o^{'}$ for all simulated plumes 42

3.16 Regressions applied to $\Delta\rho h$ and $\Delta\rho h^2$ as a function of river discharge 43

3.17 Regressions applied to $\Delta\rho h$ and $\Delta\rho h^2$ as a function of river discharge and latitude 44

3.18 Plume export timescale time of the simulated plumes as a function of the S_P number 45

3.19 Estimated freshwater budgets for the Amazon, Mississippi, and Columbia Rivers 47

3.20 Estimated export efficiency of fresh water to the open ocean for rivers in the GlobalNEWS model 48

3.21 Freshwater budgets in 10° latitude bands. 49

3.22 River mouth locations and freshwater budgets for four socioeconomic regions 50

3.23 Global riverine loads and conservative cross-shelf export of different nutrients 51

3.24 Global distribution of estimated export timescales 52

3.25 Estimated nutrient budgets for the Amazon, Mississippi, and Columbia Rivers for a processing rate of 0.75 d^{-1} 53

3.26 Global export of DIN and DON for different shelf processing timescales 54

3.27 Comparison of DIN and DSi delivery and export in 10° latitude bands 55

4.1 Percent removal of DIN and DIP as a function of export timescale according to empirical relationships 73

A.1 Cross-shelf export efficiency as a function of the S_P number for the tidally forced simulations 84

A.2 Cross-shelf export efficiency as a function of the S_P number for the alongshore dominant wind forced simulations 85

A.3 DON delivery and export in 10° latitude bands 86

A.4 DIP delivery and export in 10° latitude bands 87

A.5 DOP delivery and export in 10° latitude bands 88

A.6 DOC delivery and export in 10° latitude bands 89

A.7 Global export of DIP and DOP for different shelf processing timescales 90

A.8 Global export of DOC and DSi for different shelf processing timescales 91

ABSTRACT

Rivers connect land and sea, delivering large amounts of terrestrially derived materials (such as nutrients, sediments, and pollutants) to the coastal ocean. Understanding the fate of this delivery is critical. Nutrients can accumulate on shelves, driving high levels of primary production, which can lead to hypoxia, or they can be exported rapidly across the shelf to the open ocean where their impact is minimized. With global ocean models unable to resolve the small-scale processes of riverine export to the open ocean, they are often parameterized with an "all or nothing" approach: either all of the riverine material enters the open ocean (ignoring shelf processes), or none of it does. Both approaches potentially misrepresent riverine export. Using an idealized river plume model, I assess the impact of latitude, river discharge, winds, and tides on the cross-shelf export of riverine material. From these numerical experiments, latitude is shown to be a strong controlling factor in determining the cross-shelf export within river plumes, which can only be slightly offset by external forcing from winds. It is possible to parameterize the resulting export using the S_P number—a dimensionless number relating the cross-shelf extent of a plume to the local shelf width. I use this simple relationship to estimate global export of riverine fresh water and nutrients to the open ocean. Globally, I estimate that just 15–53% of riverine fresh water reaches the open ocean through direct transport within river plumes, with greatly reduced nutrient export due to shelf processing.

LIST OF ABBREVIATIONS AND SYMBOLS USED

Abbreviations	Description
CMIP5	Coupled Model Intercomparison Project Phase 5 (*Taylor et al.* 2012)
CPU	Central Processing Unit
DIN	Dissolved Inorganic Nitrogen
DIP	Dissolved Inorganic Phosphorus
DOC	Dissolved Organic Carbon
DON	Dissolved Organic Nitrogen
DOP	Dissolved Organic Phosphorus
DSi	Dissilved Silica
GlobalNEWS	Global Nutrient Export from WaterSheds (*Mayorga et al.* 2010)
IPCC	Intergovernmental Panel on Climate Change
ROMS	Regional Ocean Modelling System (*Haidvogel et al.* 2008)
For model run abbreviations, see Table 2.1	

Greek symbol	Description	Units
$\Gamma_{(X,A)}$	Transport of fresh water or nutrients (in the cross-shelf or alongshore direction)	$m^3\ s^{-1}$ or Mg[Nut] y^{-1}
ϕ	Latitude	$^\circ$
ρ	Density of water	$kg\ m^{-3}$
ρ_o	Ambient density (here, $1025\ kg\ m^{-3}$)	$kg\ m^{-3}$
τ_E	Exposure timescale	d
τ_P	Processing timescale	d

Roman symbol	Description	Units
C^{Nut}	Nutrient concentration	Mg[Nut] m^{-3}
D_S	Shelf width	km
$E_{(X,A)}$	Export efficiency (cross-shelf or alongshore)	-
f	Coriolis parameter	s^{-1}
F_{FW}	Fresh water fraction	-
g	Acceleration due to gravity	$m\,s^2$
h	Mean plume depth	m
H	Water depth (half depth at shelf break)	m
L^{Nut}_{River}	Riverine nutrient load	Mg[Nut] y^{-1}
N_E	Damköhler number	-
Q	River discharge	$m^3\,s^{-1}$
r	Specific rate of removal for non-conservative nutrients	d^{-1}
R'_o	Internal Rossby radius of deformation	km
$R_{Shelf/Source}$	Fraction of material retained on the shelf/near the source	-
S	Salinity	-
S_0	Ambient salinity (here, 32)	-
S_P	Dimensionless number comparing plume width to shelf width	-
T_E	Export timescale of plume	d
$u\,v$	Horizontal velocity components	$m\,s^{-1}$
$x\,y\,z$	Horizontal and vertical coordinates	-

ACKNOWLEDGEMENTS

The completion of this work is only the result of the support and opportunities provided by many people to whom I am deeply grateful.

First and foremost, thank you, Katja, for your support and guidance over the past two years. I have grown so much under your supervision; not only do you teach through instruction, but you lead by example in your dedication and tireless efforts.

I am also grateful to Dr. Michael Whitney (University of Connecticut) for serving as my external examiner, and for the input of Drs. Jinyu Sheng and Chris Algar as members of my thesis committee. Further, I am extremely thankful for the valuable and incisive input from Dr. Rachel Horwitz as an ex-officio member of my advisory committee. Throughout this entire process, Dr. Jonathan Sharples (University of Liverpool) was also always willing to share his work and make available to me any revisions to his manuscript. Funding for this work was provided in part through the NSERC CGS-M award and the Nova Scotia Scholarship. I am incredibly grateful to the granting agencies for their support.

Thank you to everyone in the Department of Oceanography who made each day at the office an enjoyable one, and who was there to help me with any number of tasks; in particular the Marine Environmental Modelling group (MEMG). I am especially grateful for the friendship and support of my fellow graduate students and my Seadogs teammates.

To my family: thank you for all of your love and support, not just throughout this degree, but for the many years that have led to this point. Thank you for always pushing my to be my best, and believing nothing short of it could even be possible from me.

Last but not least: Maaike. Thank you for all of your encouragement and love. Throughout these past two years, your unwavering support and belief in me has helped more than you will ever know. Thank you for being by my side, even with the entire country between us.

CHAPTER 1
INTRODUCTION

Freshwater plumes associated with river mouths are common features of the world's coastlines (see example in Figure 1.1). They connect the continents and the coastal ocean, bringing with them not only fresh water, but also large amounts of terrestrially derived materials (e.g., from erosion, weathering, agricultural run off, and urban and industrial activity) including nutrients, sediments, and pollutants. It is unclear, however, how much of these terrestrial materials are efficiently exported to the open ocean (defined here as ocean deeper than 200 m), and how much is retained in continental shelf systems.

A significant source of materials to the coastal ocean from adjacent continents, river loads can drive primary productivity in the coastal ocean. In cases where nutrient delivery is particularly high and export to the open ocean inefficient, eutrophication, and subsequent effects such as harmful algal blooms, hypoxia, fish kills, and habitat loss can have repercussions for human uses (e.g., *Diaz and Rosenberg* 2008; *Doney* 2010; *Galloway et al.* 2004; *Seitzinger et al.* 2010). Where cross-shelf export of riverborne materials to the open ocean is efficient, the risk of these negative effects is lower (e.g., *Chen et al.* 2003; *Gruber and Galloway* 2008).

For rivers that pass through areas of high human activity, retention and accumulation of nutrients on the shelf can be particularly problematic. The Mississippi River, for example, drains a large fraction of the continental United States (approximately 41%), including agricultural regions where fertilizer use is high. As a result, nutrient concentrations in the lower Mississippi are high and bring significant nutrient loads to the shelf of the northern Gulf of Mexico where they contribute to extensive hypoxia (e.g., *Bianchi et al.* 2010; *Rabalais et al.* 2002; *Wiseman et al.* 1997).

Globally, nutrient loads to the coastal ocean have increased dramatically compared to preindustrial levels due to increasing use of industrial fertilizers to feed the growing world population, and other human activities (*Diaz and Rosenberg* 2008; *Galloway et al.* 2004; *Seitzinger et al.* 2010). Nitrogen delivery by rivers, for example, increased by 40% from 1970 to 2000: a trend that is predicted to continue (*Galloway et al.* 2004). How these

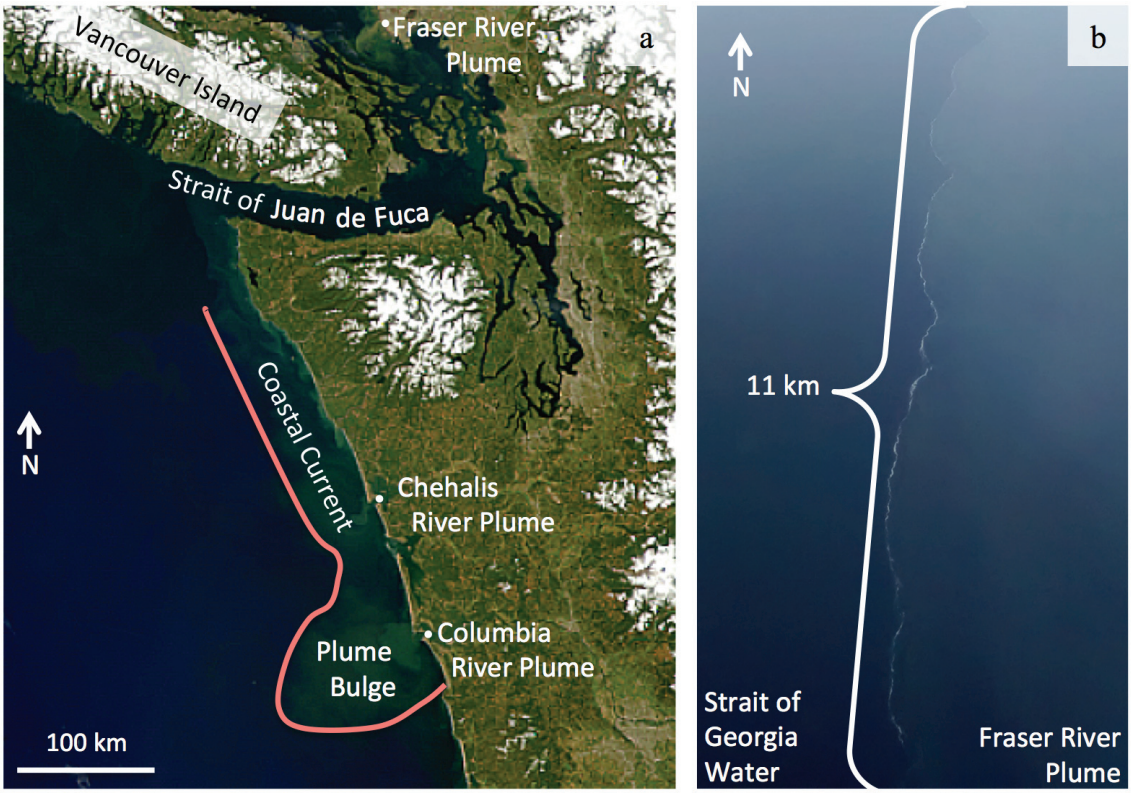

Figure 1.1: a) The Columbia River plume as seen by NASA's SeaWiFS instrument from space[1]. The plume (roughly outlined in pink and visible due to high sediment and chlorophyll concentrations) deflects to the right, forming a bulge and a coastal current that travels north toward the Juan de Fuca Strait and Vancouver Island. b) Sharp front created at the interface of the Fraser River plume in the more saline Strait of Georgia[2].
[1]Image source: NASA Visible Earth (http://visibleearth.nasa.gov/view.php?id=52924)
[2] Photograph taken at an altitude of 1200 m on 26 March, 2016

materials are transported will determine their impact on coastal systems.

A common approach for assessing the importance of different transport and transformation processes is through the analysis of freshwater and nutrient budgets. Analogous to their economic counterparts, oceanographic budgets compare the sources, sinks, and reservoirs (similar to income, expenses, and accounts) of a given material within a specific area (Figure 1.2). They can be calculated at local scales (e.g. for a single river as in *Lehrter et al.* 2013), on regional scales (like the Gulf of Mexico, *Xue et al.* 2013), and even for the global continental shelf (e.g., *Rabouille et al.* 2001).Within the context of the shelf system, riverine inputs and transports are often masked by other shelf processes such as open ocean exchange.

The question of how much riverine material reaches the open ocean is relevant for

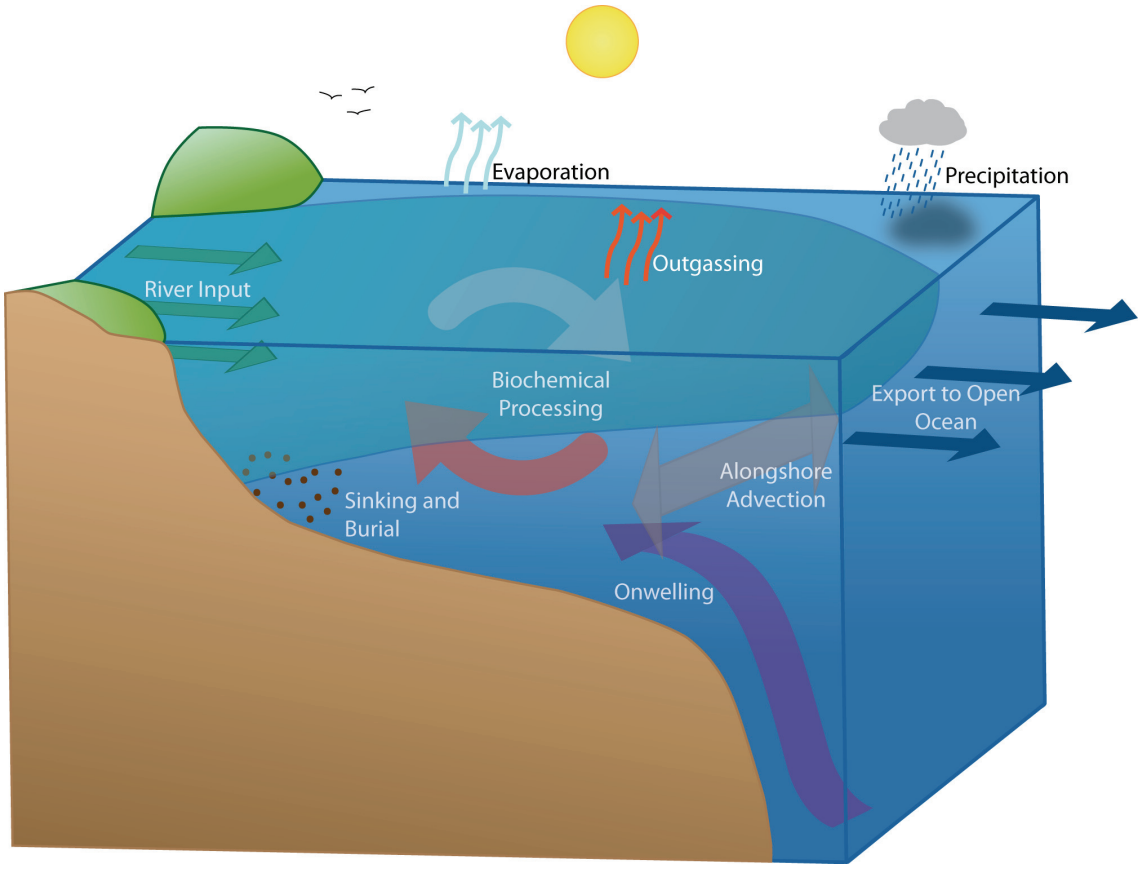

Figure 1.2: Schematic of some coastal ocean sources and sinks that could be considered in freshwater and nutrient budgets. River inputs and export are just part of the system.

global budgets and global models. Often, global models are too coarse to resolve the comparatively small-scale features of the coastal ocean, let alone individual rivers and their plumes. Presently, riverine inputs to global models are usually represented using an "all or nothing" approach: either river inputs are added directly to the open ocean (bypassing the shelf), or river inputs are ignored altogether. This can be illustrated using the most recent IPCC CMIP5 models as examples. *Bopp et al.* (2013) and *Anav et al.* (2013) assess the representation of the global carbon cycle within some of these models, ten of which are listed in Table 1.1. Of these ten models, only two consider riverine inputs (by taking the "all" approach), while the rest assume that there are no riverine inputs to the ocean.

On a local scale, box models can be useful in assessing export of riverine materials to the open ocean. For example, *Garvine and Whitney* (2006) outline the development of a box model based on the potential energy anomaly of the system to estimate fresh water export to

Model	Resolution (Lon x Lat) (Vert Levels)	Treatment of Riverine Nutrients	References
CanESM2	1.4° x 1° 40	None	*Arora et al.* (2011)
CESM1-BGC	1.25° x 0.27-0.53° 60	None	*Gent et al.* (2011); *Moore et al.* (2013)
CMCC-ESM	0.5-2° 31	None	*Vichi et al.* (2006); *Vichi et al.* (2011)
GFDL-ESM2M/G	0.3-1° 50/63	Coastal Inputs[a]	*Dunne et al.* (2012); *Dunne et al.* (2013)
HadGEM2-ES	0.3-1° 40	None	*Palmer and Totterdell* (2001)
INM-CM4	1° x 0.5° 40	None	*Volodin et al.* (2010)
IPSL-CM5A-LR/MR	0.5-2° 31	Coastal DOC Inputs[b]	*Dufresne et al.* (2013)
MIROC-ESM	1.4° x 1° 44	None	*Watanabe et al.* (2011)
MPI-ESM-LR/MR	1.5° 40	None	*Giorgetta et al.* (2013); *Ilyina et al.* (2013)
NorESM1-ME	1.125° 53	None	*Bentsen et al.* (2013); *Tjiputra et al.* (2013)

[a]Directly apply coastal DIN inputs from the GlobalNEWS1 model (*Seitzinger et al.* 2005) and DIC, alkalinity, and organic carbon estimated by *Dunne et al.* (2007).

[b]Directly apply coastal riverine DOC estimates from *Ludwig et al.* (1996).

Table 1.1: Some of the CMIP5 models compared by *Bopp et al.* (2013) and *Anav et al.* (2013) to assess the representation of the global carbon cycle. Of the ten models, just two include nutrient inputs from rivers.

the open ocean within climate models. However, such an approach is difficult to generalize on a global scale, requiring specific knowledge of individual rivers' properties. *Rabouille et al.* (2001) and *Laruelle et al.* (2009) have attempted to address coastal processing in simple, global mass balance models by assessing coastal ocean nutrient budgets and fluxes. Their approaches consider shelf processing of materials, but do not account for differences between shelf zones around the globe and make many simplifying assumptions about the physical and biochemical processes taking place.

The physical dynamics of river plumes have been investigated extensively in previous observational, experimental, and modelling studies. For example, the Columbia River

(*Horner-Devine* 2007), the Delaware Coastal Current (*Münchow and Garvine* 1993), the Hudson River (*Chant et al.* 2007), the Rhine River (*Simpson et al.* 1993), and the Yangtze (*Beardsley et al.* 1985), among many others, have been subject to dedicated observational studies. Similarly, previous modelling studies have explored the influence of estuarine properties (e.g., *Garvine* 2001; *McCreary et al.* 1997; *Sheng* 2001), bathymetry (e.g., *Chao* 1988; *Schiller and Kourafalou* 2010; *Yankovsky and Chapman* 1997), wind (e.g., *Berdeal et al.* 2002; *Fong and Geyer* 2001; *Hetland* 2005; *Jurisa and Chant* 2013), and tides (e.g., *Isobe* 2005; *Chen* 2014) on river plumes. The majority of these efforts have focused on the physical properties of the plume, including its overall shape and size, as well as their impact on the downstream coastal current. However, little attention has been paid to the potential of plumes to export riverine material across the shelf break into the open ocean.

Recently, *Sharples et al.* (in revision) proposed a simple parameterization to describe riverine export to the open ocean based on the ratio of a plume's width (assumed to scale with the internal Rossby radius of deformation) to the local shelf width. When a plume extends beyond the shelf, *Sharples et al.* (in revision) predict material will be exported to the open ocean efficiently and rapidly. Conversely, if the shelf is wider than the plume, no direct cross-shelf transport is expected to occur. Using empirical formulae to calculate biochemical nutrient removal, *Sharples et al.* (in revision) conclude that efficient transport occurs primarily within 20° of the Equator, and along continental margins where shelves are narrow. They estimate that approximately 75% DIN and 80% DIP delivered by rivers globally reach the open ocean. This simplified approach holds great potential for providing estimates of retention of riverine material on the shelf versus export to the open ocean. However, their work was based solely on theoretical scaling arguments and not a detailed numerical study. Further testing is needed to ensure that this simple relationship can be used to describe cross-shelf export of river nutrients globally before the methodology can be adopted with confidence.

Building on this previous work, my objective is a detailed assessment of how the physical dynamics of river plumes affects cross-shelf and alongshore export of materials in river plumes using a series of idealized model experiments (Section 2). The experiments focus on four factors influencing plume structure and dynamics: latitude, river discharge, winds, and tides. The first two—latitude and discharge—capture variations among rivers around the world, but neglect further external forcing. Simulations with winds and tides then aim

to characterize the impact of additional external forcing. Although many other forcing factors could be considered, the four chosen here turned out to be the most important in influencing the plume structure during initial numerical tests, and can be easily generalized to describe a wide range of plumes (as opposed to, for example, the impact of bathymetry which is more difficult to compare over a wide range of rivers).

From the idealized experiments, I develop a simple framework to describe cross-shelf plume export using easily measured properties of a river mouth (e.g., its discharge, latitude, and distance to the shelf break). I then apply this relationship to global rivers in order to estimate the export of riverine fresh water and nutrients to the open ocean. In my assessment, I focus on the direct export of materials within river plumes, as opposed to subsequent transport processes that occur on longer timescales after riverine nutrients have undergone many stages of biochemical transformation on the shelf.

CHAPTER 2
METHODS AND MODEL

2.1 Factors that Influence Cross-Shelf Transport in River Plumes

Whether riverborne materials are transported efficiently to the open ocean within river plumes or retained on shelves is strongly influenced by the physical dynamics of the plumes themselves. There are many factors that can influence the structure and transport of plumes, with careful consideration of their significance needed when developing numerical models to study plume behaviour. As a result, the simplified approach taken by *Sharples et al.* (in revision), and similar theoretical and idealized approaches may not capture all of the important dynamics. However, it is useful to study the behaviour of plumes under idealized conditions with external factors carefully controlled or removed in order to gain insight into their effects and relative importance, and it is necessary to do so when aiming to derive globally applicable parameterizations.

In an unforced setting, plume dynamics are the result of the underlying behaviour of buoyant flows entering the coastal ocean, with latitude and riverine discharge important factors in determining the shape and structure of the plume. At the river mouth, light, fresh water encounters denser, saline water within an estuary or on the shelf. While some mixing occurs, the resulting outflow often remains much less dense than the shelf water, and floats above the ambient water as a buoyant plume. Plumes and their associated fronts (sharp density gradients; see example in Figure 1.1b) occur over a wide range of spatial scales (*O'Donnell* 1990). If the plume is larger than the Rossby radius of deformation, it is influenced by the Earth's rotation through the Coriolis force (*Hill* 1998), turning toward the coast in the direction of Kelvin wave propagation (to the right in the northern hemisphere, and left in the southern hemisphere; hereafter referred to as downstream after *Garvine* 2001). Two distinct regions are predicted to occur within the resulting plume: an anticyclonically rotating bulge region near the inflow and an alongshore coastal current that remains attached to the coast as it travels downstream (e.g., *Horner-Devine et al.*

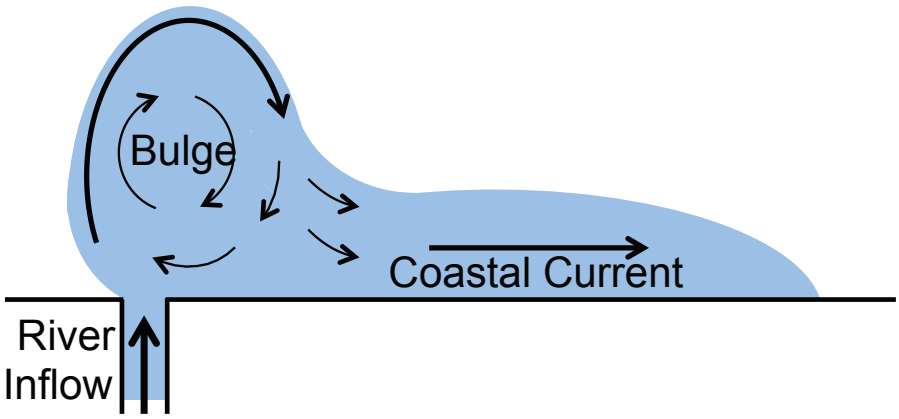

Figure 2.1: An idealized river plume in the northern hemisphere. Due to the Coriolis force, the plume is deflected to travel along the coast in the direction of Kelvin wave propagation.

2015; Figure 2.1). This theoretical structure and the associated seaward expansion of the plume is governed by three different aspects (*McClimans* 1986): 1) the balance between inertia and buoyancy forces, which determines the offshore acceleration of the plume; 2) mixing at the frontal interface between the plume and the ambient water, which ensures the plume extension is finite; and 3) the geostrophic balance between the Coriolis force and the cross-shore pressure gradient that leads to the coastal current.

Often, this well-defined theoretical structure is not observed in nature due to complex bathymetry and coastlines, and the presence of external forcing factors (e.g., wind and ambient currents), which influence plume structure and transport. For example, bulges are often absent from real world plumes (*Garvine* 2001), with the Columbia (*Horner-Devine* 2007; Figure 1.1a) and Hudson Rivers (*Chant et al.* 2007) being notable exceptions that regularly form bulges.

The depth and width of the outflow at the river mouth and bottom topography are all known to play a major role in determining a river plume's shape and size (e.g., *Kourafalou et al.* 1996; *Fong and Geyer* 2002; *Sheng* 2001; *Yankovsky and Chapman* 1997). *Fong and Geyer* (2001) note that an increase in inflow depth results in an increase in alongshore transport within the plume. *Garvine* (2001) further notes that the shape of the inflow for simulated plumes (i.e., point source versus more realistic estuary/river mouth) influences the resulting shape of the plume. When a more realistic mouth is used, plumes have a smaller bulge region (similar to those often seen in nature). Similarly, *Wright* (1989) and *Yankovsky and Chapman* (1997) point out that if a plume interacts with the seafloor it can

be advected significantly further offshore through bottom interaction, which would lead to an increase in cross-shelf plume transport. Generalizing a river domain, beyond a simple rectangular basin to address these influences, however, is beyond the scope of this study.

External forces beyond those imposed by a river's latitue and discharge, such as the presence of an ambient shelf current, lead to the plume reaching a steady state after a short period of time (e.g., *Fong and Geyer* 2002; *Garvine* 2001). *Garvine* (2001) notes that, without external forcing, simulated plumes grow continuously: a trait that is rarely observed in nature due to the presence of many overlapping forces. Another control on the offshore extent of plumes is the difference between the plume's salinity and the ambient shelf water; if the salinity of the plume is below a critical level, mixing will erode the plume front, restricting its extension (*Hetland* 2005). Forcing, though common in occurrence to all shelves, is difficult to generalize.

Consideration of all of the above factors is neither realistic nor desirable in this work where the goal is to determine a simple, general understanding of how physical plume dynamics govern cross-shelf and alongshore export that can be applied in a range of settings. As such, only some of the above factors, such as inflow depth, are considered in sensitivity analyses for the idealized model domain, but many are not addressed. The four primary factors considered in the idealized experiments are: latitude, river discharge, wind forcing and tides. They are ubiquitous, albeit variable, for global shelf systems.

Through the Coriolis force, changes in latitude are expected to influence the deflection of the plume, with higher latitude plumes more likely to remain close to the coast, causing the offshore extent and subsequent cross-shelf transport to be small. Overall, discharge and transport are directly related (more water means correspondingly more transport); however, high discharge plumes can also detach from the coast and move offshore (*McCreary et al.* 1997), which would enhance cross-shelf transport. The presence of tides has been shown to stabilize river plume bulges (*Isobe* 2005; *Chen* 2014). This is expected to cause a reduction in the offshore extent of the plume, potentially reducing cross-shelf transport.

Winds have the potential to significantly impact plume transport (e.g., *Horner-Devine et al.* 2015), and are the most complex forcing addressed in this research. *Hetland* (2005) shows that upwelling-favourable winds can drive a plume offshore, while downwelling-favourable winds force the plume toward the coast. When applied to cross-shelf transport, this suggests that upwelling winds should increase delivery of riverborne materials to the

open ocean, with the opposite occurring for downwelling winds. Further, *Kourafalou et al.* (1996) and *Jurisa and Chant* (2013) found that plume transport is driven predominantly by wind-induced Ekman transport. *Fong and Geyer* (2002) note that the response of plumes to wind forcing is much faster than plumes are able to reach a steady state, meaning that the influence of winds strongly determines plume development.

2.2 The Idealized River Plume Model

I implemented a three-dimensional idealized river plume model using the Regional Ocean Modelling System (ROMS; *Haidvogel et al.* 2008). ROMS is a primitive equation, general circulation model that can be applied to a wide range of settings and problems.

For the purposes of this research, I used an idealized rectangular domain (Figure 2.2) measuring 200 km in the cross-shore direction and 500 km in the alongshore direction, with 2.5 km horizontal resolution, 15 vertical sigma levels (with tighter spacing near the surface), three open boundaries, and no-slip conditions at the coast. The bathymetry is uniform in the alongshore direction, and has a gentle slope of 0.6 $\mathrm{m\,km^{-1}}$ from coast to the shelf break which is located 65 km offshore. Fresh water enters the domain as a point source (with salinity of 0) through a 10 m-deep, 20 km-long coastal channel (so that the inflow at the coast is not completely fresh). The ambient salinity is 32, and the water temperature is uniform throughout the domain and identical to the river inflow (no initial stratification). Shelf stratification due to non-uniform temperature would impact the results (by restricting vertical mixing), but was not addressed here for the sake of simplicity.

A series of initial tests showed that a horizontal resolution of 2.5 km is sufficient for resolving many of the plume features and instabilities without significantly limiting computational time (at 1 km resolution there is little change in the simulated plumes, but computation time increases by a factor of 7). The vertical resolution is sufficient to capture the plume's vertical structure, with simulated plumes being almost exclusively confined to the upper 20 m.

The horizontal extent of the domain, in both the cross-shelf and alongshore directions, is such that none of the simulated plumes interact significantly with the boundaries. Radiation/nudging conditions are prescribed at the open boundaries for temperature, salinity, and 3D momentum, with nudging to the ambient state (effectively erasing the plume at the boundaries). A 25 km-wide sponge region along the open boundaries,

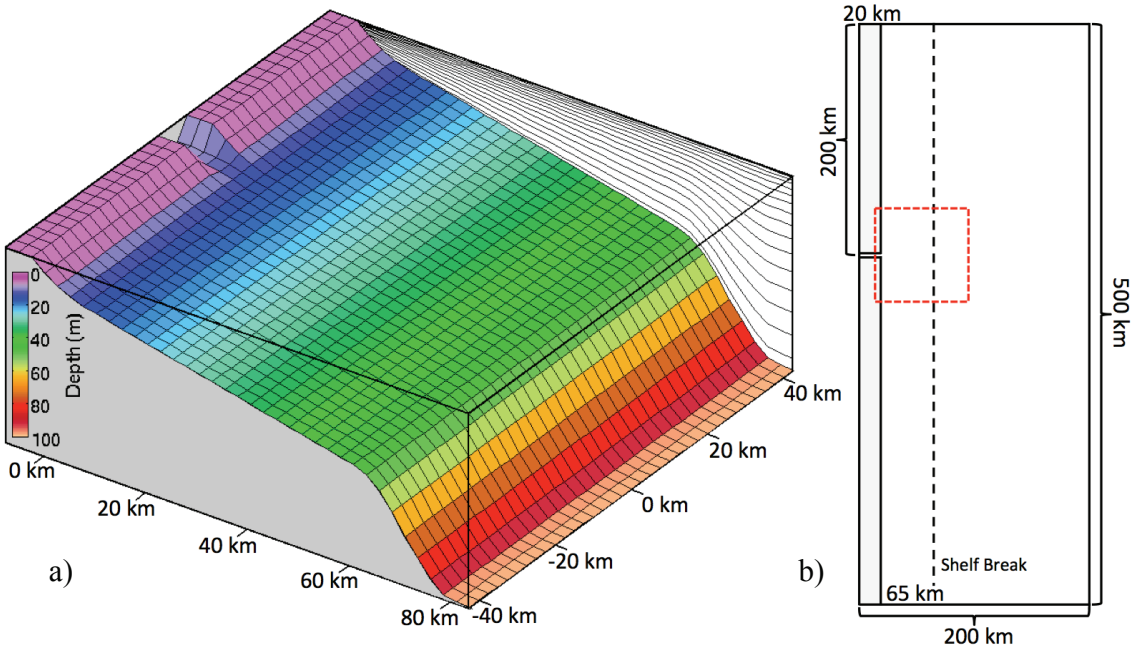

Figure 2.2: a) A portion of the model domain (red box in b) with vertical levels indicated by grey lines. b) The full domain extends 200 km in the offshore direction, and 500 km in the alongshore, with a freshwater input to a 5 km wide channel located 200 km from the northern boundary of the domain and 20 km from the coast.

where the viscosity is incrementally increased toward the boundary, further minimizes any boundary interactions. The sponge region was excluded in all subsequent analyses.

I use a k–ε turbulence closure scheme, with a background vertical mixing coefficient of 5 x 10^{-6} m^2 s^{-1}. Initial tests showed the choice of this coefficient (either doubling or increasing it by an order of magnitude) did not significantly affect the simulated plumes to justify a full sensitivity assessment of the vertical mixing parameterization.

I ran the river plume model for the various latitudes, discharges, and forcing scenarios described in Table 2.1. On an x86-64 multi-node Linux cluster using 8 CPUs (2 nodes with 4 CPUs each), 50 days of simulation time took approximately four hours of clock time to complete. An internal model time step of 120 s was sufficient for all but the highest discharge scenarios (100 000 m^3 s^{-1}), for which 60 s was used. The model state was saved every six hours of simulation time (although twelve hours proved sufficient for capturing most variability) except the tidally forced plumes, which were saved every 3 hours in order to avoid aliasing with the 12-hour tidal period (Section 2.2.1).

	Lat	f (x 10^{-4} s^{-1})	Q (x 10^3 m^3 s^{-1})	Max Wind ($m\,s^{-1}$)
Latitude and discharge varied. No tides. No wind forcing.				
DL001	0°	0	1.5	None
DL011	1°	0.025	1.5	None
DL051	5°	0.127	1.5	None
DL101	10°	0.253	1.5	None
DL151	15°	0.377	1.5	None
DL301	30°	0.729	1.5	None
DL451	45°	1.031	1.5	None
DL601	60°	1.263	1.5	None
DLxx5	0-60°	0-1.263	5	None
DLxx10	0-60°	0-1.263	10	None
DLxx20	0-60°	0-1.263	20	None
DLxx50	0-60°	0-1.263	50	None
DLxx80	0-60°	0-1.263	80	None
DLxx100	0-60°	0-1.263	100	None
DL runs with tides: 1 m tidal forcing with 12-hour period. No wind forcing.				
TDL	Same as DL runs, but with tidal forcing added.			
Wind forcing, but no tides. Winds are: – constant, unidirectional (UpW, DnW, OnW, and OffW); – periodic bidirectional (UpDnW, and OnOffW); and – synthetic real winds with either dominant alongshore (AWDL) or cross-shelf winds (XWDL). Synthetic winds equivalent to the DL runs. Others only for 1 500 m^3 s^{-1}.				
UpW	0-60°	0-1.263	1.5	$u = 0$ $v = 5$
DnW	0-60°	0-1.263	1.5	$u = 0$ $v = -5$
OnW	0-60°	0-1.263	1.5	$u = 5$ $v = 0$
OffW	0-60°	0-1.263	1.5	$u = -5$ $v = 0$
UpDnW	0-60°	0-1.263	1.5	$u = 0$ $v = \pm 5$
OnOffW	0-60°	0-1.263	1.5	$u = \pm 5$ $v = 0$
AWDL	0-60°	0-1.263	1.5-100	$u = \pm 1$ $v = \pm 5$
XWDL	0-60°	0-1.263	1.5-100	$u = \pm 5$ $v = \pm 1$
Bottom slope is doubled/halved from its base value of 0.6 $m\,km^{-1}$. Discharge is constant at 1 500 $m^3 s^{-1}$ and 50 000 m^3 s^{-1}, with no external forcing.				
DblSlp/ HlfSlp	Bottom slopes of 1.2 $m\,km^{-1}$ (double) and 0.3 $m\,km^{-1}$ (half), respectively, over all latitudes.			
River inflow depth is doubled/halved from its base value of 10 m. Discharge is constant at 1 500 $m^3 s^{-1}$ and 50 000 m^3 s^{-1}, with no external forcing.				
DpIn/ ShIn	Same as slope tests, but instead change river inflow depth to 20 m (deep) and 5 m (shallow), respectively.			

Table 2.1: Overview of the different idealized model runs performed.

2.2.1 Wind and Tidal Forcing

The model was run both with and without forcing from wind and tides (Table 2.1). For the wind-forced scenarios, I used 1) unidirectional constant speed winds (alongshore to the north and south, simulating up and downwelling conditions, and on/offshore winds); 2) bidirectional winds with a sinusoidal cycle in time (cycling weekly between up– and downwelling conditions or diurnally between on– and offshore); and 3) a synthetic wind field designed to mimic realistic variability. The latter combines an idealized sinusoidal wind that imitates upwelling and downwelling cycles with diurnal on/offshore variability and slight random perturbations (Figure 2.3, left). For this "realistic" wind scenario, I tested the influence of direction with two different wind fields: one where the alongshore components were stronger (AWDL, with a maximum wind speed of 5 m s^{-1} alongshore, and 1 m s^{-1} cross-shore; see Figure 2.3, left) and one where the cross-shore on/offshore variability was stronger (XWDL: maximum speed of 5 m s^{-1} cross-shore, and 1 m s^{-1} alongshore). Wind is applied uniformly throughout the entire domain over the complete duration of the simulations, converting wind speed to wind stress using a drag coefficient of 1.25 x 10^{-3} (*Kara et al.* 2007).

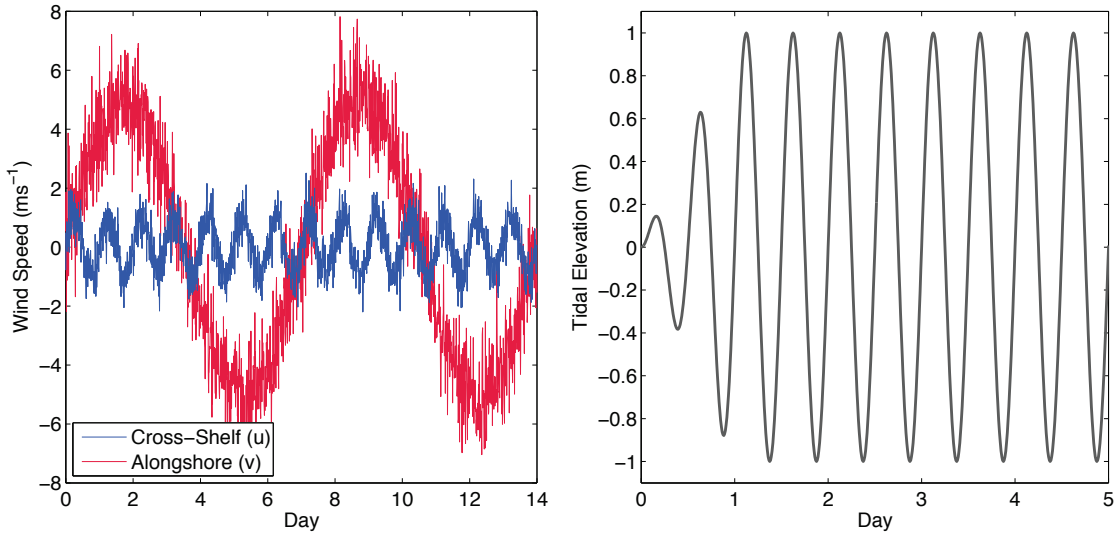

Figure 2.3: Example forcing fields. Left, the realistic alongshore-dominant wind with a weekly variation between up and downwelling winds (the alongshore direction), superimposed with a weaker diurnal land/sea breeze (cross-shore). Right, the 1 m, 12-hour tidal signal applied to the domain was ramped up over the first day.

For the tidally forced model runs, I applied a 12-hour (semi-diurnal) tidal cycle (approximately the same frequency as the primary lunar and solar semi-diurnal tides: M2 and S2, respectively) at the eastern boundary, such that the elevation at the coast is 1 m (Figure 2.3, right) and the imposed tidal currents are 0.1 $\mathrm{m\,s^{-1}}$. This tidal forcing is, of course, highly idealized when compared to tides around the world. However, it serves to assess the influence forcing on a tidal timescale. To avoid numerical instabilities, the tides ramped up to their maximum elevation over the course of one day. The model state was saved at the peak tidal amplitudes ($\pm$1 m), as well as the maximum ebb/flood conditions (at the inflection points of the sinusoidal wave).

2.3 Metrics Used to Assess the Simulated Plumes

In the literature, many metrics have been used to describe river plumes. My analysis focuses on just two primary metrics: the S_P number (*Sharples et al.* in revision), and the export efficiency. These metrics have the benefit of being easily calculated from numerical model output, and use simple and easily accessible characteristics of plume properties, such as river discharge.

2.3.1 The S_P Number

Sharples et al. (in revision) use the S_P number to relate the approximate width of a plume (estimated at twice the internal Rossby radius: $2R_o^{'}$) to the local shelf width (D_S):

$$S_P = \frac{2R_o^{'}}{D_S}. \tag{2.1}$$

When $S_P > 1$, as might occur for low latitude plumes where $R_o^{'}$ is large, or at active margins where the shelf width is small, *Sharples et al.* (in revision) assume that riverborne materials are efficiently transported to the open ocean. Conversely, a value of $S_P < 1$ indicates direct transport to the open ocean is negligible. Other studies have shown the width of the plume can be greater than twice the internal Rossby radius (potentially larger than $4R_o^{'}$; see, for example, *Yankovsky and Chapman* 1997), but the factor of two is used here to be consistent with *Sharples et al.* (in revision).

The internal Rossby radius is the length scale over which Earth's rotation becomes important for influencing fluid motion and can be defined mathematically for a two-layer stratified flow as follows (*Csanady* 1971):

$$R_o' = \frac{\sqrt{g\frac{\Delta\rho}{\rho_o}h\frac{(H-h)}{H}}}{f}, \tag{2.2}$$

where g is the acceleration due to gravity, ρ_o the ambient density (here 1025 kg m^{-3}), $\Delta\rho$ the anomaly between the mean plume density and the ambient density, H half the water depth at the shelf break, h the mean plume depth, and f the Coriolis parameter (which depends on the sine of the latitude). $\Delta\rho$ and h are calculated as the mean over the entire plume.

2.3.2 Export Efficiency

Export efficiency, E_D^M, is defined here simply as the ratio of the total, time-integrated cross-shelf transport, Γ_D^M, where D refers to either the cross-shelf or alongshelf direction (X or A, respectively) and M to the material being transported (e.g., fresh water or nutrients) divided by the total, time-integrated river input/load of the component, L_{River}^M (discharge, Q, in the case of fresh water). Export efficiency thus provides a measure of the fraction of riverborne materials being exported either in the cross-shelf direction to the open ocean, or downstream from the source in the coastal current:

$$E_D^M = {}^{\Gamma_D^M}\!/_{L_{River}^M}. \tag{2.3}$$

It then follows that the amount retained on the shelf is simply:

$$R_{Shelf}^M = 1 - E_X^M, \tag{2.4}$$

which can be broken further into the near and far field as the fraction retained near the source (R_{Source}), and the amount exported alongshore:

$$R_{Shelf}^M = R_{Source}^M + E_A^M. \tag{2.5}$$

The transport of a material is calculated as the net flux through a transect at either a constant distance cross-shelf (x-direction), or alongshore (y-direction) (e.g., *Fong and Geyer* 2002). The cross-shelf transport is calculated as:

$$\Gamma_X^M(x) = \sum_{y,z} C^M(x,y,z)\cdot u(x,y,z)\Delta y\Delta z(z), \tag{2.6}$$

where C^M is the concentration of the material, and u is the cross-shelf velocity at each grid cell. The alongshore transport is calculated analogously. For fresh water, C^M is the "fresh water fraction" (F_{FW}, following *Lehrter et al.* 2013), a measure of the proportion of river water (salinity of 0) within a given parcel or grid cell, calculated as:

$$F_{FW} = \frac{S_0 - S}{S_0}. \tag{2.7}$$

S is the salinity of the parcel/grid cell, and S_0 is the ambient salinity (here, 32). Export efficiency is easy to calculate from a numerical simulation, but much harder (if not impossible) to obtain in the field.

I calculated cross-shelf freshwater transport at both a near shore location (15 km; just wide enough to exclude the coastal current in each of the simulated plumes) and at the model shelf break (65 km), as well as the alongshore transport at 150 km downstream of the river mouth, which is well outside the bulge region.

2.4 Global River Data

One thesis objective is to estimate the global freshwater and nutrient export to the open ocean. To do this, I used estimates of freshwater and nutrient discharges for the world's rivers from the Global Nutrient Export from WaterSheds (GlobalNEWS) model (*Mayorga et al.* 2010). This model includes around 5800 rivers that discharge directly into the ocean (Figure 2.4).

Available information includes the rivers' locations (latitude and longitude of river mouth on a 0.25° grid), their discharges and nutrient loads (in $\mathrm{Mg\,y^{-1}}$) including dissolved inorganic and organic nitrogen (DIN and DON), dissolved inorganic and organic phosphorus (DIP and DOP), dissolved organic carbon (DOC), and dissolved silicate (DSi).

In addition to the river load data from GlobalNEWS, I used NOAA's ETOPO1 Topography (*Amante and Eakins* 2009) to calculate the shelf width for each river as the distance from the river mouth to the 200 m isobath (see Figure 2.5 for an example). I calculated the shelf widths of most rivers using an automatic algorithm to determine the distance between the coast and shelf break. In some cases (such as complex coastlines or bathymetry), the algorithm miscalculated the shelf width (for example, predicting very different shelf widths than for neighbouring rivers). These rivers were either flagged by the program, or through

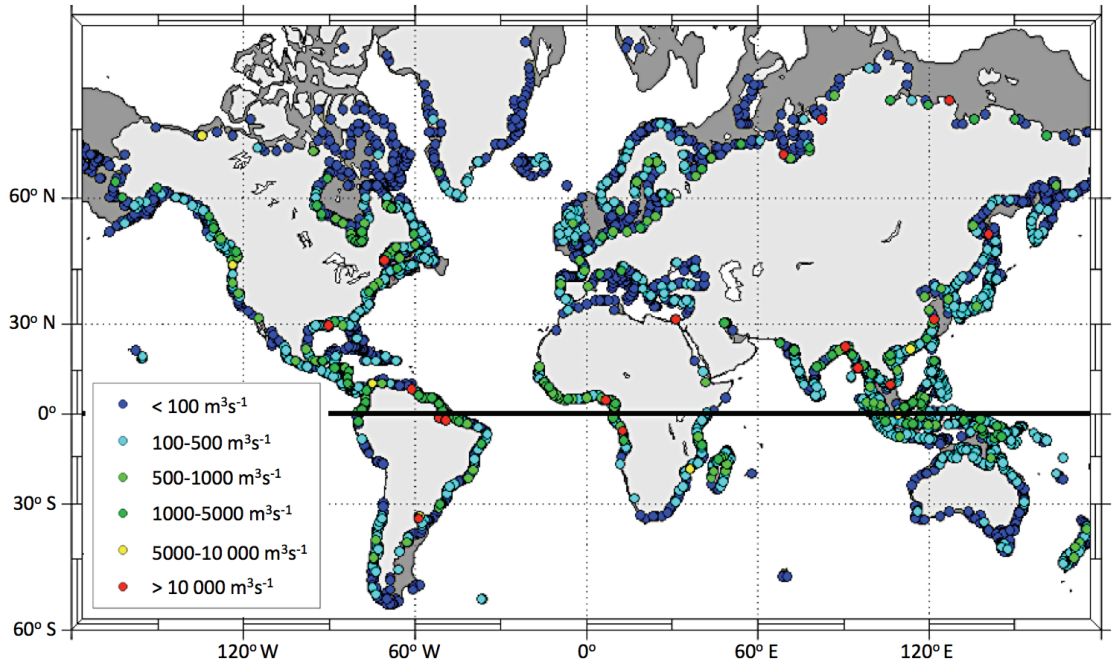

Figure 2.4: Map of global mean annual river discharge as listed for the rivers that flow into the ocean in the GlobalNEWS model (only rivers that discharge into the ocean at more than 10 $m^3\ s^{-1}$ are included). Shelf regions, defined by the 200 m isobath, are shown in dark grey.

manual inspection. Each of the flagged shelf widths was then recalculated manually by taking the mean distance of at least three cross-shelf transects. I also calculated the shelf width manually for the 50 largest rivers to ensure their accuracy. Shelf widths ranged from just tens of kilometres (e.g., 20 km for the Congo River) up to hundreds of kilometres (e.g. for Arctic rivers).

Globally, rivers vary significantly in discharge, nutrient load and latitude (Figures 2.6 and 2.7, and Table 2.2) and, hence, are expected to vary in plume dynamics and cross-shelf export efficiency. Riverine nutrient loads and freshwater discharge covary (larger rivers deliver more nutrients; Figure 2.6a); however, nutrient concentrations are independent of river discharge, with often greater nutrient concentrations in the low to mid-latitudes of the northern hemisphere (Figure 2.6b). Most of the world's rivers have low discharges (less than 100 $m^3\ s^{-1}$), with overall more rivers in the northern hemisphere (Figure 2.7a). Total freshwater discharge is also higher in the northern hemisphere, as are shelf widths (Figure 2.7b). The Amazon River dominates global discharge, delivering approximately $1/6^{th}$ of the global annual freshwater input.

River	Country/ Continent	Outflow Region and Approximate Latitude		Q ($m^3\ s^{-1}$)	D_S (km)
Amazon	South America	Atlantic Ocean	1°S	204 340	304
Congo	Africa	Atlantic Ocean	6°S	40 533	20
Ganges	Asia	Indian Ocean	23°N	36 268	230
Orinoco	South America	Atlantic Ocean	9°N	35 360	100
Yangtze	China	East China Sea	31°N	28 706	460
Mississippi	United States	Gulf of Mexico	30°N	19 661	52
Irrawaddy	Southeast Asia	Andaman Sea	16°N	19 633	170
Yenisei	Russia	Arctic Ocean	71°N	18 910	500
Lena	Russia	Arctic Ocean	73°N	15 237	370
Mekong	Southeast Asia	South China Sea	10°N	13 740	170
Ob	Russia	Arctic Ocean	67°N	12 461	470
Tocantins	Brazil	Atlantic Ocean	2°S	12 157	220
St. Lawrence	North America	Gulf of St. Lawrence	47°N	11 252	260
Nile	Africa	Mediterranean Sea	31°N	11 029	56
Amur	Asia	Sea of Okhotsk	53°N	10 705	390
Niger	Africa	Gulf of Guinea	5°N	10 298	60
Zambezi	Africa	Indian Ocean	19°S	9 811	76
Mackenzie	Canada	Arctic Ocean	69°N	9 180	90
Zhujiang	Asia	South China Sea	22°N	8 229	200
Columbia	United States	Pacific Ocean	46°N	7 624	47

Table 2.2: Overview of the world's 20 largest rivers considered in the GlobalNEWS model (*Mayorga et al.* 2010) and approximate shelf widths determined using NOAA's ETOPO1 topography (*Amante and Eakins* 2009).

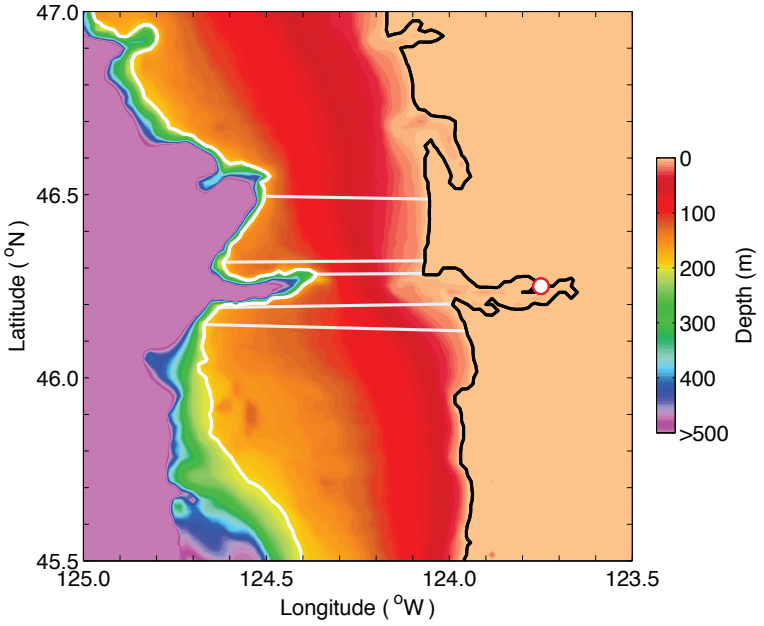

Figure 2.5: Bathymetry at the outflow of the Columbia River (GlobalNEWS coordinate indicated by the circle). The black line is the coast and the white line the shelf break (200 m water depth). The grey lines show the 5 transects whose mean value was used to approximate the shelf width of 47 km.

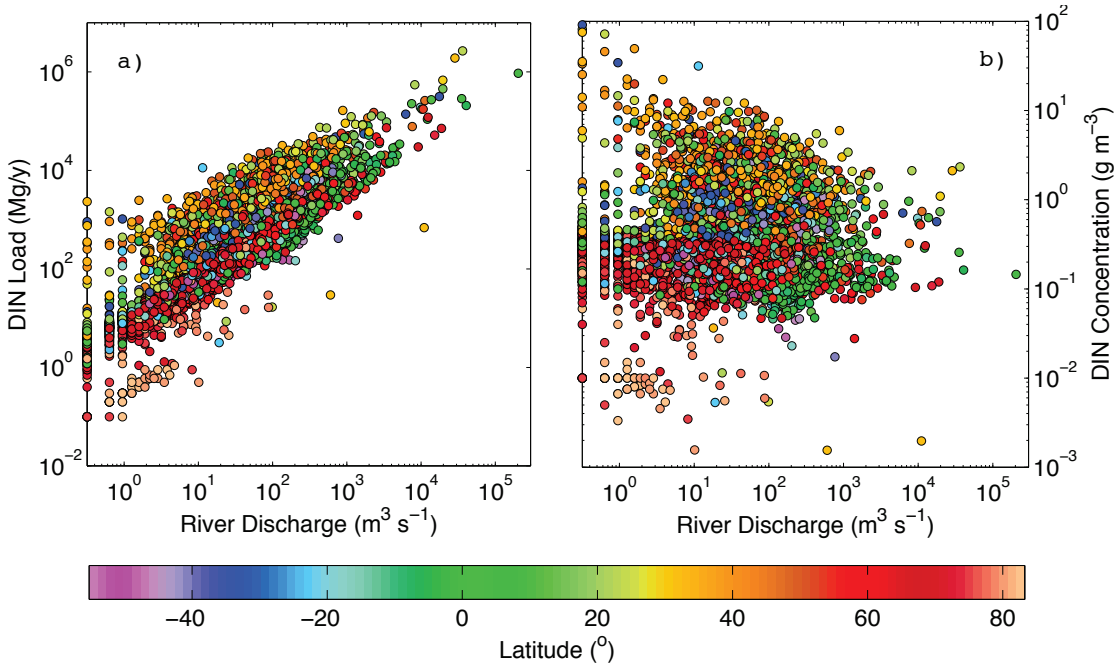

Figure 2.6: GlobalNEWS riverine DIN load (a) and concentration (b) as a function of discharge and latitude.

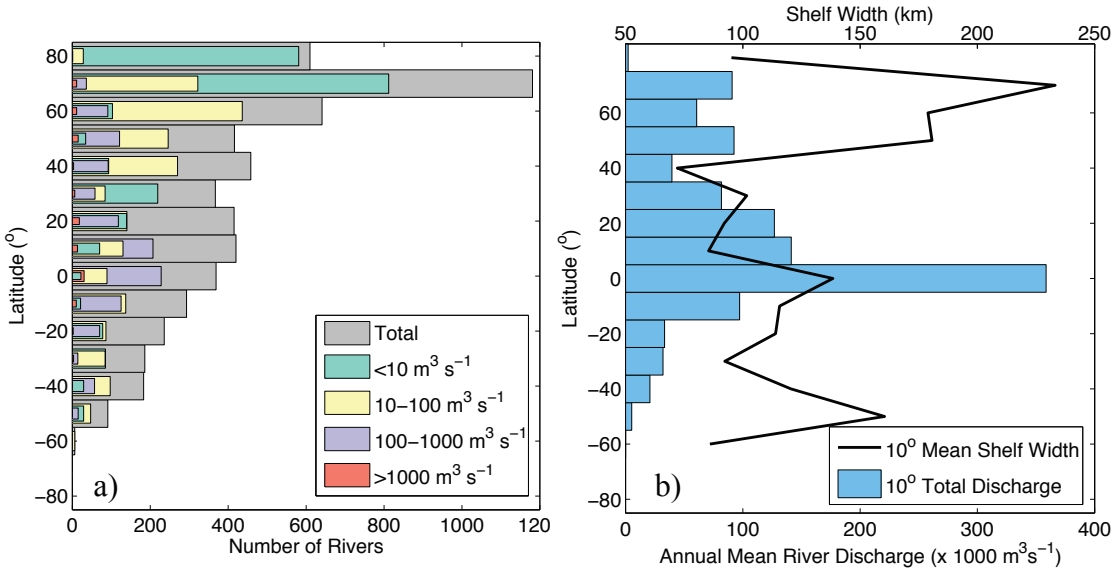

Figure 2.7: a) Histogram of rivers in 10° latitude bands grouped by discharge. b) Mean shelf width (black line) and total freshwater discharge (blue bars) for 10° latitude bands.

CHAPTER 3
PHYSICAL CONTROLS ON CROSS-SHELF TRANSPORT

3.1 Results of the Idealized Model Experiments

3.1.1 The Influence of Latitude and Discharge

In order to assess the impact of changing latitude and discharge on plume structure and export efficiency, I first ran the model without any forcing from wind and tides (DL runs in Table2.1). Below 5°, the simulated plumes do not form a coastal current due to the weak Coriolis force. Instead, they spread offshore from the inflow in a near symmetric, non-rotational plume. At latitudes 5° and above, a bulge forms at the river mouth and the plume is deflected forming the expected downstream coastal current (Figure 3.1). The bulge is smaller for higher latitude plumes, and more spread out at low latitudes.

Most of the simulated plumes remain near the surface, detaching from the bottom close to shore and reaching less than 10 m in mean depth. Only the higher discharge plumes penetrate deep enough to interact with the bottom of the domain over significant distances (Figures 3.2 and 3.3). At the high latitudes, the highest discharge plumes (80 000 $m^3\,s^{-1}$ and 100 000 $m^3\,s^{-1}$) remain attached almost out to the shelf break at 65 km offshore.

In all cases, the bulge grows and evolves continuously in time; however, cross-shelf transport reaches an established state in which transport oscillates about a mean value after no more than 20 days (Figure 3.4). During the established-transport phase, instabilities develop along the plume front, which vary depending on latitude, discharge, and external forcing. For all simulated plumes above 5°, the entire bulge eventually becomes unstable, causing it to detach and reattach on varying timescales (Figure 3.5). High-latitude and high-discharge plumes are much less stable than those at lower latitudes and for small discharges, and have overall much more dynamic bulge regions. All of the results presented here are for greater than 20 days, i.e. once the plumes are established.

Simulated cross-shelf export of fresh water, E_X^{FW}, varies with latitude and discharge.

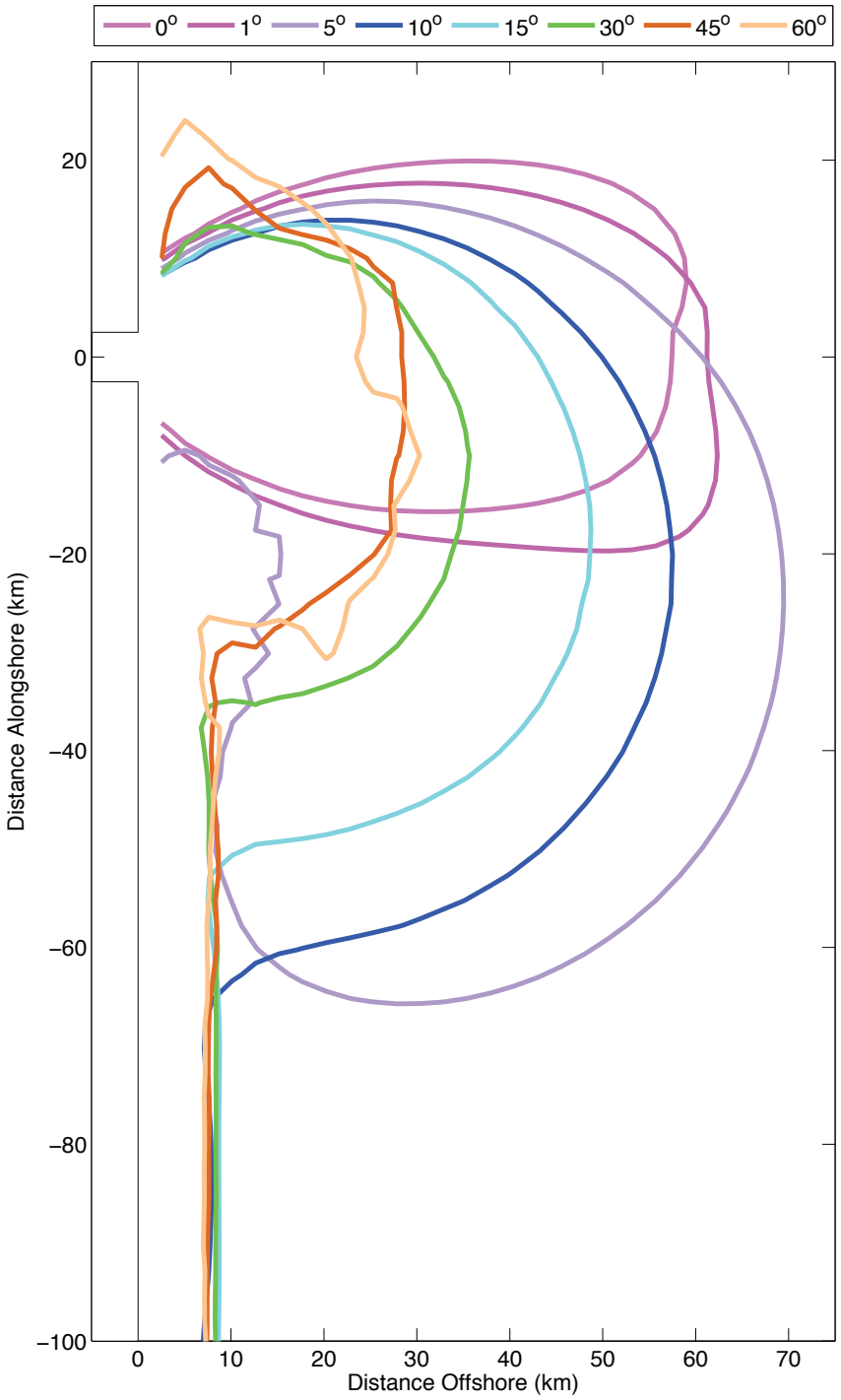

Figure 3.1: Plume shape at various latitudes indicated by the 29 surface salinity contour after 20 days of simulation with a constant discharge of 1 500 m^3 s^{-1}.

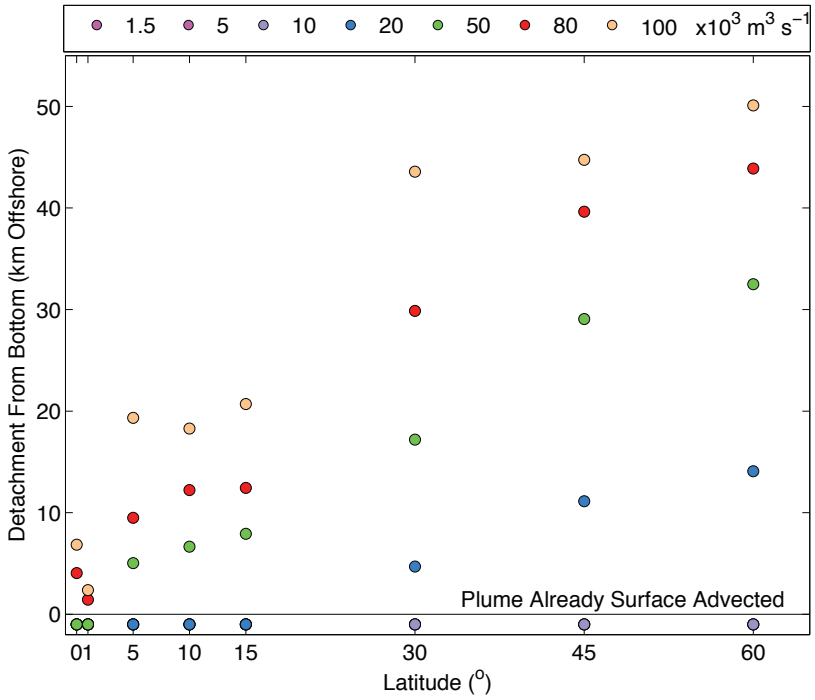

Figure 3.2: Distance offshore that simulated plumes detach from the bottom after 20 days as a function of latitude and discharge. Circles below 0 km represent the maximum discharge that is already detached from the bottom upon leaving the inflow channel.

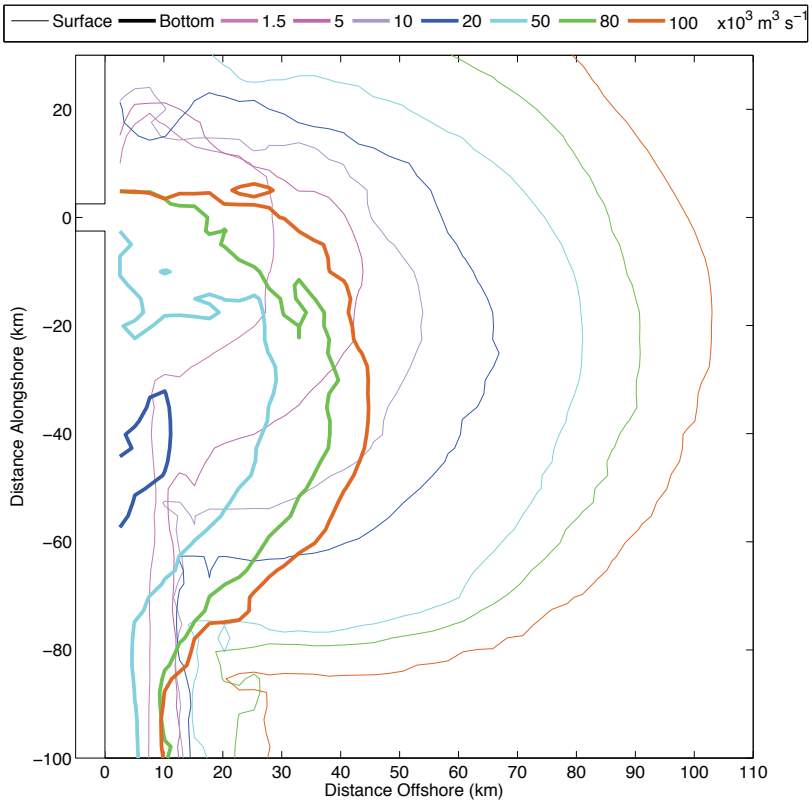

Figure 3.3: Surface (thin lines) and bottom (thick lines) 29 salinity contours after 20 days for different discharges at 45°. Plumes below a discharge of 20 000 m^3 s^{-1} are all detached from the bottom.

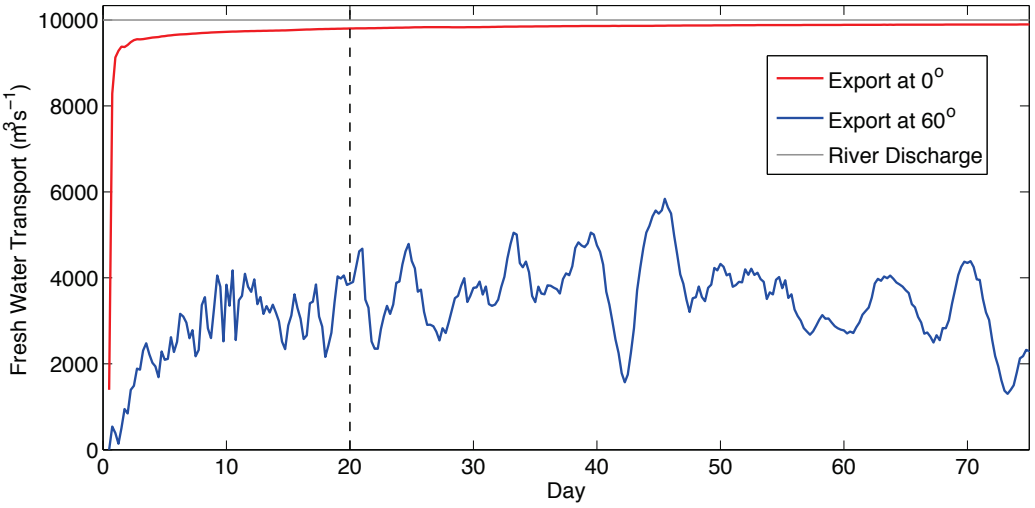

Figure 3.4: Cross-shelf freshwater transport, Γ_X^{FW}, beyond 15 km from the coast for a constant river discharge of 10 000 m^3 s^{-1} at 0° and 60°.

At a constant discharge, E_X^{FW} decreases with increasing latitude from close to 100% efficiency near the equator to almost no transport at high latitudes (Figure 3.6a and b). Conversely, cross-shelf export efficiency increases with increasing discharge by as much as 30% between the lowest discharge case (1 500 m^3 s^{-1}) and the highest discharge case (100 000 m^3 s^{-1}). Low latitude and high discharge plumes are much more efficient exporters than high-latitude, low-discharge plumes. Across all discharge scenarios, the simulated cross-shelf export efficiency for the higher latitude plumes is less than 65% beyond 15 km from the shore, and less than 50% beyond 65 km from the shore. For discharges less than 10 000 m^3 s^{-1}, export efficiency beyond 65 km is less than 5% above 45° latitude. Comparing Figure 3.6 to Figure 3.2, plumes that are attached to the bottom further offshore have greater export efficiencies than plumes that detach earlier at the same latitude. The purely surface-advected plumes (for lower discharges) have similar export efficiencies, while the bottom-attached plumes (for higher discharges) have up to 30% higher export efficiency.

The simulated alongshore export efficiency of fresh water, E_A^{FW}, follows a trend that is opposite to cross-shelf export efficiency (Figure 3.6c). At low latitudes, the alongshore transport is close to zero for all discharges, with increasing export efficiency toward higher latitudes. The lower discharge plumes have greater alongshore export efficiency than the

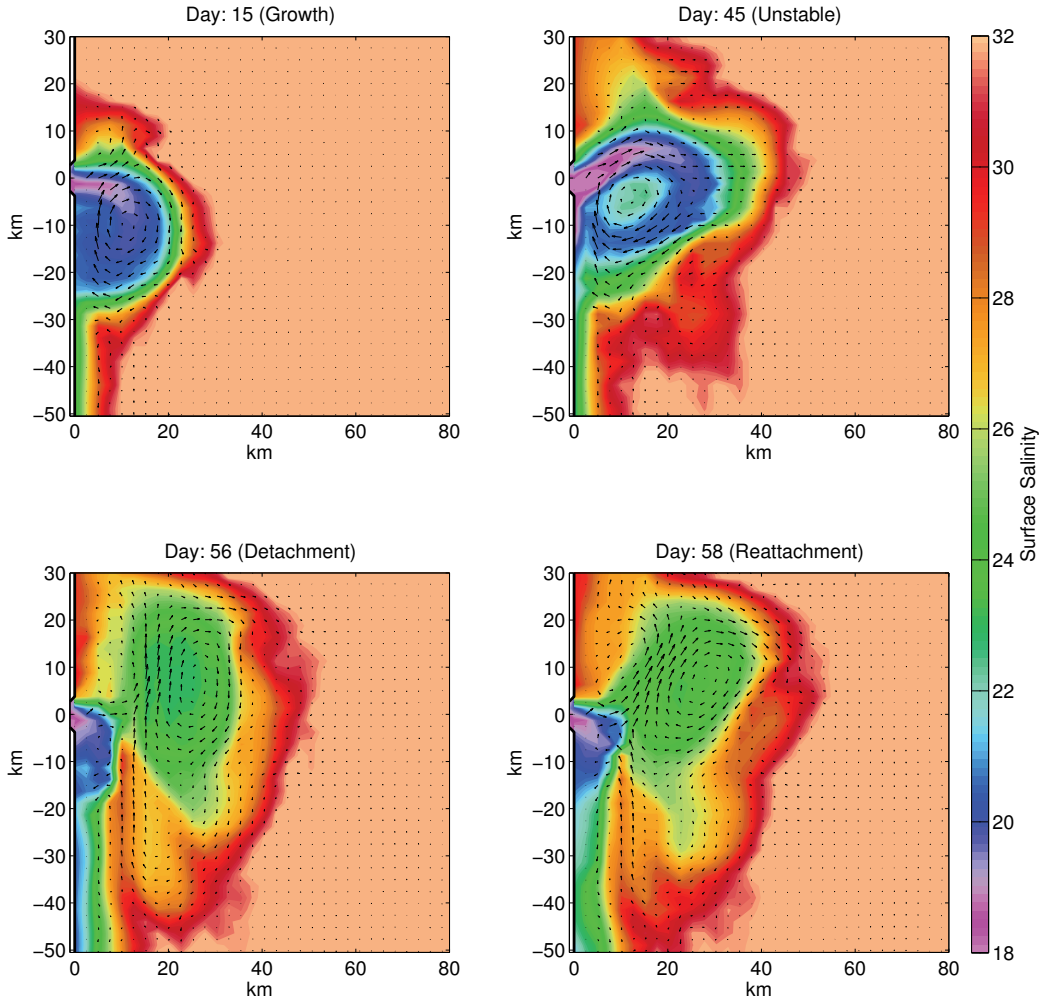

Figure 3.5: Snapshots of plume evolution at 45° for a discharge of 1 500 $m^3\ s^{-1}$ illustrating different stages of bulge detachment and reattachment. From top left to bottom right: initial growth of the bulge (< 20 days); the plume becomes unstable (> 30 days); the unstable bugle detaches at day 56; and the bulge reattaches at day 58.

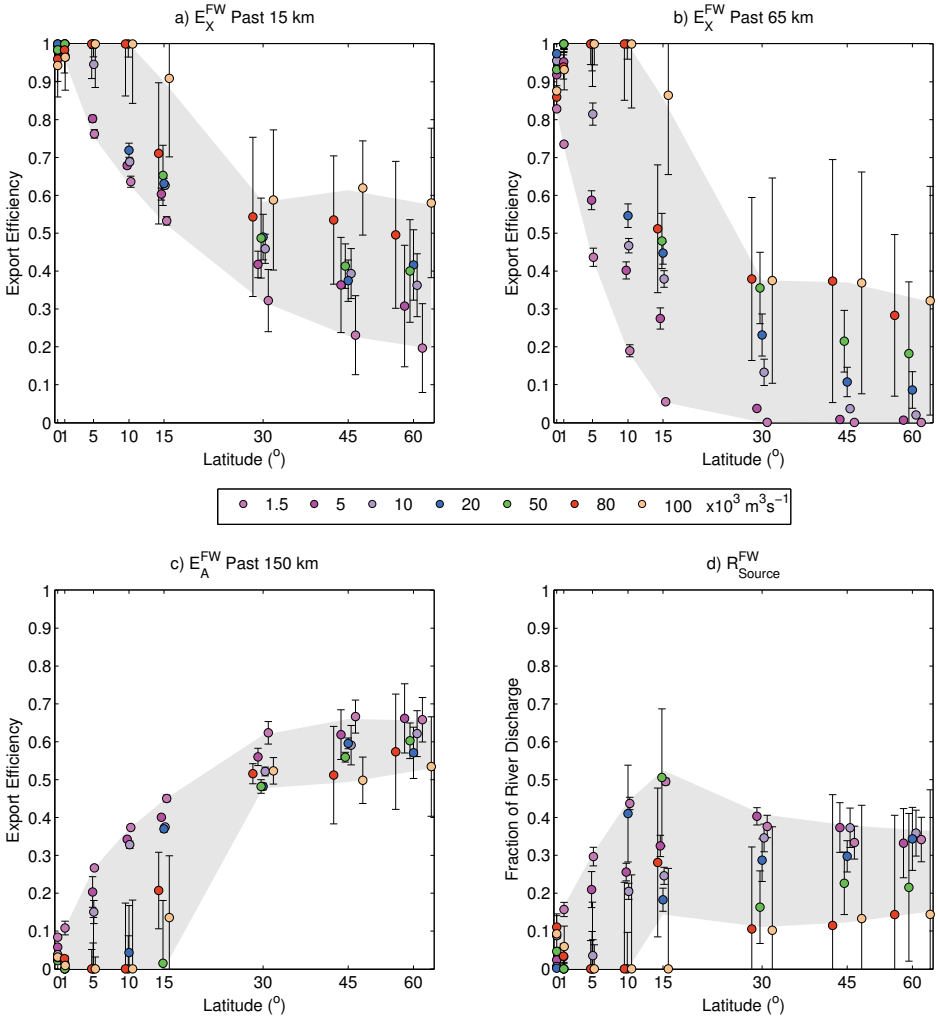

Figure 3.6: Simulated export efficiency and retention of fresh water as a function of latitude for all discharge scenarios (coloured markers) without any forcing from wind or tides (DL; Table 2.1). The grey shading shows the maximum and minimum range of the data. a) Cross-shelf export efficiency past 15 km and b) past 65 km. c) Alongshore export in the coastal current. d) Retention near the source. The data are slightly offset from their respective latitudes (by up to $\pm 2\%$) in order to distinguish overlapping data.

high discharge plumes. At high latitudes, the alongshore export efficiency is between 55% and 70%. Overall, the amount of fresh water retained near the source (Figure 3.6d) is just 0–40%, with higher retention at higher latitudes and lower discharges.

Uncertainties in the estimates were calculated as the standard deviation of the calculated transport at each time step, divided by river discharge. The uncertainties are larger for the larger plumes, and at higher latitudes, due to less stable flows. In some cases, the uncertainties span as great a range as 65% of the river discharge (for example, the 80 000 $m^3\,s^{-1}$ plume at 45° in Figure 3.6b). Although this is large, most uncertainties are smaller, and the general pattern of decreasing transport is still obvious.

I assessed the sensitivity of the model results to the choice of domain by halving/doubling the depth of the inflow channel (ShIn/DpIn in Table 2.1) and halving/doubling the bottom slope (HlfSlp/DblSlp) for the 1 500 $m^3\,s^{-1}$ (low) and 50 000 $m^3\,s^{-1}$ (high) discharge scenarios (Figure 3.7).

For the low discharge case, halving (doubling) the bottom slope of the domain consistently results in decreased (increased) export efficiency at both 15 km and 65 km offshore for all latitudes (Figure 3.7a). Between 5° and 15°, doubling (halving) the depth of the inflow channel decreases (increases) the cross-shelf export efficiency of fresh water beyond the base case at a distance of 15 km from shore (Figure 3.7b). The same is true for all latitudes above 5° at 65 km offshore. The opposite occurs outside of these latitude ranges.

For the high discharge, both halving and doubling the bottom slope results in greater export efficiency than the base case above 10° (Figure 3.7c). Halving the slope leads to greater overall transport for most latitudes, except at 60° where the doubled slope scenario results in the greatest transport. Halving the inflow depth results in greater export efficiency at higher latitudes, while doubling it leads to slightly reduced export efficiency from the base case (Figure 3.7d). The decrease with latitude is reduced compared to the base case, with near constant export efficiency 15 km from shore at higher latitudes. Overall, making the domain shallower increases the export efficiency by up to 30% from the base case.

The simulated cross-shelf export efficiency is more sensitive to changes in the domain at 15 km offshore than 65 km, and for the higher latitude simulations. Cross-shelf export efficiency is also more sensitive to changes in the depth of the inflow channel than to changes in the bottom slope. Overall, however, the qualitative results do not change upon changing the domain: high latitude plumes are still restricted in their cross-shelf export,

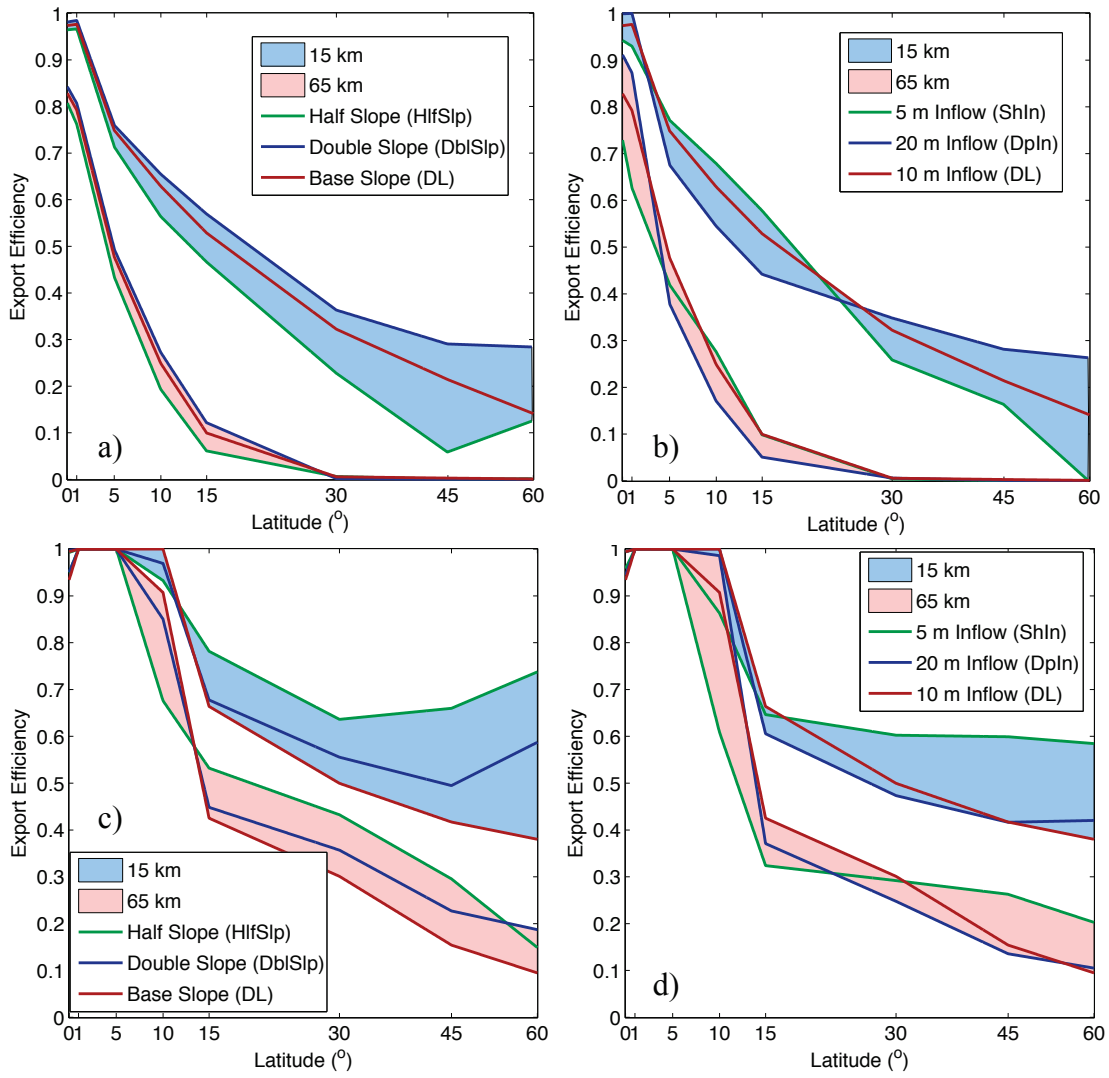

Figure 3.7: Comparison of cross-shelf export efficiency of fresh water at 15 km and 65 km offshore as a function of latitude for (a/c) different bottom slope scenarios (DL, DblSlp, and HlfSlp) and (b/d) different inflow depths (DL, ShIn, DpIn) as described in Table 2.1. a) and b) are for the 1 500 $m^3\,s^{-1}$ discharge tests, and c) and d) 50 000 $m^3\,s^{-1}$ discharge.

with less than 5% and 20% export efficiency for the low discharge and high discharge cases, respectively, beyond 65 km offshore above 15° latitude.

3.1.2 Influence of Tide and Wind Forcing

I tested the influence of external forcing by repeating the variable discharge and latitude tests with the addition of either a 1-m, semi-diurnal tidal forcing (TDL as in Table 2.1) or a synthetic wind (ADWL and XWDL). The addition of the tide causes only slight on– and offshore motion of the plume with the tidal ebb and flood (Figure 3.8a and b). At 15 km from shore, the tidal forcing increases the overall export efficiency of fresh water beyond the unforced DL cases at all latitudes and discharges (by approximately 5–15%), but results in decreased export at 65 km from shore (a reduction of approximately 5–10%) (Figure 3.9a and b). The variance in freshwater export efficiency with latitude is also smaller for the tidally forced plumes beyond 15 km. In both cases, the freshwater export efficiency decreases with increasing latitude, dropping below 50% and 30% at 60°, past both 15 km and 65 km, respectively, regardless of the discharge. The alongshore export efficiency was also similar to the unforced case (Figure 3.9c), with 40–55% exported away from the source and a greater near-source retention of up to 60% of the riverine input (Figure 3.9d). The uncertainties for the tidally forced simulations, calculated by first removing the tidal signal from the data, are overall smaller than for the unforced case.

Adding the alongshore-dominant wind (AWDL; see Table 2.1) either forces the plume offshore during upwelling conditions, leading to a significant increase in fresh water offshore, or onshore during downwelling conditions, supressing the plume bulge and enhancing the coastal current (Figure 3.8c and d). The simulated export efficiency of fresh water beyond 15 km from the coast is more uniform than for the base case, with the impact of latitude greatly reduced (higher export efficiency at higher latitudes; Figure 3.10a). At 65 km offshore (Figure 3.10b), the export efficiency is highly variable for the low latitude plumes ($< 15°$), with the low discharge plumes suppressed by the wind forcing. Above 15°, the export efficiency is approximately equal for the different discharge simulations. Overall, the reduction in export efficiency with increasing latitude that occurs in the unforced and tidally forced cases is less pronounced. Compared to the unforced efficiency of approximately 20–60% and 0–30% beyond 15 km and 65 km offshore, respectively, cross-shelf freshwater transport is enhanced at higher latitudes with wind forcing, with efficiencies between 50–75% and 20–30%. The upper limits are similar for the high

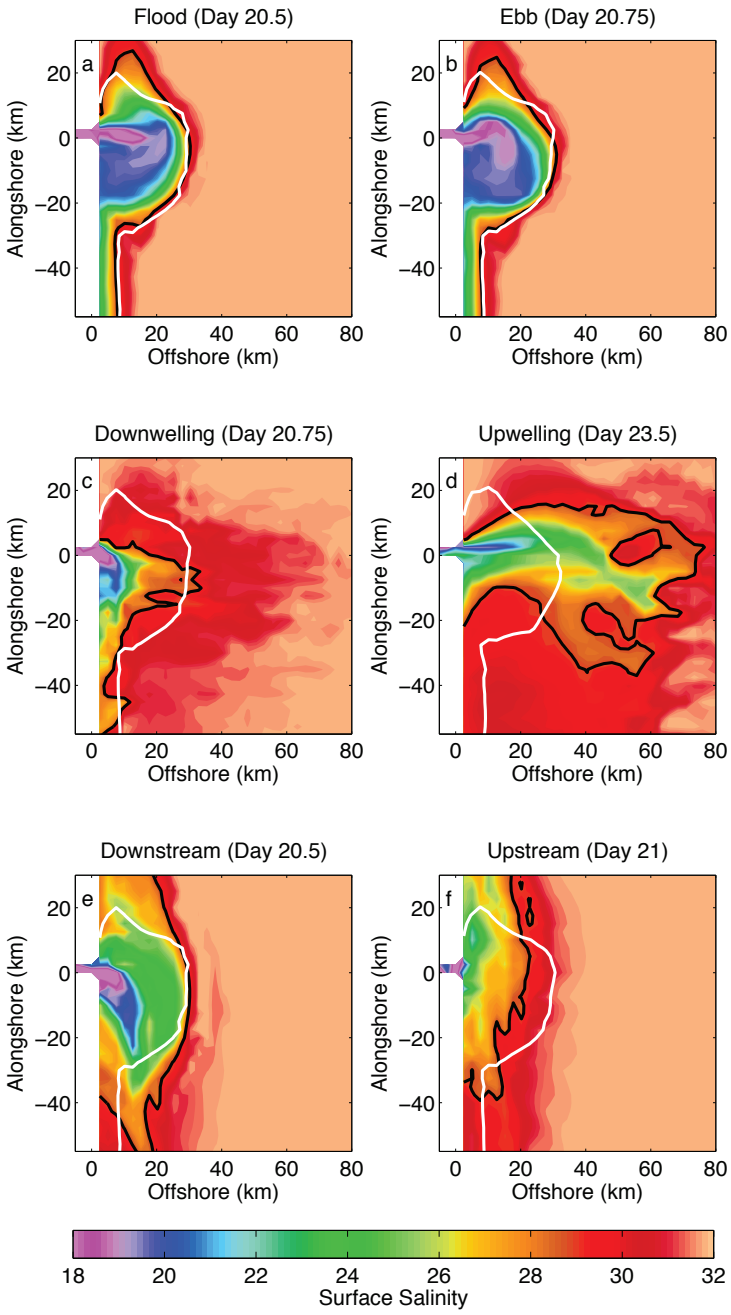

Figure 3.8: Simulated plumes under different forcing conditions at 45° for a discharge of 1 500 $m^3\ s^{-1}$. a and b) The ebb and flood cycles of the tidally forced simulations (TDL); c and d) the down– and upwelling components of the alongshore-dominant wind forcing (AWDL); e and f) the downstream and upstream transport from the on/offshore wind cycle in the cross-shelf-dominant wind forcing (XWDL). The 29 salinity contour is shown in black. The same salinity contour from the unforced simulation is also shown (white line).

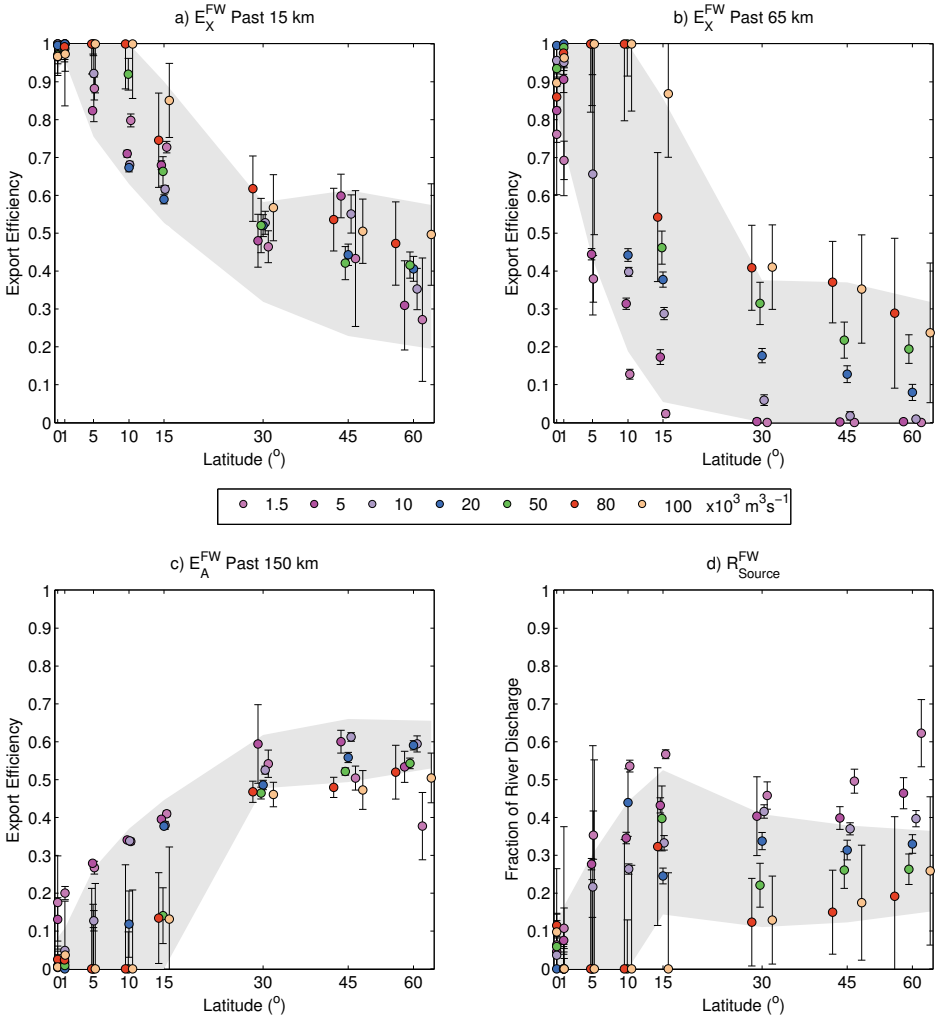

Figure 3.9: Simulated export efficiency and retention of fresh water as a function of latitude for all discharge scenarios (coloured markers) with tidal forcing (TDL; Table 2.1). The grey shading shows the range of base (DL) data (Figure 3.6). a) Cross-shelf export efficiency past 15 km, and b) past 65 km. c) Alongshore export in the coastal current. d) Retention near the source. The data are slightly offset from their respective latitudes (by up to $\pm 2\%$) in order to distinguish overlapping data.

discharge plumes, but low discharge plumes have increased cross-shelf export.

Forcing the simulated plumes with the cross-shore dominant synthetic wind (XWDL; Table 2.1) leads to either an enhancement of the coastal current at mid-latitudes (due to downstream Ekman transport from the offshore wind), or a complete reversal of the coastal current (from upstream transport with the onshore winds) (Figure 3.8e and f). At low latitudes, the on/offshore winds lead to up– and downwelling. This results in a similar overall increase in cross-shelf export efficiency of fresh water as for the alongshore-dominant winds, particularly beyond 15 km from the coast and at the lower latitudes where most of the scenarios result in 100% freshwater export (Figure 3.11). The higher latitude plumes have export efficiencies that are similar to the tidally forced and unforced simulations. The variance between the different discharge simulations is greater than for the alongshore wind and tidally forced plumes, but still smaller than for the unforced plumes.

Again, the overall alongshore export efficiency, E_A^{FW}, varies opposite to the cross-shelf transport under the influence of the winds, with greater export efficiency occurring when the plume is pushed closer to shore as in the case of downwelling or downstream Ekman transport with offshore winds. The winds also lead to upstream alongshore transport in the case of onshore winds, reversing the flow of the coastal current. At high latitudes, the winds lead to approximately 25–60% alongshore export and 20–80% near source retention at high latitudes. At low latitudes, as with the cross-shelf export, the alongshore export is extremely variable, with between 0 and 70% export efficiency for the alongshore dominant winds and 0–40% for the cross-shore-dominant winds.

For both the unforced simulations and those with the external forcing, cross-shelf export efficiency is in general greater for higher discharges, but decreases with increasing latitude (the opposite is true for the alongshore export). Without any external forcing, plumes at high latitudes have very low cross-shelf export efficiency (less than 5% beyond 65 km above 45°). Tidal forcing reduces the overall transport 65 km offshore, but the wind forcing is able to overcome some of the influence of latitude and increases transport at higher latitudes, with the low discharge plumes having similar export efficiencies to the high discharge plumes. For both the wind-forced and tidally forced simulations, the lower discharge plumes are more affected by the added forcing than the higher discharge plumes, especially at the lower latitudes. Overall, wind forcing has a greater impact than tidal

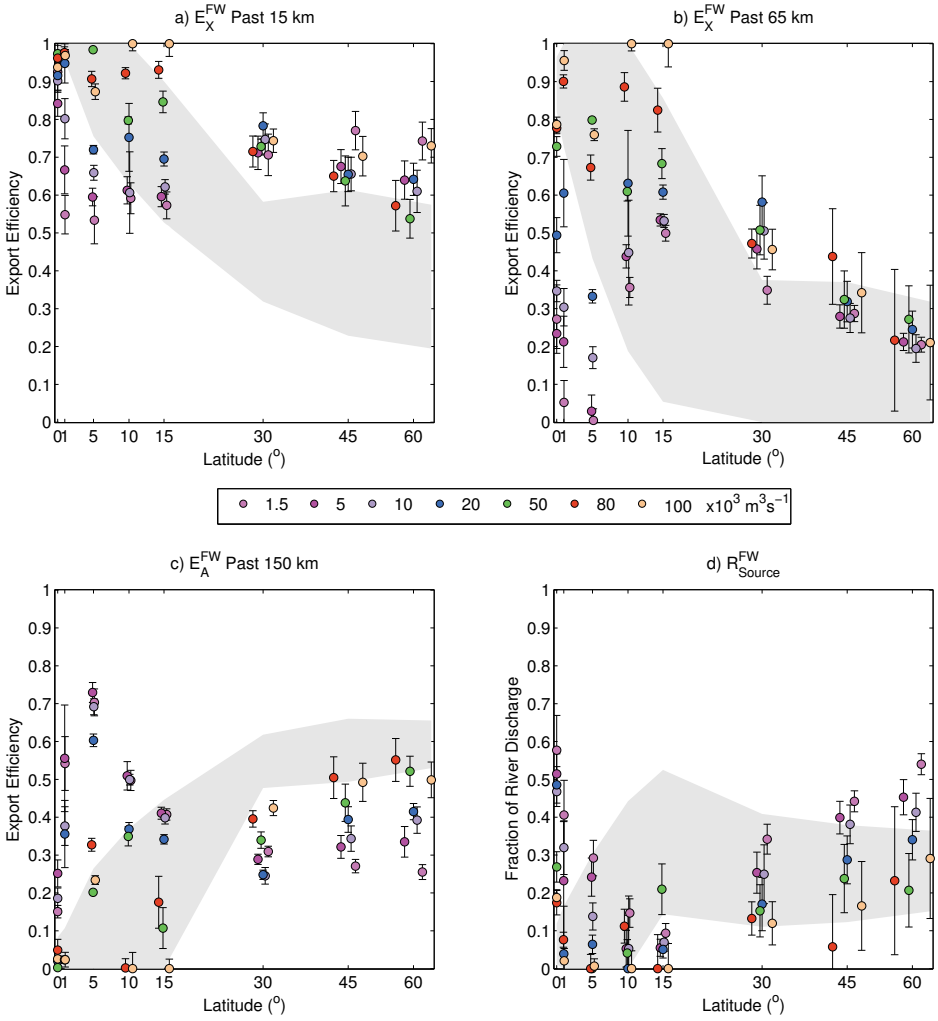

Figure 3.10: Simulated export efficiency and retention of fresh water as a function of latitude for all discharge scenarios (coloured markers) forced with the alongshore-dominant synthetic winds (AWDL; Table 2.1). The grey shading shows the range of the base (DL) data (Figure 3.6). a) Cross-shelf export efficiency past 15 km, and b) past 65 km. c) Alongshore export in the coastal current. d) Retention near the source. The data are slightly offset from their respective latitudes (by up to $\pm 2\%$) in order to distinguish overlapping data.

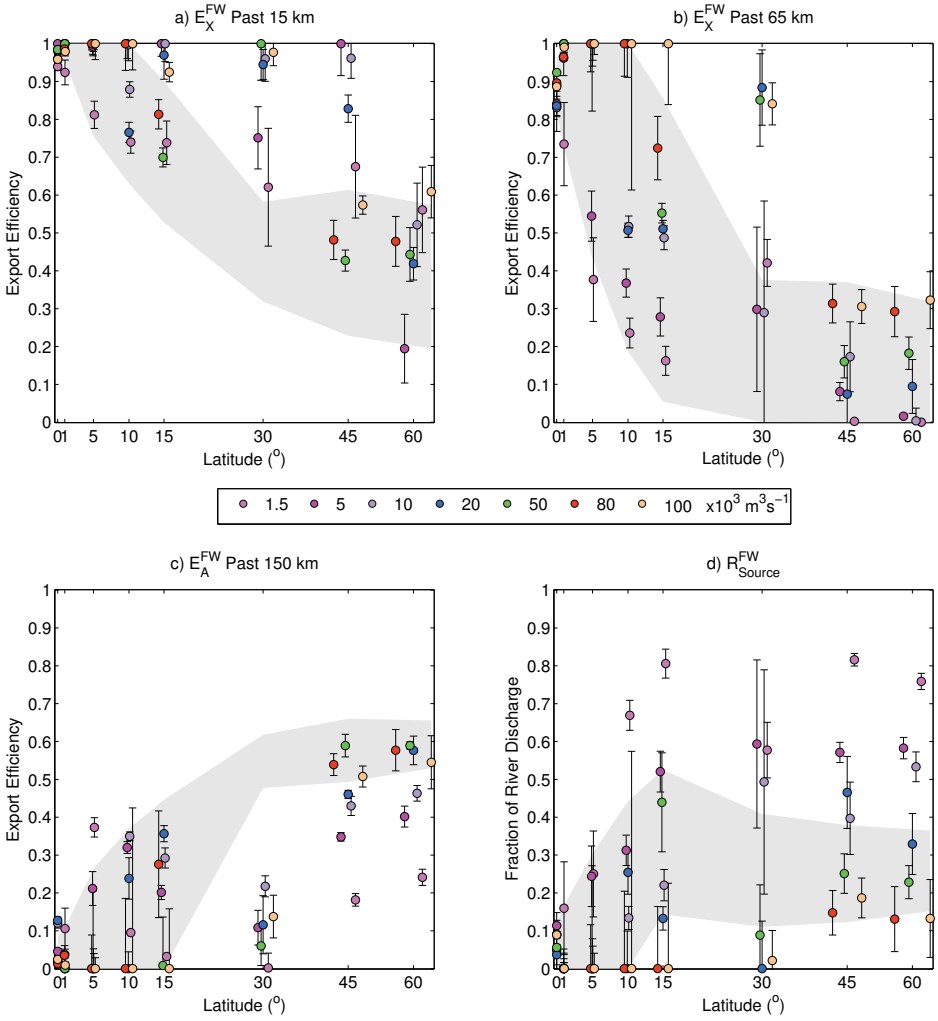

Figure 3.11: Simulated export efficiency and retention of fresh water as a function of latitude for all discharge scenarios (coloured markers) forced with the cross-shore dominant synthetic winds (XWDL; Table 2.1). The grey shading shows the range of the base (DL) data (Figure 3.6). a) Cross-shelf export efficiency past 15 km, and b) past 65 km. c) Alongshore export in the coastal current. d) Retention near the source. The data are slightly offset from their respective latitudes (by up to $\pm 2\%$) in order to distinguish overlapping data.

forcing on the simulated plumes.

3.2 Describing River Plumes with Simple Metrics

One of the goals of this thesis is to estimate plume transport using simple, general relationships. To this end, the following presents a series of relationships derived through applying a series of regressions to the simulated data. I attempted to ensure realistic values are predicted by the regressions, but they are primarily based on statistical best fits, rather than physical derivations. As such, they are used as means of estimating the various parameters, but not to provide physical meaning.

3.2.1 Cross-Shelf Export as a Function of the S_P Number

I compared the export efficiency of the simulated plumes at 15 km and 65 km offshore to their S_P number. For all forcing scenarios, I use linear regression to fit an asymptotic function of the form:

$$E_X^{FW} = 1 - \frac{1}{aS_P^{1/2} + b} \tag{3.1}$$

The functional form was chosen to ensure that export eficiency approaches 100% as S_P increases, but never predicts greater than 100% effiency, with the power of 1/2 dependence on S_P consistently providing the best fit (other asymptiotic forms were attempted, but they were not able to fit the data well). In order to ensure realism of the regression, b is bounded by 0 and 1, and $a > 0$. Where E_X is less than 0 (S_P values below the x-intercept of $((1-b)/a)^2$), all estimates are 0.

The asymptotic regression does very well in predicting the cross-shelf export efficiency with the plumes' S_P number for each of the unforced (DL) (Figure 3.12), tidal forcing (TDL), and alongshore-dominant wind forcing (AWDL) scenarios (Appendix A). In each case, the regression results in a positive x-intercept, indicating that a certain value of S_P must be reached before export can occur.

When applied to the cross-shore dominant wind simulations (XWDL), b was negative. As such,the regression was recalculated with b forced to 0 (Figure 3.13).

The same regression can be applied to the entire data set (all forcing scenarios combined) to obtain a means of estimating export under a range of forcing scenarios (Figure 3.14).

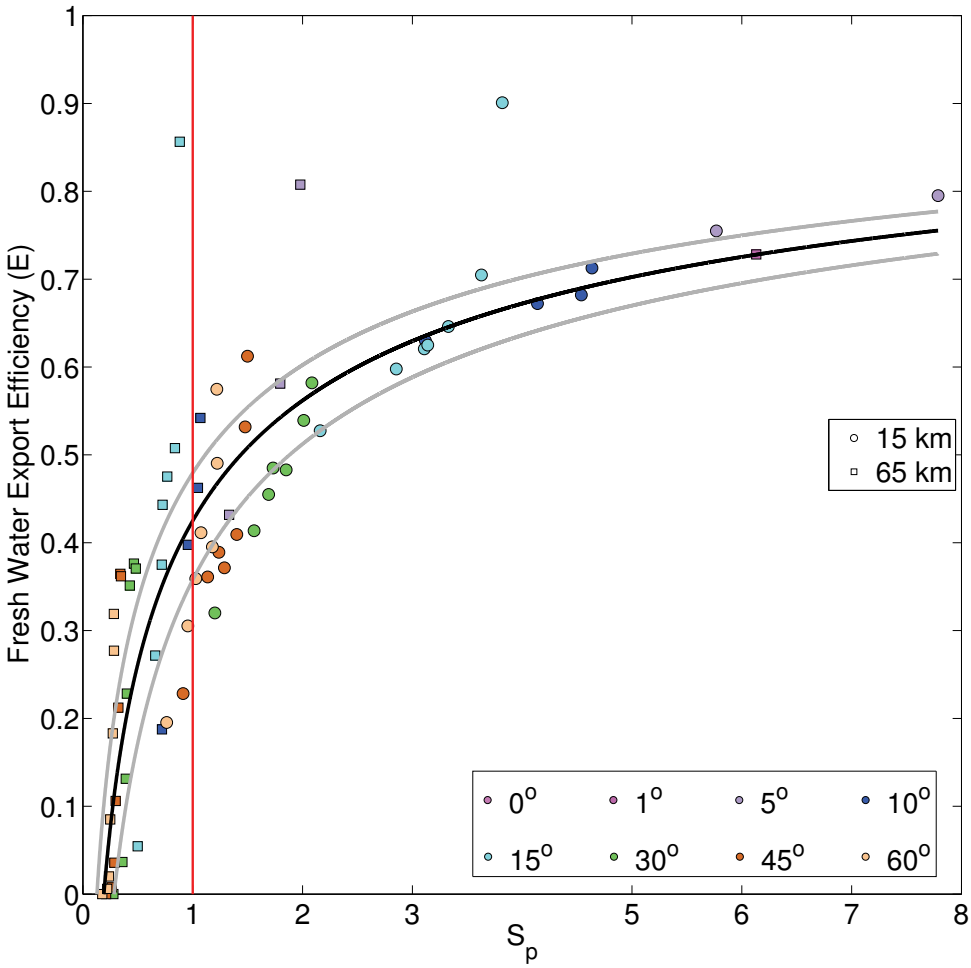

Figure 3.12: Freshwater export efficiency beyond 15 km and 65 km for the unforced runs as a function of the S_P number. An asymptotic regression was applied following Equation 3.1 with $a = 1.4 \pm 0.5$ and $b = 0.4 \pm 0.3$. The fit is excellent, with an r^2 value of 0.93 and a p-value of 0.

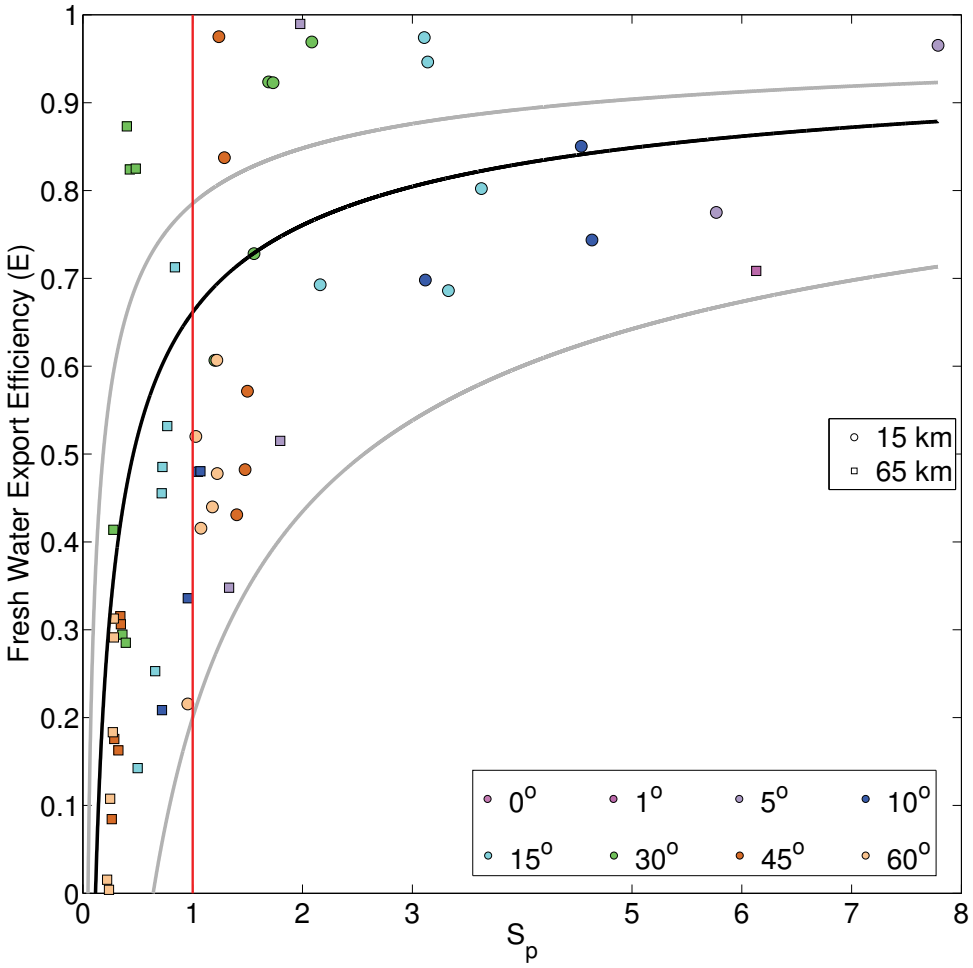

Figure 3.13: Freshwater export efficiency beyond 15 km and 65 km as a function of the S_P number for the simulated plumes forced with the cross-shelf dominant winds (XWDL). An asymptotic regression was applied following Equation 3.1 with $a = 3.0 \pm 1.7$ and b forced to 0 to ensure E_X is not unrealistically predicted to be greater than 0 for $S_P = 0$. The fit is good, with an r^2 value of 0.55 and a p-value of 0.001.

The uncertainty ranges for the regression capture roughly 80% of the total simulated data points.

Table 3.1 lists the regression coefficients in Equation 3.1 and their uncertainties (95% confidence intervals) for the different forcing scenarios as well as for the fit for all simulations. I use the regression applied to all scenarios to estimate the export for real rivers.

Scenario	a	b	r^2
DL	1.4 ± 0.5	0.4 ± 0.3	0.93
TDL	1.4 ± 0.3	0.4 ± 0.1	0.91
AWDL	1.5 ± 0.7	1.0 ± 0.4	0.77
XWDL	3.0 ± 1.7	0	0.55
All	1.5 ± 0.6	0.5 ± 0.3	0.77

Table 3.1: Regression coefficients for Equation 3.1 as found for the different model scenarios. Each regression was very significant with p-values of 0.

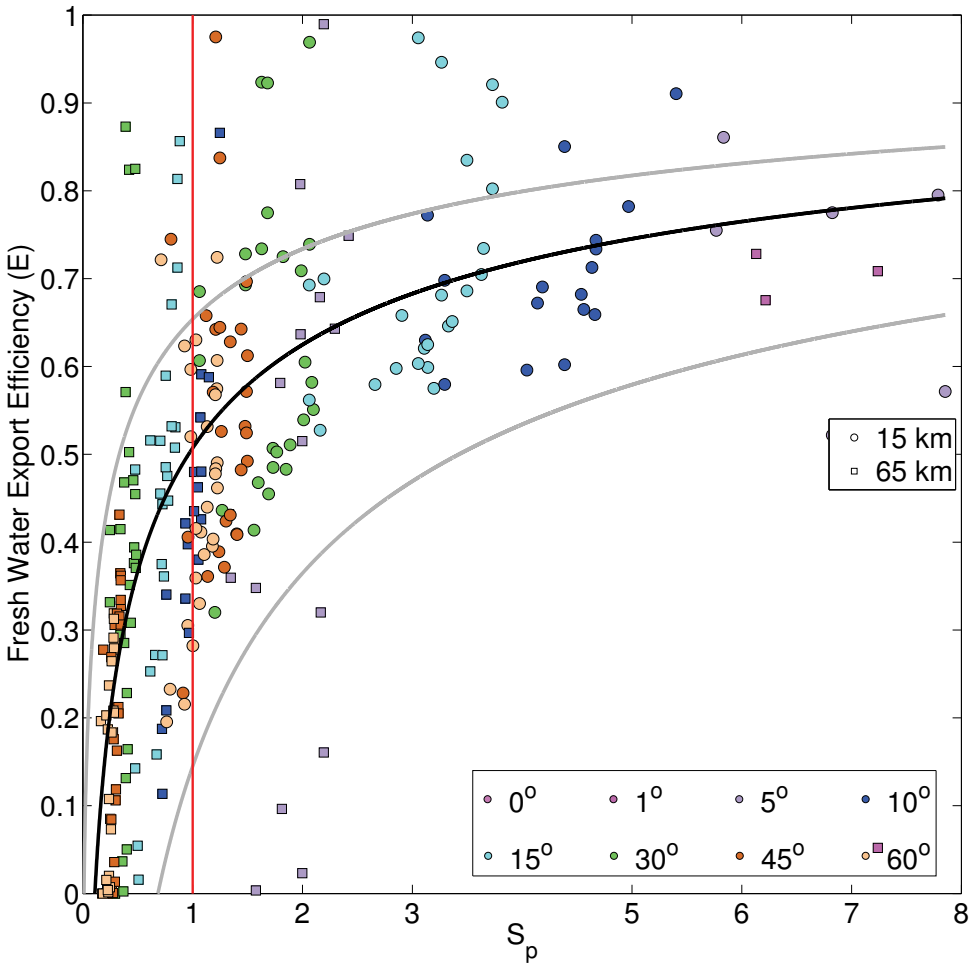

Figure 3.14: Freshwater export efficiency beyond 15 km and 65 km as a function of the S_P number for all simulated plumes under the different forcing scenarios. An asymptotic regression was applied following Equation 3.1 with $a = 1.5 \pm 0.6$ and $b = 0.5 \pm 0.3$. The fit was very good, with an r^2 value of 0.77 and a p-value of 0.

3.2.2 Other Plume Properties

Other plume properties can also be estimated using simple relationships. The alongshore freshwater export efficiency (E_A^{FW}) 150 km downstream from the river mouth, for example, increases with increasing latitude, and scales according to $R_o^{'-1/2}$ (Equation 3.2 and Figure 3.15). The regression is not as strong as those calculated for the cross-shelf export, with an r^2 value of 0.53, but is still significant with a p-value of 0. Using this equation to estimate E_A, it can predict values greater than 1 (for $R_o < 2$ km) as well as values less than 0 ($R_o > 256$ km). When used with Equation 3.1, it is also possible that $E_A + E_X$ could be greater than 1. Of course, these values are not physically possible, so I constrain all of my estimates for real rivers such that $0 \leq E_A \leq 1 - E_X$.

$$E_A^{FW} = \frac{1.6 \pm 0.2 \text{ km}^{1/2}}{\sqrt{R_o'}} - (0.10 \pm 0.02) \tag{3.2}$$

Rewriting Equation 2.2, the Rossby radius depends on the products $\Delta\rho h$ and $\Delta\rho h^2$:

$$R_o^{'} = \sqrt{\frac{g}{f^2\rho_o}\left(\Delta\rho h - \frac{\Delta\rho h^2}{H}\right)}, \tag{3.3}$$

where $\Delta\rho$ is the density anomaly between the plume and ambient water, and h is the mean depth of the plume. While the other parameters are easily obtained, $\Delta\rho h$ and $\Delta\rho h^2$ are difficult to measure in field studies of real plumes. *Sharples et al.* (in revision) estimate these parameters as linear functions of river discharge (Q). Similarly, $\Delta\rho h$ and $\Delta\rho h^2$ increase approximately linearly with discharge for the simulated plumes (r^2 values of 0.67 and 0.62, respectively), however, there is also a strong dependence on latitude (Figure 3.16). As such, I looked for regresions with dependece on both the discharge and the Coriolis parameter (f; Equation 3.4 and Figure 3.17). Based on pysical scaling arguments, the two parameters were expected to be proportional to $\sqrt{Q}f$; however, better regressions were obtained for each using $\sqrt{Qf}$ and Qf, respectively. By including the latitude dependence, the goodness of fit increased significantly, resulting in r^2 values of 0.95 and 0.93, respectively.

$$\begin{aligned} \Delta\rho h &= (70 \pm 5.7)\sqrt{Qf} + (43 \pm 5.2)\, kg\, m^{-2} \\ \Delta\rho h^2 &= (270 \pm 17)\, Qf + (223 \pm 51)\, kg\, m^{-1} \end{aligned} \tag{3.4}$$

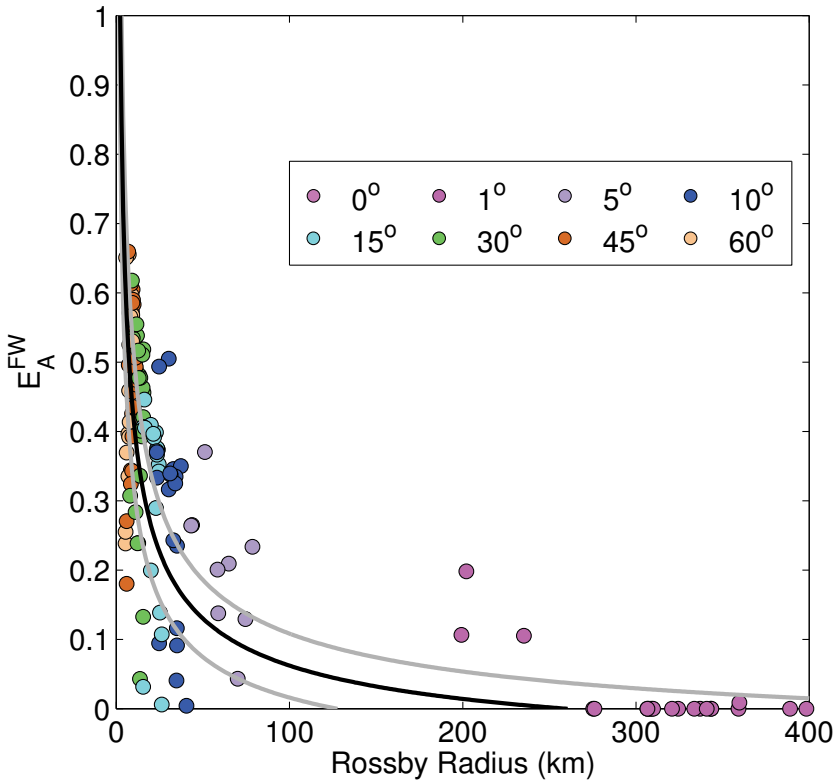

Figure 3.15: Alongshore freshwater export (past 150 km downstream) for all simulated plumes as a function of $R_o^{'}$. The regression is shown with the black line and the uncertainties (95% confidence intervals) in grey (Equation 3.2).

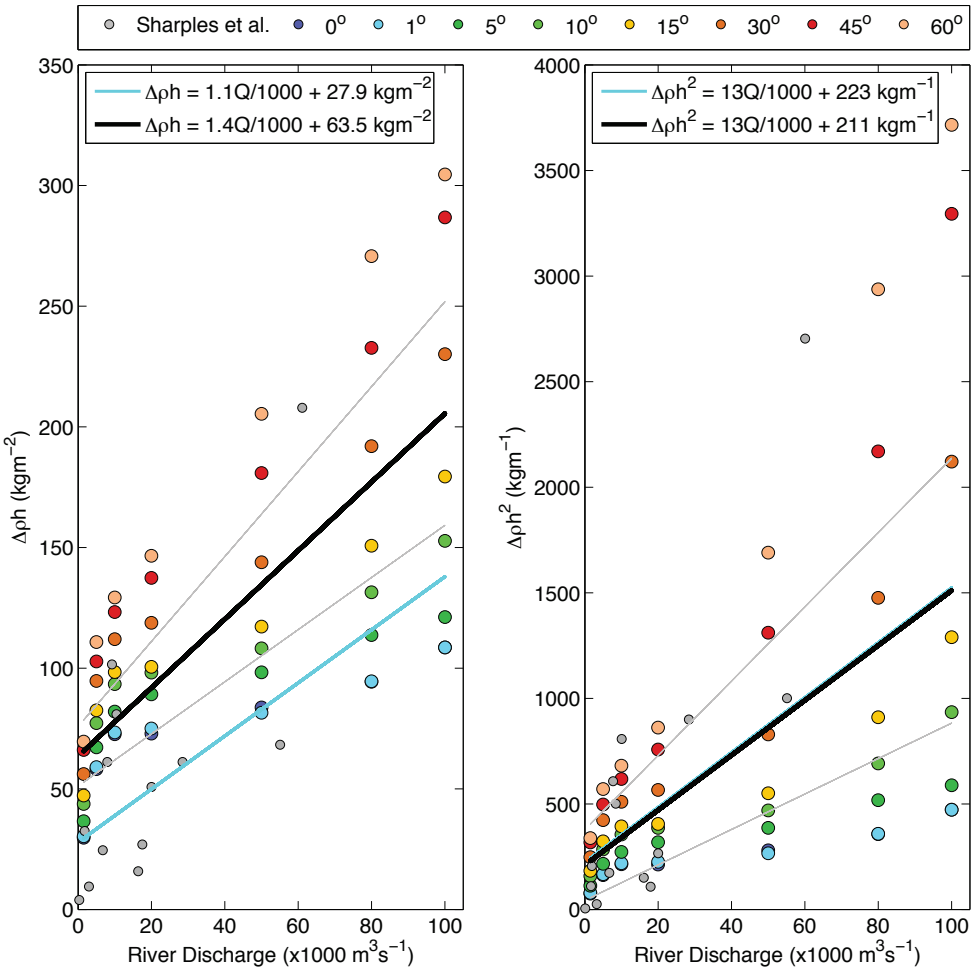

Figure 3.16: Regressions applied to $\Delta\rho h$ and $\Delta\rho h^2$ as a function of river discharge only. The black line is the regression fit to the model data with r^2 values of 0.67 and 0.62, respectively (with grey lines the 95% confidence intervals) while the cyan line is the fit calculated by *Sharples et al.* (in revision), whose data are shown with the grey circles.

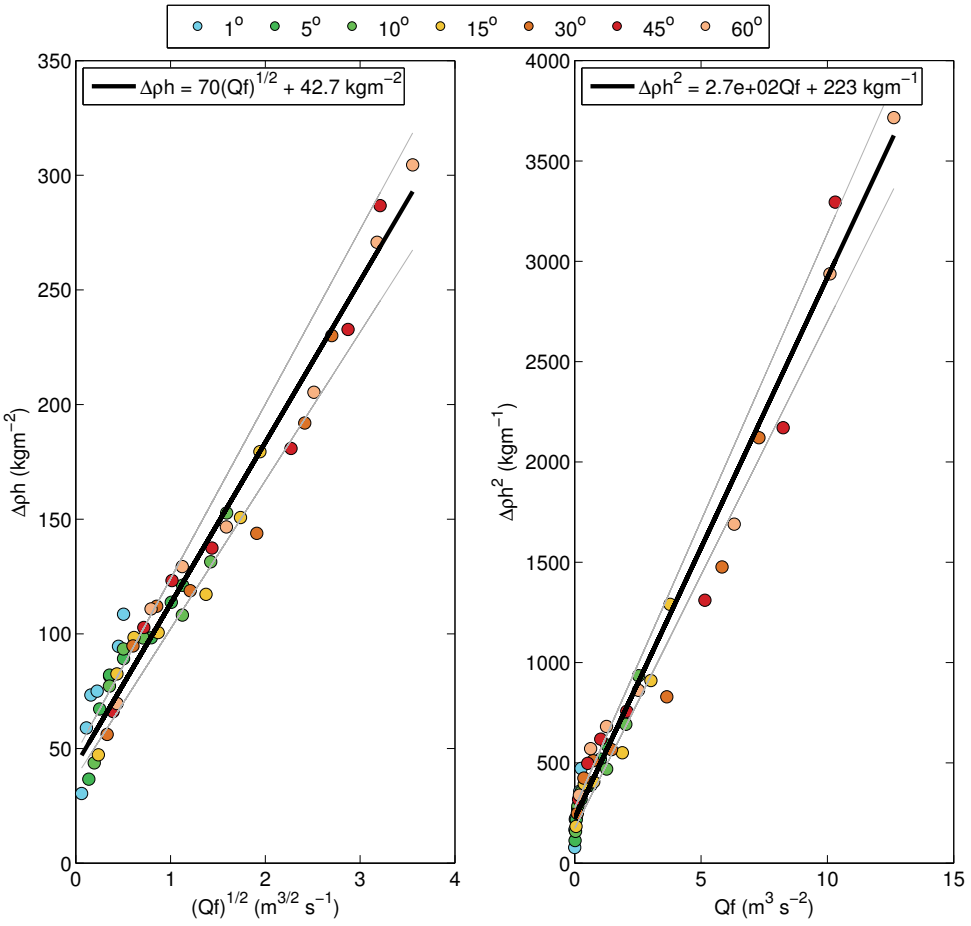

Figure 3.17: Regressions applied to $\Delta\rho h$ and $\Delta\rho h^2$ as a function of both river discharge and the Coriolis parameter (excluding the points at 0°). The black line is the regression fit to the model data (Equation 3.4) with r^2 values of 0.95 and 0.93, respectively (with grey lines the 95% confidence intervals).

As with cross-shelf export, the S_P number can also be used to predict the export timescale (T_E) of the simulated plumes (the time it takes for the plume to first reach the shelf break), scaling best as linearly proportional to S_P^{-3} (Figure 3.18). The regression (Equation 3.5) has an r^2 value of 0.72. As with the estimation of the alongshore export efficiency, T_E can also be negative for large values of S_P when estimated using the 95% confidence intervals for the regression. As such, all negative values are set to zero when I use the relationship to estimate nutrient processing for real rivers. Other regressions were attempted (such as different powers and different parameter dependencies), but this regression proved the best fit to the data.

$$T_E = (0.3 \pm 0.2) S_P^{-3} + (0.8 \pm 1.3) \tag{3.5}$$

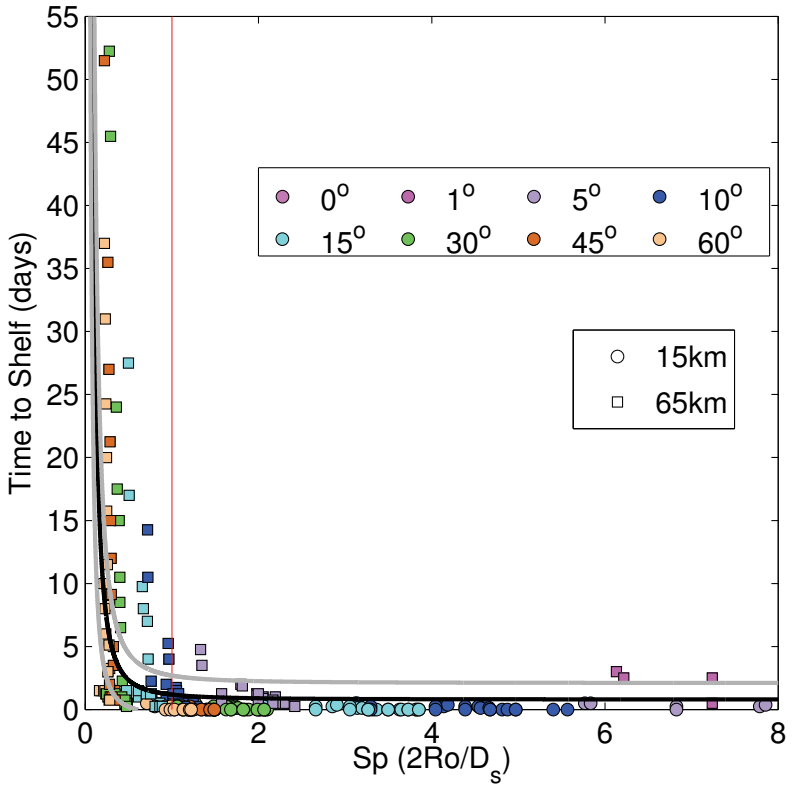

Figure 3.18: Plume export timescale as a function of the S_P number for all simulated plumes. The black line is the linear regression with an r^2 value of 0.72 and the grey lines show the 95% confidence intervals.

3.3 Obtaining a Global Estimate of Open Ocean Export

3.3.1 Freshwater Export

Using the idealized relationships described in Section 3.2, I estimated the freshwater export efficiency for all rivers in the GloablNEWS database (Section 2.4; *Mayorga et al.* 2010). First, I calculated the internal Rossby radius at the mouth of each river following Equation 3.3 and using the regressions for $\Delta\rho h$ and $\Delta\rho h^2$ in Equation 3.4. I then calculated the S_P number for each of the rivers, and estimated the cross-shelf and alongshore export efficiencies using Equation 3.1, with the coefficient values in Table 3.1 obtained from a regression applied to all of the simulated data.

As an illustration, Figure 3.19 presents the individual freshwater budgets for the Amazon, the Mississippi, and the Columbia Rivers. The Amazon River, which is closest to the equator, has the highest estimated cross-shelf export efficiency (31–73%) of the three rivers, and no downstream transport away from the source region. Much greater downstream advection is estimated for the Mississippi and Columbia Rivers, and much higher overall shelf retention within the plume. The Columbia River has the greatest downstream transport, with 34–51% of the river discharge advected away from the source region in the coastal current.

On a global scale, I estimate that between 15 and 53% of riverine fresh water is exported by river plumes (equivalent to approximatey 6–20 x 10^3 km^3 annually). Figure 3.20 shows that the highest efficiencies are confined to a narrow band spanning roughly 15° on either side of the equator, and on the narrow active margins of the continental shelves (such as the west coast of North America).

Combined freshwater budgets for 10° latitude bands (Figure 3.21) show that, in general, the estimated cross-shelf export of fresh water in plumes is higher in the northern hemisphere than the southern hemisphere, with a decrease in cross-shelf export and corresponding increase in alongshore export with increasing distance from the equator in both hemispheres. Cross-shelf export is dominant in the low latitudes. Retention near the source peaks in the mid-latitudes in both hemispheres. Alongshore export is greatest in the higher latitudes. Within 10° of the equator, 60% riverine fresh water is exported to the open ocean, while 60% of fresh water is retained in the coastal current above 45°.

Combined freshwater budgets for eastern and western North America, northwestern Europe, and south Asia are shown in Figure 3.22. Of the four regions, the highest estimates

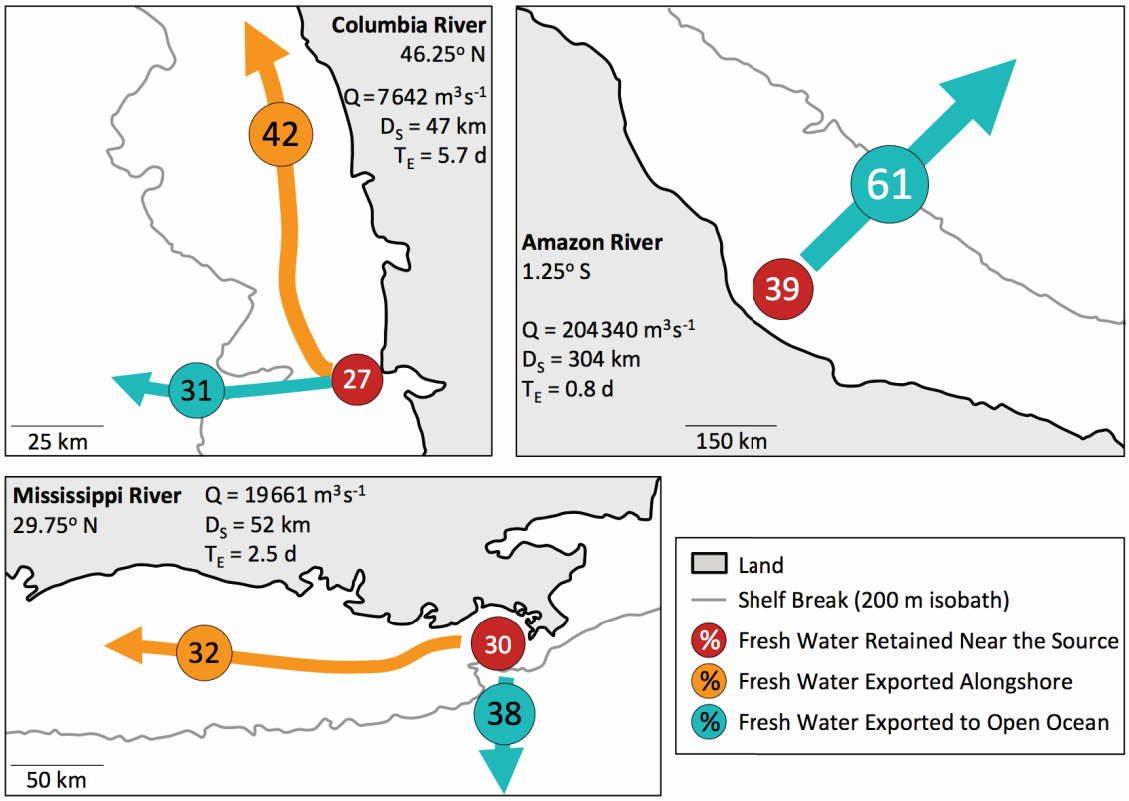

Figure 3.19: Estimated freshwater budgets for the Amazon, Mississippi, and Columbia Rivers. The shelf width was calculated to the 200 m isobath.

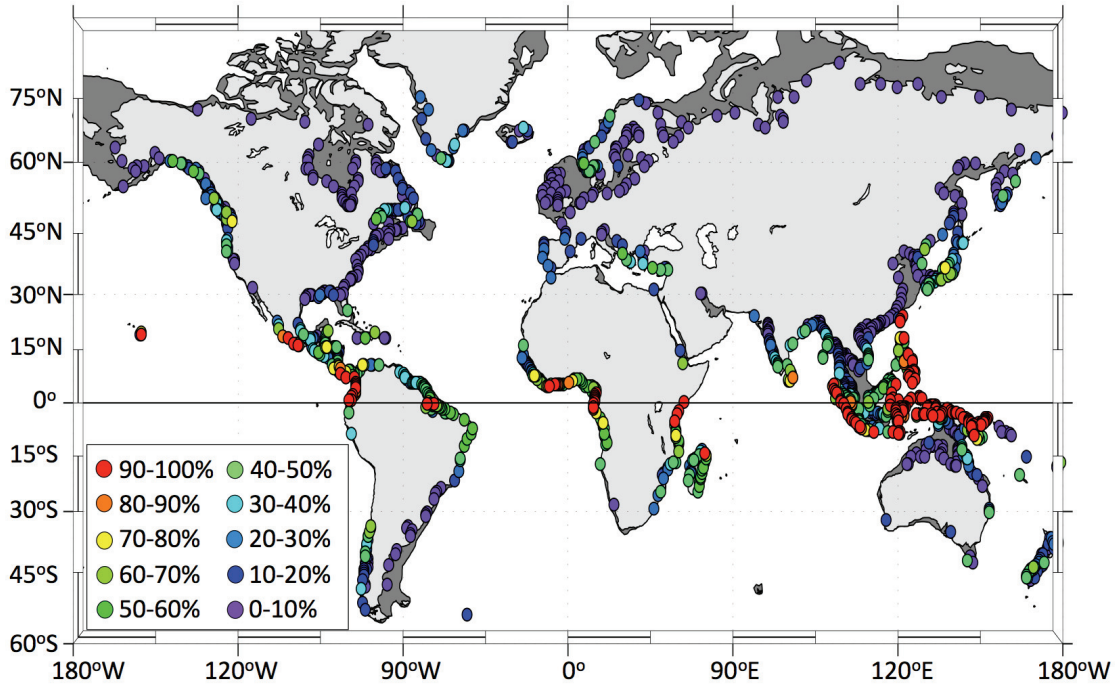

Figure 3.20: Estimated export efficiency of fresh water to the open ocean for rivers in the GlobalNEWS model (only rivers that discharge into the ocean at more than 100 $m^3\ s^{-1}$ are included). Shelf regions, defined by the 200 m isobath, are shown in dark grey.

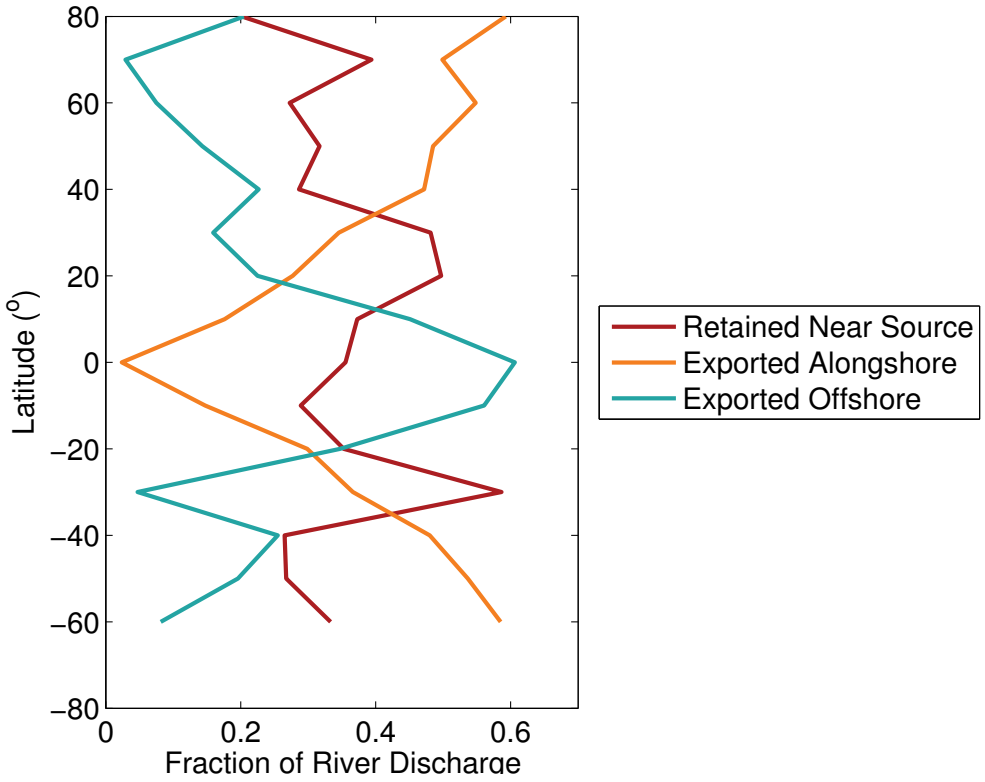

Figure 3.21: Freshwater budgets in 10° latitude bands.

of cross-shelf export are along the west coast of North America (33%), with the lowest retention near the sources (18% within 150 km). Along the east coast of North America only 13% of the riverine fresh water is estimated to be exported to the open ocean, with 39% retained near the sources. The largest retention occurs in south Asia, where an estimated 50% of riverine fresh water remains on the shelf within 150 km of the source, with 30% exported to the open ocean. The greatest alongshore export occurs in northwest Europe (56%), with the lowest cross-shelf export (just 9%).

3.3.2 Nutrient Export

In order to estimate nutrient export, I first assumed that nutrients are conservative, i.e. that they are not affected by biochemical processing and essentially behave as conservative tracers:

$$\Gamma_{XC}^{Nut} = E_X^{FW} L_{River}^{Nut}, \tag{3.6}$$

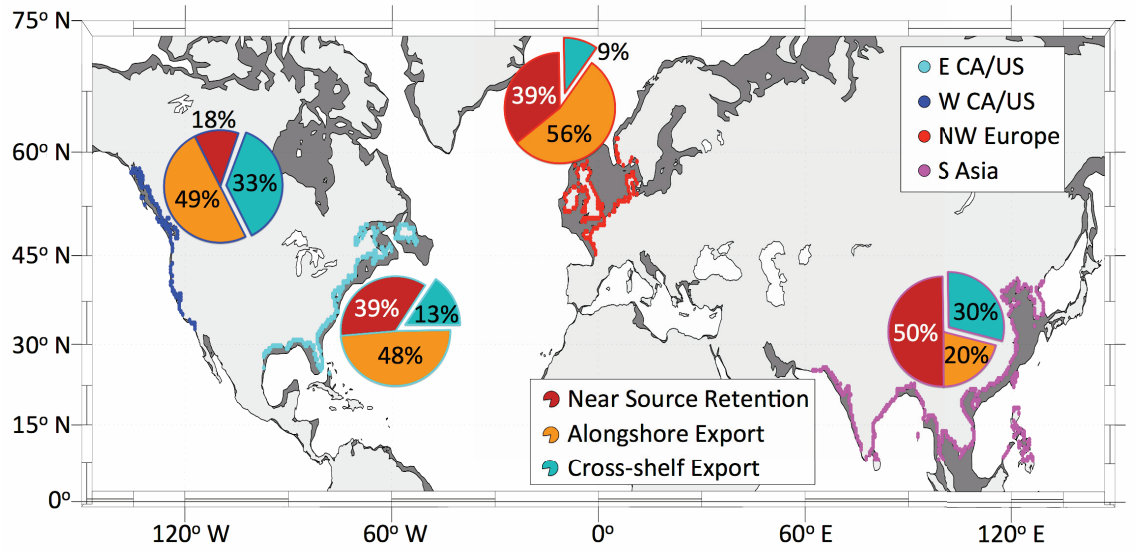

Figure 3.22: River mouth locations and freshwater budgets for the four socioeconomic regions: east and west coasts of Canada and the United States, northwestern Europe, and south Asia.

which is simply the cross-shelf freshwater export efficiency (E_X^{FW}) multiplied by the riverine load of the nutrient (L_{River}^{Nut}). These estimates represent upper limits for the actual nutrient export occurring. From this, I calculated an upper bound of global nutrient export for DIN, DON, DIP, DOP, DOC, and DSi (Figure 3.23 and Appendix B). Even with conservative export, the upper bounds are low. DSi is exported globally with the highest efficiency of all the nutrients (18.2–56.4%), while DIN has the lowest conservative export efficiency (7.3–44.3%).

I also estimated export of non-conservative nutrients using a range of removal rates as follows. For a given removal rate, r (in days^{-1}), the exported amount of a nutrient is the product of the conservative export ($E_X^{FW} L_{River}^{Nut}$; Equation 3.6) and the fraction of material removed:

$$\begin{aligned} \Gamma_{X\overline{C}}^{Nut} &= \frac{1}{1+rT_E} E_X^{FW} L_{River}^{Nut} \\ &= \frac{1}{1+rT_E} \Gamma_{XC}^{Nut}, \end{aligned} \tag{3.7}$$

where T_E is the export timescale of the plume (how long it takes for the plume to reach the shelf break). The inverse of the removal rate is the processing timescale, which is

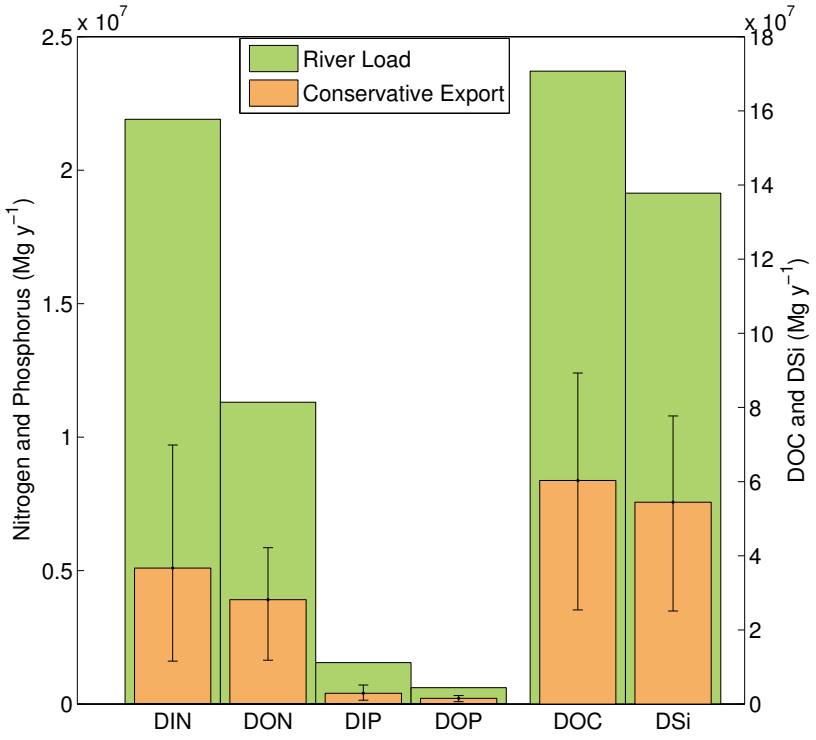

Figure 3.23: Global riverine loads and conservative cross-shelf export of different nutrients.

an indicator of the amount of time it takes for nutrients to be removed from the system through biological and chemical uptake and transformations.

I calculated the export timescale for each river in the GlobalNEWS database using Equation 3.5. The global pattern of estimated export timescales (Figure 3.24) is opposite to the freshwater export efficiency in Figure 3.20: higher export times for smaller rivers, higher latitudes, and wider shelves (lower S_P). Most rivers have estimated export timescales greater than two weeks.

I then estimated nutrient export using Equation 3.7 for a range of removal rates. As with the freshwater budgets in Section 3.3.1, I calculated nutrient budgets for the Columbia, Mississippi, and Amazon Rivers. Figure 3.25 shows the results of assuming a nutrient removal rate of 0.75 d^{-1}; even the Amazon River (which has a short export timescale of just 0.8 d) has significantly reduced nutrient export beyond the 200 m isobath, with the Missisippi River (export timescale of 2.5 d) and Columbia River (export timescale 5.7 d) having very high near source retention due to significant nutrient removal. The

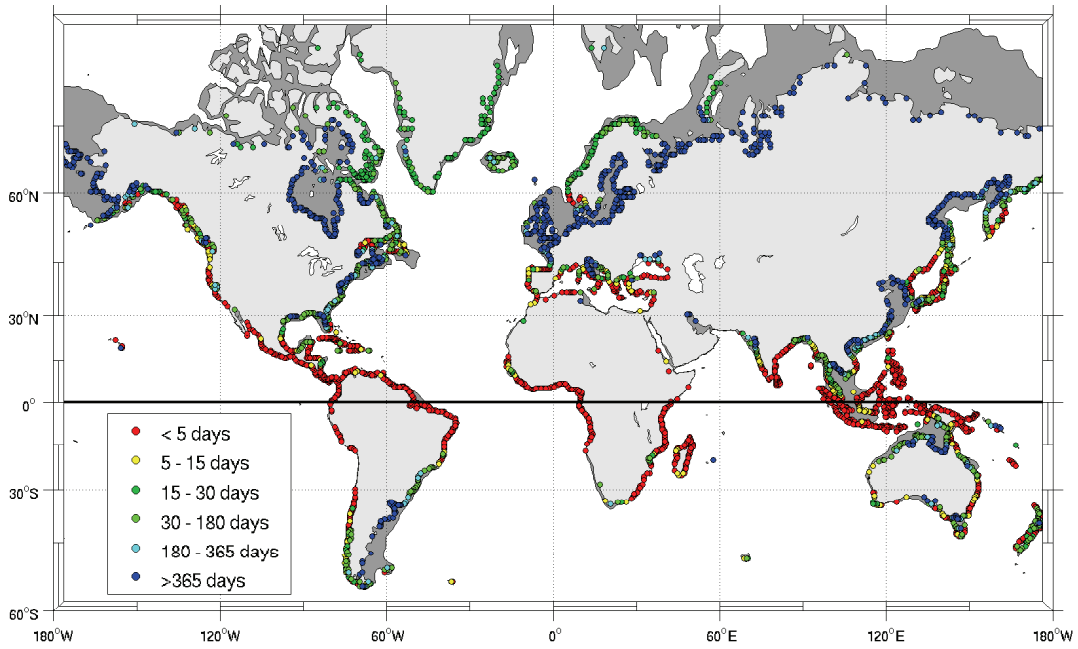

Figure 3.24: Global distribution of estimated plume export timescales (only rivers that discharge into the ocean at more than 10 $m^3\ s^{-1}$ are included). Shelf regions, defined by the 200 m isobath, are shown in dark grey.

conservative nutrient export efficiency is the same as for freshwater export in Figure 3.19.

For the highest and lowest processing rates ($r > 10\ d^{-1}$ and $r < 0.01\ d^{-1}$, corresponding to processing timescales of less than 0.1 day or greater than 100 days), the global amount of material exported is approximately constant and not sensitive to changes in r. Between processing timescales of one day to a few months, however, export is more sensitive to the rate chosen, with a significant decrease in exported nutrients for shorter processing timescales (Figure 3.26, and Appendices A and B). Within this range, increasing the removal rate by one order of magnitude results in approximately a factor of 2 decrease in the number of rivers that are estimated to export to the open ocean, and an equivalent decrease in the overall nutrient export. Of the six nutrients considered, DIN and DIP are depleted the quickest for the lowest nutrient removal rates, while DSi and DOC not only have the largest riverine loads, but are also exported with the greatest efficiency.

Global comparisons are presented in Figure 3.27 for DIN and DSi under different removal scenarios: no removal (conservative export), low removal ($r = 0.15\ d^{-1}$; used by *Rabouille et al.* 2001 as a global rate of shelf uptake of DIN by phytoplankton) and

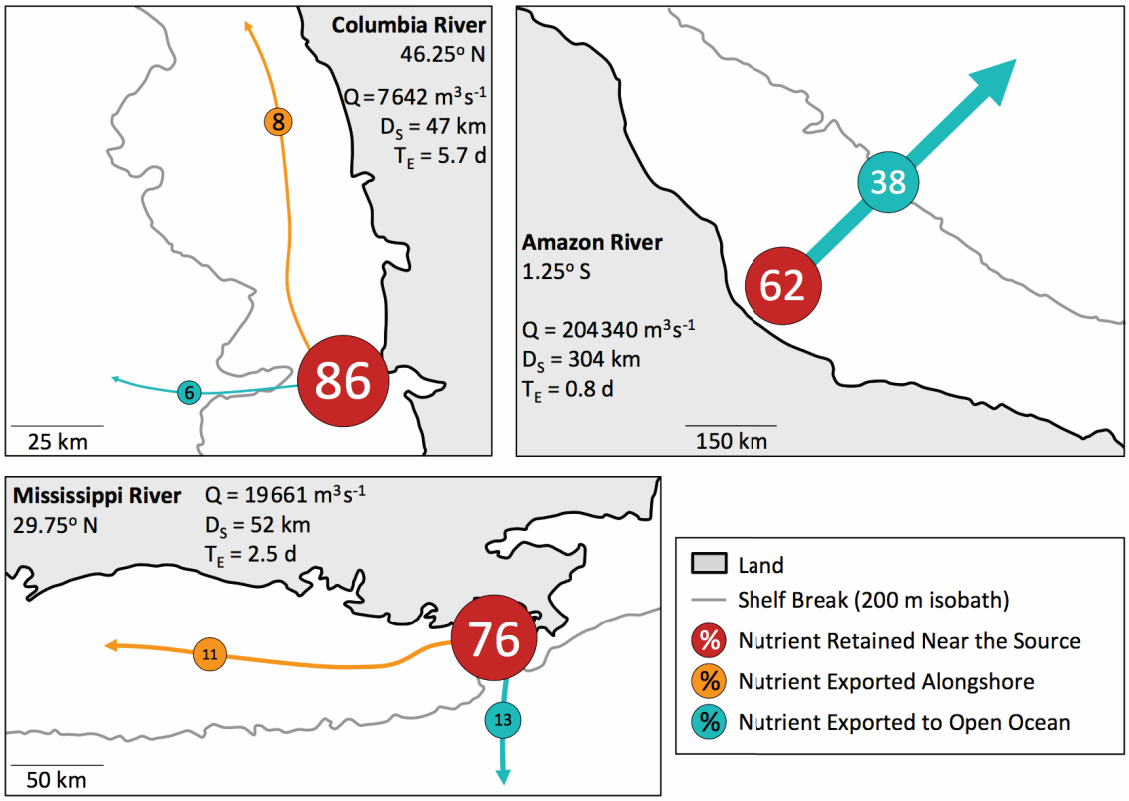

Figure 3.25: Estimated nutrient budgets for the Amazon, Mississippi, and Columbia Rivers for a processing rate of 0.75 d^{-1}. The shelf width was calculated to the 200 m isobath.

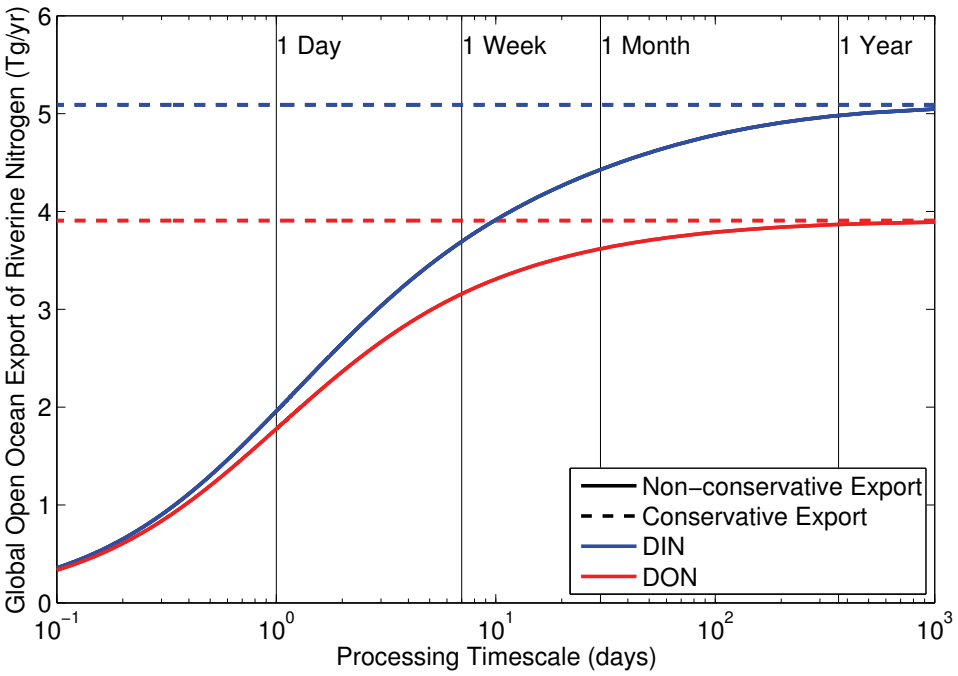

Figure 3.26: Global export of DIN and DON for different shelf processing timescales. The dashed line represents the conservative export.

high removal ($r = 0.75$ d^{-1}; 5 times that of the low rate and where the global nutrient export begins to level off and is less sensitive to further increases in r). DSi is delivered in the greatest amounts near the equator, while DIN delivery is highest in the 15–25° latitude band. The highest export occurs in the low latitudes, and decreases with higher latitudes. Under the removal scenarios, the combination of long export timescales and already-reduced freshwater export efficiency at high latitudes results in very little to no estimated nutrient export above 30°. A summary of all nutrient estimates is in Appendix B. The overall global ranges of nutrient export estimates (from the lowest at $r = 0.75$ d^{-1} to the highest under conservative behaviour) are:

DIN:	2.8–44.3%	DIP:	3.5–45.9%
DON:	5.6–51.8%	DOP:	5.5–51.9%
DOC:	5.7–52.3%	DSi:	7.0–56.4%

Table 3.2 summarizes the freshwater and nutrient budgets for different regions, from individual river systems up to the global shelves, with comparisons to available estimates.

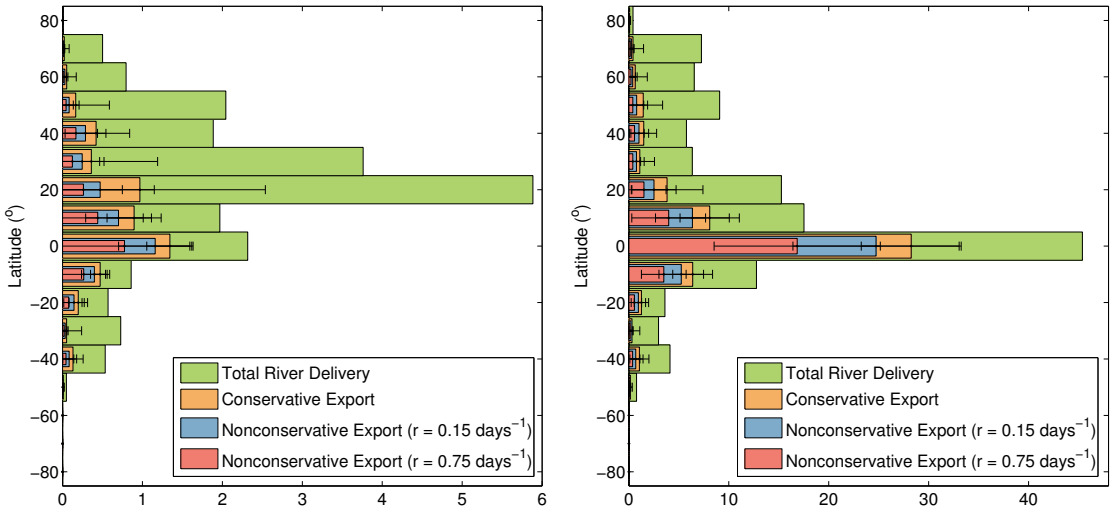

(a) Annual DIN (Tg/year) (b) Annual DSi (Tg/year)

Figure 3.27: Comparison of a) DIN and b) DSi delivery and export in 10° latitude bands

River/Shelf System		Fresh Water ($m^3\ s^{-1}$)	DIN ($Mg\ yr^{-1}$)	DIP ($Mg\ yr^{-1}$)	DOC ($Mg\ yr^{-1}$)	DSi ($Mg\ yr^{-1}$)
Amazon	L_{River}	2.04 x 10^5 [1.9 x 10^5]^a	9.3 x 10^5 [1.0-3.0 x 10^6]^a	2.7 x 10^4 [2.1-2.5 x 10^5]^a	2.9 x 10^7	2.0 x 10^7 [2.2 x 10^7]^a
	E_X	31-73%	12-73% [50%]^a	12-73% [100%]^a	12-73%	12-73% [92%]^a
	E_A	0-3%	0-3%	0-3%	0-3%	0-3%
	R_{Source}	24-69%	24-88%	24-88%	24-88%	24-88%
Mississippi†	L_{River}	1.97 x 10^4 [1.34 x 10^4]^b	6.8 x 10^5 [9.5 x 10^5 TN]^b	2.7 x 10^4 [1.1 x 10^5 TP]^b	2.9 x 10^6	1.5 x 10^6
	E_X	19-69% [-33%*]^b	7-69% [-60%*]^b	7-69% [-53%*]^b	7-69%	7-69%
	E_A	25-39% [47%]^b	9-39% [127%*]^b	9-39% [88%]^b	9-39%	9-39%
	R_{Source}	8-56%	8-84% [18%]^b	8-84% [62%]^b	8-84%	8-84%
Gulf of Mexico†	L_{River}	3.60 x 10^4	1.1 x 10^6 [1.9 x 10^6]^c	5.3 x 10^4	5.3 x 10^6	3.8 x 10^6
	E_X	14-65%	5-64% [-7.7%*]^c	4-63%	5-64%	5-64%
	E_A	26-41%	7-42% [-4%*]^c	5-43%	6-42%	6-42%
	R_{Source}	6-59%	6-88%	5-90%	6-88%	6-89%

River/Shelf System		Fresh Water ($m^3\ s^{-1}$)	DIN ($Mg\ yr^{-1}$)	DIP ($Mg\ yr^{-1}$)	DOC ($Mg\ yr^{-1}$)	DSi ($Mg\ yr^{-1}$)
Mid Atlantic Bight	L_{River}	4.12 x 10^3	2.16 x 10^5	2.31 x 10^4	6.54 x 10^5	4.49 x 10^5
	E_X	0-28%	0-8% [-3.5 x 10^5*][d]	0-28%	0-28%	0-28%
	E_A	39-57%	0-58%	0-58%	0-57%	0-57%
	R_{Source}	15-61%	15-100%	15-100%	14-100%	15-100%
Global	L_{River}	1.18 x 10^{12}	2.19 x 10^7 [2.3[g] x 10^7/3.1[e] x 10^6]	1.5 x 10^6 [1.6 x 10^6][g]	1.71 x 10^8 [4.1 x 10^7][e]	1.37 x 10^8 [1.7 x 10^8][f]
	E_X	15-53%	3-44% [75%[g] / 7%[e]]	3-46% [80%][g]	6-52% [15%][e]	7-56% [9%][f]
	R_{Shelf}	47-85%	66-97% [25%[g] / 93%[e]]	64-97% [20%][g]	48-94% [85%][e]	48-93% [91%][f]

* Transport is net onshore/toward source or is greater than riverine input

† calculated to 50 m isobath for consistency with previous estimates

[a] Reported as fraction of total input by *DeMaster and Aller* (2001)

[b] From combined obervational and numerical study, *Lehrter et al.* (2013)

[c] Annual total from numerical study of entire Gulf of Mexico region *Xue et al.* (2013)

[d] Total nitrogen (TN) budget from numerical study of the Mid Atlantic Bight *Fennel et al.* (2006)

[e] From global mass balance model of *Rabouille et al.* (2001)

[f] From global mass balance model of *Laruelle et al.* (2009)

[g] Estimates from *Sharples et al.* (in revision)

Table 3.2: Comparison of local, regional, and global freshwater and nutrient budgets with previously published values. The percentage ranges span the maximum and minimum values for each material, with the nutrients bounded by assuming an uptake rate of $r = 0.75\ d^{-1}$, and the conservative export estimate (no removal).

CHAPTER 4
DISCUSSION

4.1 The Idealized Model Experiments

I conducted a series of idealized model experiments to assess the influence of four primary factors on the cross shelf transport of river plume water. The four factors are: latitude, river discharge, tidal forcing, and wind forcing.

In general, the simulated plumes form and behave as predicted by theory (see, for example, *Horner-Devine et al.* 2015 for a review of plume dynamics). At latitudes 5° and above, the buoyant outflow at the river mouth is deflected by the Coriolis force, resulting in the formation of a bulge and coastal current (Figure 3.1). With increasing latitude this downstream deflection intensifies, and the plumes become deeper at higher latitudes and for higher discharges (Figure 3.2). Without any external forcing, this classical shape persists for the duration of the simulations; however, when external forcing is applied the shape of the simulated plumes changes (Figure 3.8) and plumes can be pushed offshore or onshore depending on the forcing. All of the simulated plumes—forced and unforced—reach a point of established plume transport where instabilities osciallate about a mean value (Figure 3.4); however, the bulge never completely stabilizes to a steady-state shape and size. In the unforced case, this is the result of continuous growth of the bulge region (as discussed by *Garvine* 2001), while the dynamic nature of the plumes in the forced scenarios leads to continual reshaping of the plumes. Overall, the simulated plumes for high discharge and low latitude cases extend further across the shelf than those for low discharge and high latitude cases.

The main pathway for cross-shelf export within the simulated plumes is through direct advection within the bulge region. This occurs in two ways: 1) through cross-shelf growth and advection of the plume, and 2) through the development instabilities along the front demarcating the plume. In the absence of external forcing, the continuous growth of the bulge region carries riverine water offshore. In all of the unforced cases, the initial bulge eventually grows so large that it becomes unstable and detaches from the rest of the plume

before recirculating, and eventually reattaching on different timescales depending on the latitude and discharge of the plumes (Figure 3.5). Such large-scale instabilities were also described by *Oey and Mellor* (1992). Similarly, smaller instabilities develop along the plume front, enhancing cross-shelf transport via offshore movement of the resulting eddies.

4.1.1 The Influence of Different Factors on Plume Transport

Through the different model experiments, I tested the influence of changing latitude, river discharge, tidal forcing, and wind forcing on cross-shelf export of riverine water.

In all simulations, latitude provides a strong control on the efficiency of cross-shelf transport (Figures 3.6 and 3.9–3.11). With increasing latitude, the cross-shelf export decreases significantly, with the greatest decrease in transport occurring for the unforced case (approximately 70% from 0° to 60°; Figure 3.6). Correspondingly, as the cross-shelf transport decreases with increasing latitude, the alongshore transport within the coastal current increases, while the near source retention remains approximately constant above 5° at roughly 30%.

Increasing discharge has a slightly non-linear effect on plume transport. In most simulations, export efficiencies at low discharges are similar; but, the higher discharge simulations are more spread out, resulting in a 30% change between the lowest and highest transport values at 60° (e.g., Figure 3.6). At first, this non-linearity is surprising. Given that export efficiency is normalized by the discharge (Equation 2.3), the efficiencies were expected to be approximately similar for all discharges. Upon closer inspection, it is apparent that the greater cross-shelf transport efficiency for high discharges (and subsequently reduced alongshore transport efficiencies) is consistent with the process of bottom advection as described, for example, by *Yankovsky and Chapman* (1997). Looking at Figure 3.2 and Figure 3.6, the plumes that are entirely surface-advected (i.e., below the 0 km line in Figure 3.2) are generally similar in their export efficiencies. However, the plumes that are attached to the bottom much further offshore (i.e., the higher discharge cases) have higher cross-shelf transport efficiencies than the surface-advected plumes, and lower alongshore transport efficiencies. At 45°, for example, the plumes with discharges less than 10 000 $m^3\ s^{-1}$ are all surface-advected (Figure 3.2) and cross-shelf transport is less than 5% beyond 65 km for each of them (Figure 3.6). The plumes with discharges above 20 000 $m^3\ s^{-1}$ are all attached to the bottom at least 10 km from the coast (Figure 3.2), and have correspondingly increased cross-shelf transport: all the way up to the 100 000 $m^3\ s^{-1}$

plume, which reaches almost to the shelf break after 20 days, and has an export efficiency of almost 40% (Figure 3.6). The impact of bottom advection is greater at higher latitudes due to deepening of the plume, but is less noticeable for the forced plumes than the unforced plumes, where the external forcing exerts greater control over the plume dynamics.

Tests to assess the impact of the shelf bathymetry on the results provide further evidence for bottom advection within the simulations. Shelf bathymetry was changed by varying the minimum depth, or the slope of the shelf in the DpIn/ShIn and DblSlp/HlfSlp simulations (Table 2.1). Two discharges were used in these tests: 1 500 $m^3\,s^{-1}$ and 50 000 $m^3\,s^{-1}$ (low and high, respectively). The low discharge plumes are completely surface advected at all latitudes (Figure 3.2) and so should not be influenced greatly by changing the depth of the domain, while the high discharge plumes are attached to the bottom of the domain for most latitudes and should have increased cross-shelf transport when the domain is shallower. This is exactly what happens. The low discharge plumes (Figure 3.7a and b) are not very sensitive to changes in the domain. The high discharge plumes (Figure 3.7c and d), however, are sensitive to changes in the shelf depth and slope; consistent with the idea of bottom advection, the plumes have higher cross-shelf export efficiencies when the domain is shallower (ShIn and HlfSlp) leading to an approximate 20% spread in export efficiency between the deep domain (where the plume detaches from the coast closer to shore) and the shallow domain (where the plume remains attached to the bottom further offshore). As such, bottom advection is a mechanism for overcoming some of the influence of latitude in shallow seas, or high discharge plumes.

Adding tidal forcing to the model simulations (TDL) does not have a significant impact on the plumes. Cross-shelf transport is between 30–50% 15 km offshore, and 0–30% 65 km offshore at higher latitudes (Figure 3.9), compared to the unforced case of 20–60% and 0–30% (Figure 3.6), respectively. As in the unforced case, there is still a roughly 70% decrease in cross-shelf export efficiency between the low and high latitudes. Near shore, the motion of the tides enhances the cross-shelf motion of the plume slightly for the low discharge plumes, but does not change the high discharge plumes. Offshore transport beyond 65 km is reduced slightly, in spite of the increased near shore transport, because the tides stabilize the plume bulge (as seen by the more uniform export values and previously described by, for example, *Isobe* 2005). The tides I used were very simple (semi-diurnal,

uniform amplitude, and perpendicular to the coast) in comparison to tides around the world, and thus may oversimplify the influence of tides under different conditions. However, *Isobe* (2005) used an alongshore Kelvin wave to simulate the tide (perpendicular to my tides), with similar results, which suggests that the presence of any tide stabilizes the bulge (similar to the effect *Fong and Geyer* 2002 noticed for an ambient current), and the direction may not be important.

Winds increase the cross-shelf transport at high latitudes by up to 70% compared to the unforced case, and provide a mechanism for overcoming some of the constraints on export posed by latitude (Figures 3.10 and 3.11). When the simulated winds are strong in the cross-shore direction (XWDL; see Table 2.1), the low latitude plumes are pushed directly offshore due to the lack of Coriolis force near the equator, and almost all plumes have an export efficiency of 100% (Figure 3.11). In the unforced case, these low discharge plumes have transport efficiencies around 70–80% (Figure 3.6). At high latitudes, the XWDL winds also enhance cross-shelf transport, with the alongshore component of the synthetic wind leading to cross-shelf Ekman transport (an increase of 30–70% 15 km offshore).

The alongshore-dominant winds (AWDL in Table 2.1), drive offshore export at high latitudes through enhanced Ekman transport as a result of the strong upwelling cycle (Figure 3.10). Overall, latitude has less of an impact on the plumes such that the cross-shelf export efficiency remains above 20% at all latitudes (recall that in the unforced case it is 0–30%). It is interesting to note, though, that the alongshore winds lead to a reduction (to below 50%) in cross-shelf export in the low latitudes for the smaller plumes (Figure 3.10b). This is likely due to the idealized domain and wind fields, where the strong up and downwelling winds cause suppression of the plume at the rectangular outflow. A more realistic coastline might not have the same impact in suppressing the flow.

Overall, the wind-forced scenarios (XWDL and AWDL) have the highest cross-shelf export efficiencies of all the simulations, increasing cross-shelf export efficiency by up to 70% compared to the unforced case, and overcoming some of the influence of latitude. However, in all of the model experiments, cross-shelf transport decreases with latitude (by as much as 70% in the unforced case and 50% with wind forcing between 0–60°). Consistent with *Sharples et al.* (in revision), the fact that the Coriolis force exerts a strong control in all cases suggests that it is the main factor determining whether riverborne materials are exported to the open ocean, reducing the offshore extent of river plumes and

subsequent cross-shelf transport. External forcing is only able to overcome some of the overriding influence of the Coriolis force.

4.1.2 Describing River Plume Export with Simple Metrics

One of the objectives of this research is to describe river plumes—in particular their associated open ocean export—using simple, general relationships. Despite the variability of the simulated plumes with the different influencing factors, clear statistical relationships emerge between simple plume descriptors and properties of the simulated plumes.

The alongshore export efficiency of the simulated plumes is related to the inverse of the square root of the Rossby radius (Figure 3.15). The Rossby radius, which depends on latitude through the inverse of the Coriolis parameter (Equation 2.2) also provides an indication of a plume's ability to spread offshore. The higher the latitude, the stronger the Coriolis force, resulting in greater downstream deflection of the plume, and correspondingly less cross-shelf export and increased transport in the coastal current.

Similarly, I found that the S_P number (Equation 2.1) predicts the cross-shelf export efficiency extremely well for most scenarios through a simple asymptotic relationship. As discussed by *Sharples et al.* (in revision), cross-shelf export efficiency is qualitatively different for plumes with an S_P less or greater than 1. However, whereas *Sharples et al.* (in revision) assume complete export for $S_P > 1$, and no export for $S_P < 1$, I estimate the export using a continuos function (Equation 3.1; e.g., Figure 3.12). For $S_P < 1$, the export efficiency is low, but increases rapidly with increasing S_P. Above 1, the overall export efficiency is higher, but the rate of increase in export efficiency with increasing S_P is much lower as the curve levels off. The unforced (DL) and tidally forced (TDL) scenarios result in similar regressions, while the wind-forced scenarios (AWDL and XWDL) result in an overall increase in export (Table 3.1). Important to note is that all of the regressions have positive x-intercepts. This indicates that plumes below a given S_P number do not directly export material to the open ocean.

When estimating export for real rivers, I use the regression applied to the simulated data from all forcing scenarios (Table 3.1). The confidence intervals on the estimates cover just over 80% of the variability in the simulated plumes, indicating they are reliable for estimating export in more complex forcing environments. To further improve the estimates, an immediate next step would be to test and refine the relationships in more realistic plume models and to assess how they apply under the influence of more complex forcing

scenarios.

These relationships all describe export as a function of the internal Rossby radius (the S_P number is calculated with $R_o^{'}$ in the numerator) and can be used to estimate export for real rivers. This, of course, relies on knowing the internal Rossby radius for real plumes, which is not always straightforward. In Equation 3.3, the Rossby radius depends on the parameters $\Delta\rho h$ and $\Delta\rho h^2$, which are difficult to measure for real plumes, even in dedicated field studies ($\Delta\rho$ is the density difference between the plume and ambient water, and h is the mean plume depth). *Sharples et al.* (in revision) estimate these paramters from linear regressions with the river discharge as the independent variable (see Figure 3.16) using measurements of 20 real world plumes. However, my simulations show an apparent latitude dependence as well, so I apply regressions that depend on both the river discharge and the Coriolis parameter (Equation 3.4 and Figure 3.17). These regressions provide extremely good fits for the simulated plumes (r^2 values over 0.9), and as such are assumed to be good predictors for real world plumes as well, making it easy to estimate the Rossby radius of a real plume.

Also important in calculating export in real rivers is the time the plume remains on the shelf. The longer water remains on the shelf before being exported, the greater the potential for nutrients to be processed and transformed into forms less likely to be exported. Figure 3.18 shows that the export timescale for all of the simulated plumes (calculated as the time before cross-shelf transport first occurs) can be estimated as a linear function of S_P^{-3}. Intuitively, this makes sense: a larger S_P number means either a large plume, or a small shelf, such that cross-shelf export is direct and efficient (and the export timescale short). Smaller S_P, on the other hand, indicates a small plume in relation to the shelf, with export taking much longer.

It should be noted again that the forcing used here is highly idealized compared to the forcing expected for real world systems. In reality, the plume environment can change on various timescales, including seasonally (e.g., changes in thermal stratification or wind fields). The environment of every plume is unique and highly variable, with other factors not addressed here (such as ambient currents, complex coastlines and bathymetry, the absence of bulges in many plumes, etc.) influencing offshore export. However, for the purposes of this research, where my goal is to obtain a general description of plume behaviour, the simplifications presented here help to elucidate the underlying influences

that can affect the plumes, while the use of the range in regression coefficients captures some of the potential for otherwise unexplained variability due to external factors that have not been addressed here.

The main result of the first part of this thesis is to demonstrate that plume dynamics, despite their complexity, can be described using simple relationships, at least as a first-order approximation. Given the complex nature of the different forcings that can influence plumes, I would expect that the simplified relationships do not apply for all situations; however, the fact that the simple relationships apply for most of the idealized scenarios builds confidence that rough estimates of plume transport can be obtained through this framework. My results support the findings of *Sharples et al.* (in revision), and extend their work by parameterizing export in terms of continuous functions. Overall, these relationships allow for the easy estimation of plume export for real world plumes, by first calculating the Rossby radius, and subsequently the cross-shelf and alongshore transport within the plumes. From these simple estimates, budgets of freshwater and nutrient transport can be calculated for any river.

4.2 Estimates of River Plume Export

The relationships described in Section 4.1.2 provide a straightforward means of estimating plume export for real world rivers. Although they are simple, their power lies in their generality and easy application. While they were developed from highly idealized numerical simulations, they still provide a means of estimating—even if only approximately—riverine export, with the wide range of parameter values accounting for some of the uncertainty in the estimates resulting from more complex dynamics and settings.

4.2.1 Estimating Nutrient Removal

From the relationships discussed in Section 4.1.2, calculating freshwater export for real rivers is trivial. Estimating nutrient export, however, is more challenging. In the absence of a full biogeochemical model, assessing the impact of non-conservative nutrient removal requires further assumptions about the processes involved and the rates at which nutrients are removed from the plume.

Overall, most riverine material is eventually exported to the open ocean from the shelf. However, this is only after undergoing many transformations and through circuitous

routes of export, rather than direct export within river plumes, which is the focus of my research. Some processes that can completely remove a nutrient from the system before it is exported, as opposed to simply delaying export, include burial within sediments, and alternate respirations pathways.

Sediment burial typically occurs on long timescales. Particulate organic matter that is produced in the surface layer through primary production sinks to the bottom of the water column, settling on the sediments. Much of the labile material is remineralized; however, the continual rain of particulates from above eventually covers the refractory material. With time, the material becomes permanently buried (or at least buried on long timescales as to be considered permanent burial).

In the absence of oxygen, alternate respiration pathways can be utilized that convert bioavailable nutrients to unavailable forms. Denitrification is one such pathway, converting DIN species (such as NO_3^-) to nitrogen gas (N_2), which is then lost to the system through outgassing (*Seitzinger et al.* 2006). A similar process involves the respiration of ammonium (NH_4^+) with nitrite (NO_2^-): anaerobic ammonium oxidation (annamox) (*Thandrup* 2012). Due to the requirement for low oxygen, these processes typically occur in the lower water column, or upper sediments; as such, riverine material must first sink out of the surface layer. These processes can be significant, however, with shelf denitrification removing large amounts of riverine nitrogen from shelf seas (e.g., *Christensen* 1987). *Fennel et al.* (2006), for example, estimate denitrification removes 90% of the total nitrogen input to the continental shelf of the Mid Atlantic Bight.

In my analysis, I do not explicitly simulate any specific removal processes. Instead, my generalized framework can cover the permanent removal processes such as sediment burial and denitrification, but also allows for the consideration of processes that may not remove nutrients from the system as a whole, but only from the plume itself. While not strict removal, this allows for the separation of export that occurs directly as a result of plume transport from other processes that transport material across the shelf, including those that occur on longer timescales after transformations of the riverine nutrients on the shelf.

This becomes particularly important when assessing more complete nutrient budgets or the accumulation of riverine nutrients on the shelf and their ability to influence local biochemical cycles, potentially leading to harmul effects such as eutrophication and

hypoxia. Immediate export of the material within river plumes leads to direct removal from the source region, minimizing the impact of terrestrial nutrient delivery. Other processes (such as entrainment of shelf waters in offshore eddies) represent alternative transport pathways which can also remove nutrients from the shelf. Some of these processes enhance plume transport beyond my estimates and act rapidly, while others potentially occur after the nutrients have undergone transformations on the shelf. My methods also distinguish river plume export from the total nutrient transport that occurs on the shelf. For example, most shelf systems act as a net sinks for oceanic nitrogen (*Fennel et al.* 2006; *Seitzinger and Giblin* 1996), with greater nitrogen removal through denitrification than is delivered by rivers. This extra removal is the result of onshore transport of nitrogen from the open ocean, entirely distinct from river plume processes.

I assessed a range of nutrient uptake scenarios in order to examine the sensitivity of the results to the choice of removal rate. First, I assumed nutrients behave conservatively, and applied the freshwater export efficiency to the riverine nutrient loads; this provides an upper limit on nutrient export estimates (Equation 3.6). This estimate ignores all processes that remove riverine nutrients from the water. Then I derived estimates assuming non-conservative behaviour of nutrients for a range of removal rates (Equation 3.7). Using a range of removal rates provides an indication of the sensitivity of the estimated export to the choice of uptake rate. The resulting export estimates are dependent on both the freshwater export efficiency, and the removal rate.

The role of the export timescale as it relates to nutrient removal can be quantified by the Damköhler number (*Oldham et al.* 2013): a dimensionless ratio that acts as an indicator of processing by relating an "exposure timescale" (τ_E: analogous to the export timescale, T_E), to a "processing timescale" (τ_P: here, the inverse of the removal rate, r):

$$N_E = \frac{\tau_E}{\tau_P} = rT_E. \tag{4.1}$$

The Damköhler number expressed in this form is the same as the term that appears in the denominator of Equation 3.7 (rT_E). For large N_E, processing and subsequent removal of nutrients is high, with the nutrient being removed much more rapidly than it is exported.

A global analysis with a mean removal rate, while not accounting for regional variation in removal processes, allows for simple analysis of the shelf regions. *Rabouille et al.* (2001) and *Laruelle et al.* (2009) make use of global mass balance models to assess global shelf

budgets, while *Sharples et al.* (in revision) more recently used similar globally averaged assumptions to estimate export. Here, my use of a single parameter for all global regions provides comparable analysis, along with the ability to test the sensitivity of the model to different processing rates. At the same time, however, the framework presented here also allows for the estimation of individual river export that accounts for different rates in shelf processing through presenting an analysis of sensitivity of global export to a range of values for r. I also take into account latitudinal variation of export efficiency, which is not possible in global mass balance models such as those constructed by *Rabouille et al.* (2001) and *Laruelle et al.* (2009). As such, my estimates not only provide insight on the global shelf budgets, but can also account for potential regional differences in removal rates when applied in model parameterizations through analysis of individual rivers.

4.2.2 Budgets of Fresh Water and Nutrients

I calculated freshwater and nutrient budgets for individual rivers (Figures 3.19 and 3.25), specific regions (Figure 3.22), and globally (Figures 3.21, 3.23, and 3.27). A summary of some of these budgets is presented in Table 3.2, with comparisons to previously reported estimates. Each of these budgets highlights the variability between river systems, while at the same time, also highlighting the complexity and difficulties of assessing budgets of the shelf environment.

I calculated the fresh water and nutrient budgets for the Amazon, Columbia, and Mississippi rivers. These three rivers are among the largest 20 rivers by annual discharge (1st Amazon, 6th Mississippi, and 20th Columbia), and span a range of latitudes and shelf widths with 1.25° S and 304 km, 29.75° N and 52 km, and 46.25° N and 47 km, respectively (Table 2.2). The resulting fresh water budgets (Figure 3.19) are as expected. The Amazon has a wide shelf, but is still an efficient cross-shelf exporter of fresh water with up to 73% cross-shelf export efficiency, and negligible downstream transport in the coastal current; this is due to its high discharge and close proximity to the Equator leading to minimal deflection by the Coriolis force. The Mississippi and Columbia rivers show much greater downstream advection and thus much higher retention on the shelf, as one would expect for higher latitude plumes. When assessing the non-conservative export of nutrients for these rivers (Figure 3.25), the Mississippi and Columbia rivers have longer export timescales than the Amazon (2.5 and 5.7 days, compared to less than 1 day, respectively), resulting in very high near source retention. Even under high nutrient processing with a rate of

$r = 0.75$ d^{-1}, a significant portion of the Amazon's nutrients are exported to the open ocean.

DeMaster and Aller (2001) reported nutrient budgets for the Amazon River, which are similar to my estimates for DIN, DIP, and DSi export to the open ocean (Table 3.2). They estimate 50% N, 100% P, and 92% Si delivered to the shelf (including both riverine inputs and advective fluxes) are exported to the open ocean. My estimate of 11–73% riverine nutrient export spans very rapid processing ($r = 0.75$ d^{-1}) to conservative export ($r = 0$ d^{-1}), indicating that phosphorous and silicate behave almost conservatively on the Amazon shelf (which I underestimate), while nitrogen is subject to moderate rates of processing.

Zhang et al. (2012) conducted a detailed numerical study of the Mississippi and Atchafalaya River outflows onto the Texas-Louisiana shelf. Using two numerical dyes, they tracked the fresh water discharge from the two rivers, and estimate the cross-shelf export beyond the 100 m isobath to be approximately 57% and 36% of the riverine discharges, respectively. My estimates of cross-shelf export agree extremely well for the two rivers, with my relationships leading to estimates up to 61% and 42%, respectively.

Lehrter et al. (2013) also conducted a detailed study of the Texas-Louisiana shelf near the outflow of the Mississippi River using both observations of freshwater and nutrient concentrations and 3D simulations from a realistic physical model. In their budgets, they account for freshwater and nutrient inputs from the Mississippi River, advective exchange fluxes between the open Gulf of Mexico and the shelf, and alongshore transport into the region. They estimate the annual alongshore freshwater transport within the 50 m isobath to be 47% of the riverine input in the region, which, along with estimates of 43% by *Etter et al.* (2004) and 53% by *Dinnel and Wiseman* (1986), is slightly larger than my estimate of 25–39%, but not alarmingly so. They also calculate cross-shelf transport beyond the 50 m isobath of both fresh water and nutrients to be net onshore, indicating a return flow of pre-existing offshore water to the shelf that is equivalent to 33% of the riverine fresh water and 50-60% of the nutrient inputs. In contrast, I estimate a cross-shelf export at this location of 19–69% of the riverine fresh water, and 7–69% of the nutrients. The discrepancy between the estimates is the direct consequence of my estimates only assessing riverine export, while the estimates of *Lehrter et al.* (2013) consider other processes not captured within my parameterization.

A similar problem exists when comparing to regional shelf-wide budgets. Expanding to the entire Gulf of Mexico, I estimate up to 64% of riverine DIN is exported beyond the 50 m isobath, and up to 42% export alongshore. Again, this is in contrast to a previous budget of the region. *Xue et al.* (2013) calculated 7.9% cross-shelf export of DIN, and a net negative alongshore transport of DIN with their regional model. *Fennel et al.* (2006) estimate a similar regional nitrogen budget for the Mid Atlantic Bight using a realistic 3D coupled hydrodynamic and biogeochemical model. They also estimate a net onshore transport of DIN, whereas I predict a 0–8% export of the riverine load. *Whitney* (2010) has further shown that the fresh water in the MAB region is controlled not only by local rivers, but also far-field fresh water inputs (such as from the St Lawrence River). My simple parameterization is unable to capture such influences due to only considering local sources. As with *Lehrter et al.* (2013), the regional budgets of *Xue et al.* (2013) and *Fennel et al.* (2006) consider not only riverine sources of DIN, but also offshore sources. With this, the riverine export is obscured by the more dominant processes, which are not considered in my model.

Globally, the highest export efficiency occurs within a narrow band extending approximately 15° on either side of the Equator where the low latitude dictates large Rossby radii. High export rates also occur at active margins where the shelf width is narrow (high S_P regions). This is consistent with *Sharples et al.* (in revision) who predict most cross-shelf export occurs within 20° of the Equator and along narrow shelves. Interestingly, the two largest rivers, the Amazon and the Congo, which account for approximately 20% of the world's freshwater discharge, are very close to the Equator where export efficiency is high; however, the majority of global rivers fall outside of the efficient regions of export and have much weaker discharges, such that much of the riverine material is retained on the shelf (Figure 2.7).

Due to S_P generally decreasing with increasing latitude (resulting from a smaller Rossby radius and often wider continental shelf), cross-shelf export efficiency decreases overall, while alongshore export increases (Figure 3.21). There is also a slight difference between the two hemispheres, with the northern hemisphere generally estimated to have higher cross-shelf export efficiency than the southern hemisphere for equivalent latitudes. Overall discharge levels are also higher in the northern hemisphere as well (Figure 2.7).

Correspondingly, where a greater fraction of the plume's fresh water reaches the shelf

break (higher export efficiency of fresh water) the export timescales are also shorter (Figure 3.18). As such, rivers that transport more material to the open ocean also do so faster, meaning less non-conservative nutrient removal can occur before the plume reaches the shelf break. Conversely, rivers that have high onshelf retention of river water also have long export timescales, meaning that by the time river plumes reach the shelf break, they have already been significantly depleted of nutrients by on shelf biochemical processing.

Globally, estimated plume export timescales mostly fall between a few days to a few months. As a result, the Damköhler number (Equation 4.1) for rivers around the world changes from less than one to greater than one (export to no export) within the range of equivalent processing times of a few to approximately 100 days. As the processing timescale decreases, more and more rivers have a Damköhler number greater than 1, and all nutrients are removed before export. Only the plumes with rapid export (as seen near the equator, or along narrow shelves) export nutrients to the deep ocean in large amounts at higher processing rates.

The resulting global export estimates are most sensitive within the range of processing timescales of one to one hundred days (between r values of 0.01 d^{-1} to 1 d^{-1}), days—the same as the range of global export timescales. Within this range, global nutrient export changes by a factor of approximately 10. However, the overall estimates are not very sensitive to this choice, with, for example, values of $r = 1$ d^{-1} and $r = 0.1$ d^{-1} (an order of magnitude difference) only resulting in a factor of two change in overall nutrient export. Above one hundred days, or below processing timescales on the order of one day, the estimated nutrient export levels are approximately constant. For rapid processing ($r > 1$ d^{-1}), I estimate very little nutrient export. At very low processing rates ($r < 0.01$ d^{-1}), on the other hand, nutrient export expectedly approaches the conservative levels.

Most of the global riverine nutrient supply is delivered to the ocean through rivers in the northern hemisphere (DIN in the highest proportion at 80% of the total load); however, even when simply assuming conservative behaviour, the estimated export of nutrients to the deep ocean is significantly reduced due to the influence of latitude. Assuming non-conservative removal rates, the export of nutrients is confined almost exclusively to the lower latitudes where export is more direct, and export timescales are shorter (Figure 3.27).

The estimates of global nutrient export efficiencies are greatest for dissolved silica (DSi;

7.0% for high processing, and up to 56.4% assuming conservative export), due to the highest riverine loads occurring in the low latitudes where export timescales are short and freshwater export is the most efficient (Figure 3.27b). Estimated export of DIN to the deep ocean, on the other hand, is not efficient (2.8–44.3%). Given that high DIN loads can result from agricultural runoff (e.g., *Seitzinger et al.* 2010), its delivery to the ocean is correlated with regions of high agricultural activity, such as South East Asia and North America, with maximum riverine delivery to the coastal ocean in the 20° latitude band (Figure 3.27a). These regions, however, are outside of the zone of efficient plume export, with correspondingly greater time before export, and therefore higher amounts of nutrient removal. Appendix B lists all nutrient export estimates in 10° latitude bands.

The global patterns of shelf retention and export timescales correspond to global patterns of hypoxia and eutrophication. In particular along the coast of northwestern Europe and the eastern United States, where the shelf is wide, the majority of river water is retained on the shelf (87%; Figure 3.22), with long export timescales (on the order of several months to years; Figure 3.18). As a result, riverborne nutrients, which are delivered in high amounts to these areas, accumulate on the shelves, driving eutrophication and hypoxia. This high shelf retention corresponds directly with global patterns of hypoxia (e.g., Diaz and Rosenberg, 2008), with the east coast of North America and the shelves of northwestern Europe having much higher occurrences of hypoxia than anywhere else in the world.

Previous global shelf budgets exist for DIN and DIP (*Sharples et al.* in revision), DON and DOC (*Rabouille et al.* 2001), and DSi (*Laruelle et al.* 2009). *Sharples et al.* (in revision), estimated 75% of riverine DIN, and 80% of riverine DIP is exported to the deep ocean from the shelves; I estimate that just 2.8–44.3% DIN and 3.5–45.9% DIP is exported to the deep ocean globally. Overall, we both estimate similar global patterns of export timescales, with efficient export near the equator, and low export efficiency at the high latitudes; however, the way we use export timescales estimates to assess nutrient removal is different. I estimate nutrient removal by first assessing the amount of river water that reaches the shelf break (the export efficiency of fresh water), and then calculate the fraction of nutrients removed based on the assumed rate of uptake and the export timescale (Equation 3.7). Nutrient export is thus not only controlled by removal processes, but also by plume circulation. For example, 20% of the riverine nutrient load might be removed

before export occurs, but at the same time, only 50% of plume water may be reaching the open ocean, such that nutrient export is not 80%, but rather 40%). *Sharples et al.* (in revision), on the other hand, inherently assume that all of the plume water crosses the shelf break when $S_P > 1$ ($E_X^{FW} = 1$), and then estimate nutrient removal using empirical relationships, such as the relationship for DIN removal in *Seitzinger et al.* (2006):

$$\%\text{DIN}_{rem} = 23.4 T_E^{0.204}, \tag{4.2}$$

and DIP export as per the relationship in Nixon et al. (1996):

$$\%\text{DIP}_{exp} = -31.83 \ln T_E + 80.8, \tag{4.3}$$

with the export timescale (T_E) in months. Overall, these equations predict low removal, particularly for DIN, with less than 60% DIN removed for export timescales as long as one year (Figure 4.1). Comparatively, my nutrient removal estimates can be higher (depending on the value of r), with removal rates as low as 0.01 d^{-1} exceeding the nutrient removal for rivers with export timescales longer than one month. Even assuming conservative export, however, my estiates of nutrient export are still much lower than the estimates of *Sharples et al.* (in revision) due to the constraints of the S_P number on the overall fraction of river water that makes it to the shelf break.

The global mass balance models by *Rabouille et al.* (2001) (DON and DOC) and *Laruelle et al.* (2009) (DSi) also predict much lower riverine export of nutrients than *Sharples et al.* (in revision), with my estimates agreeing reasonably well with theirs (Table 3.2). Globally, *Rabouille et al.* (2001) estimate 7% riverine DON and 15% riverine DOC are exported to the deep ocean. Similarly, I estimate a range of 5.6–51.8% and 5.7–52.2% export of the two nutrients, respectively, indicating predominantly non-conservative export. My estimate of 7.0–56.4% riverine DSi export also agrees with that of *Laruelle et al.* (2009) who estimate a global deep ocean export of 9%, suggesting global removal of DSi on shelves is high. It should be noted that both models of *Rabouille et al.* (2001) and *Laruelle et al.* (2009) only assess globally averaged values. My framework provides similar estimates, while at the same time also a means of estimating spatial patterns of export.

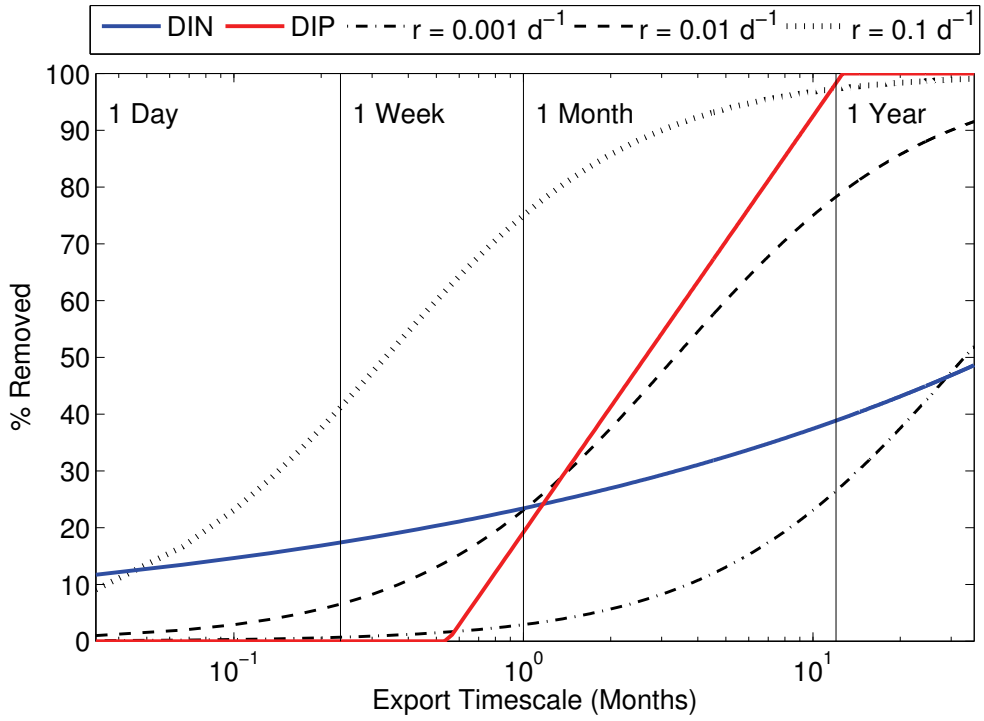

Figure 4.1: Percent removal of DIN and DIP as a function of the export timescale according to the empirical relationships from *Seitzinger et al.* (2006) and *Nixon et al.* (1996) (DIN removal following Equation 4.2 and DIP removal as 100%-Equation 4.3)

Each of these comparisons, from individual rivers to the global continental shelf, highlight the usefulness of the simple methodology for estimating riverine export to the open ocean, while illustrating the challenges of the simplified approach. My method addresses solely the riverine component of shelf nutrient budgets; it does not include other shelf processes that are external to river plume dynamics, such as onwelling of deep ocean nutrients. My estimates of cross-shelf export of riverine materials are in general agreement with the previous literature (e.g., studies by *DeMaster and Aller* 2001; *Zhang et al.* 2012; *Laruelle et al.* 2009; *Rabouille et al.* 2001) except for the global nutrient export calculated by *Sharples et al.* (in revision). The methodology is useful in providing a simple estimate of the riverine component of shelf nutrient budgets, which include many other competing and overlapping processes (Figure 1.2).

CHAPTER 5
CONCLUSIONS

I conducted a series of idealized model experiments to assess the impact of different factors on the export of terrestrially derived materials to the open ocean. Latitude appears to be the dominant controlling factor in determining the efficiency with which cross-shelf export occurs: the greater the latitude, the stronger the Coriolis force, and the greater the deflection of the plume. As a result of this deflection, the plume remains near the coast and cross-shelf export is supressed. External forcing from winds can enhance cross-shelf transport at high latitudes, but it cannot completely overcome the influence of the Coriolis force.

The idealized experiments showed that simple, latitude-dependent metrics can be used to estimate plume transport across different forcing scenarios. In particular, the cross-shelf export of riverine material is related to the S_P number of a plume through a simple asymptotic relationship, allowing for easy estimation of export for real plumes.

Using my relationships between S_P and the cross-shelf export efficiency, I estimated riverine export for global rivers. Due to the influence of the Coriolis force, export is most efficient near the equator where riverine material is most directly transported across the shelf. At higher latitudes, indirect transport and long export timescales mean very little riverine material is exported directly to the open ocean. Overall, I estimate just 15–53% of the total riverine fresh water is transported to the open ocean in river plumes, with much lower export for nutrients due to biochemical processing that occurs on the shelves.

The primary advantage of the method outlined in this thesis is its simplicity and generality. By using an idealized model, various factors were explored in isolation, allowing for a general description about a wide range of distinct regions.

The derived relationships between S_P and export can be used to estimate riverine export for any river, and can easily be used within global ocean and Earth system models. Cross-shelf export can be estimated either individually on a river-by-river basis (using the regressions obtained relating export efficiency to S_P), or by applying the global export

estimates obtained herein. The integration of such estimates into global models should be straightforward.

This work represents one of the first studies to explore the possibility of a general relationship to describe the cross-shelf export of materials in river plumes, following *Sharples et al.* (in revision). As work continues in this area, the relationships will undoubtedly be improved and investigated further. As a starting point, it would be beneficial to explore the use of the S_P number in more complex scenarios, including in specific regional models of river systems. This would enable further understanding of where the relationship is valid, and under what conditions it breaks down beyond the idealized test cases presented here. Such conditions could be regions of complex bathymetry, areas of complex shelf dynamics and with variable forcing. With increased assessment and refinement, the predictive power of the idealized S_P number and the relationships outlined here may be greatly enhanced, while also allowing for improved understanding of the limitations of such simple assumptions (e.g., simple domain geometry and idealized wind fields), and their influence on the results.

BIBLIOGRAPHY

Amante, C., and B. W. Eakins, ETOPO1 1 arc-minute global relief model: Procedures, data sources and analysis. NOAA Technical Memorandum NESDIS NGDC-24, 2009.

Anav, A., P. Friedlingstein, M. Kidston, L. Bopp, P. Ciais, P. Cox, C. Jones, M. Jung, R. Myneni, and Z. Zhu, Evaluating the land and ocean components of the global carbon cycle in the CMIP5 earth system models, *J Climate*, *26*, 6801–6843, 2013.

Arora, V. K., J. F. Scinocca, G. J. Boer, J. R. Christian, K. L. Denman, G. M. Flato, V. V. Kharin, W. G. Lee, and W. J. Merryfield, Carbon emission limits required to satisfy future representative concentration pathways of greenhouse gasses, *Geophys Res Lett*, *38*, L05805, 2011.

Beardsley, R. C., R. Limeburner, H. Yu, and G. A. Cannon, Discharge of the Changjiang (Yangtze River) into the East China Sea, *Cont Shelf Res*, *4*, 57–76, 1985.

Bentsen, M., I. Bethke, J. B. Debernard, T. Iversen, A. Kirkevåg, Ø. Seland, H. Drange, C. Roeland, I. A. Seirstad, C. Hoose, and J. E. Kristjánsson, The Norwegian Earth System Model, NorESM1-M - part 1: Description and basic evaluation of the physical climate, *Geosci Model Dev*, *6*, 687–720, 2013.

Berdeal, I. G., B. M. Hickey, and M. Kawse, Influence of wind stress and ambient flow on a high discharge river plume, *J Geophys Res*, *107*, 13–1, 2002.

Bianchi, T. S., S. F. DiMarco, J. H. Cowan Jr., R. D. Hetland, P. Chapman, J. W. Day, and M. A. Allison, The science of hypoxia in the Northern Gulf of Mexico: A review, *Sci Total Environ*, *408*, 1471–1484, 2010.

Bopp, L., L. Resplandy, J. C. Orr, S. C. Doney, J. P. Dunne, M. Gehlen, P. Halloran, C. Heinze, T. Ilyina, R. Séférian, J. Tjiputra, and M. Vichi, Multiple stressors of ocean ecosystems in the 21st century: projections with CMIP5 models, *Biogeosciences*, *10*, 6225–6245, 2013.

Chant, R. J., S. M. Glenn, E. Hunter, J. Kohut, R. F. Chen, R. W. Houghton, J. Bosch, and O. Schofield, Bulge formation of a buoyant river outflow, *J Geophys Res*, *113*, 1–16, 2007.

Chao, S.-Y., River-forced estuarine plumes, *J Phys Ocean*, *18*, 72–88, 1988.

Chen, C.-T., K.-K. Liu, and R. Macdonald, Continental margin exchanges, in *Ocean Biogeochemistry*, edited by M. J. R. Fasham, pp. 53–97, Springer-Verlag, 2003.

Chen, S.-N., Enhancement of alongshore freshwater transport in surface-advected river plumes by tides, *J Phys Ocean*, *44*, 2951–2971, 2014.

Christensen, J. P., Denitrification in continental shelf sediments has major impact on the oceanic nitrogen budget, *Glob Biogeochem Cycle*, *1*, 97–116, 1987.

Csanady, G. T., Baroclinic boundary currents and long edge-waves in basins with sloping shores, *J Phys Ocean*, *1*, 92–104, 1971.

DeMaster, D. J., and R. C. Aller, Biogeochemical processes on the Amazon Shelf: Changes in dissolved and particulate fluxes during river/ocean mixing, in *The Biogeochemistry of the Amazon Basin*, edited by M. E. McClain, R. L. Victoria, and J. E. Richey, pp. 328–357, Oxford University Press, 2001.

Diaz, R. J., and R. Rosenberg, Spreading dead zones and consequences for marine ecosystems, *Science*, *321*, 926–929, 2008.

Dinnel, S. P., and W. J. Wiseman, Fresh water on the Louisiana and Texas shelf, *Cont Shelf Res*, *6*, 765–784, 1986.

Doney, S. C., The growing human footprint on coastal and open-ocean biogeochemistry, *Science*, *328*, 1512–1516, 2010.

Dufresne, J.-L., M.-A. Foujols, S. Denvil, A. Caubel, O. Marti, O. Aumont, Y. Balkanski, S. Bekki, H. Bellenger, R. Benshila, S. Bony, L. Bopp, P. Braconnot, P. Brockmann, P. Cadule, F. Cheruy, F. Codron, A. Cozic, D. Cugnet, N. de Noblet, J.-P. Duvel, C. Ethé, L. Fairhead, T. Fichefet, S. Flavoni, P. Friedlingstein, J.-Y. Grandpeix, L. Guez, E. Guilyardi, D. Hauglustaine, F. Hourdin, A. Idelkadi, J. Ghattas, S. Joussaume, M. Kageyma, G. Krinner, S. Labetoulle, A. Lahellec, M.-P. Lefebvre, F. Lefevre, C. Levy, Z. XLi, J. Lloyd, F. Lott, G. Madec, M. Mancip, M. Marchand, S. Masson, Y. Meurdesoif, J. Mignot, I. Musat, S. Parouty, J. Polcher, C. Rio, M. Schulz, D. Swingedouw, S. Szopa, C. Talandier, P. Terray, N. Viovy, and N. Vuichard, Climate change projections using the IPSL-CM5 earth system model: from CMIP3 to CMIP5, *Clim Dynam*, *40*, 2123–2165, 2013.

Dunne, J. P., J. L. Sarmiento, and A. Gnanadesikan, A synthesis of global particle export from the surface ocean and cycling through the ocean interior and on the seafloor, *Glob Biogeochem Cycle*, *21*, GB4006, 2007.

Dunne, J. P., J. G. John, A. J. Adcroft, S. M. Griffies, R. W. Hallberg, E. Shevliakova, R. J. Stouffer, W. Cooke, K. A. Dunne, M. J. Harrison, J. P. Krasting, S. L. Malyshev, P. C. D. Milly, P. J. Phillips, L. T. Sentman, B. L. Samuels, M. J. Spelman, M. W. Winton, A. T. Wittenberg, and N. Zadeh, GFDL's ESM2 global coupled climate-carbon earth system models. Part I: Physical formulation and baseline simulation characteristics, *J Climate*, *25*, 6646–6665, 2012.

Dunne, J. P., J. G. John, E. Shevliakova, R. J. Stouffer, J. P. Krasting, S. L. Malyshev, P. C. D. Milly, L. T. Sentman, A. J. Adcroft, W. Cooke, K. A. Dunne, S. M. Griffies, R. W. Hallberg, M. J. Harrison, H. Levy, A. T. Wittenberg, P. J. Phillips, and N. Zadeh, GFDL's ESM2 global coupled climate-carbon earth system models. Part II: Carbon

system formulation and baseline simulation characteristics, *J Climate*, *26*, 2247–2267, 2013.

Etter, P. C., M. K. Howard, and J. D. Cochrane, Heat and freshwater budgets for the Texas-Louisiana shelf, *J Geophys Res*, *109*, C02024, 2004.

Fennel, K., J. Wilkin, J. Levin, J. Moisan, and J. O'Reilly, Nitrogen cycling in the Middle Atlantic Bight: results from a three-dimensional model and implications for the North Atlantic nitrogen budget, *Glob Biogeochem Cycle*, *20*, 1–14, 2006.

Fong, D. A., and W. R. Geyer, Response of a river plume during an upwelling favorable wind event, *J Geophys Res*, *106*, 1067–1084, 2001.

Fong, D. A., and W. R. Geyer, The alongshore transport of freshwater in a surface-trapped river plume, *J Phys Ocean*, *32*, 957–972, 2002.

Galloway, J. N., F. J. Dentener, D. G. Capone, E. W. Boyer, R. W. Howarth, S. P. Seitzinger, G. P. Asner, C. C. Cleveland, P. A. Green, E. A. Holland, D. M. Karl, A. F. Michaels, J. H. Porter, A. R. Townsend, and C. J. Vörösmarty, Nitrogen cycles: past, present, and future, *Biogeochemisty*, *70*, 153–226, 2004.

Garvine, R. W., The impact of model configuration in studies of buoyant coastal discharge, *J Mar Res*, *59*, 193–225, 2001.

Garvine, R. W., and M. M. Whitney, An estuarine box model of freshwater delivery to the coastal ocean for use in climate models, *J Mar Res*, *64*, 173–194, 2006.

Gent, P. R., G. Danabasoglu, L. J. Donner, M. M. Holland, E. C. Hunke, S. R. Jayne, D. M. Lawrence, R. B. Neale, P. J. Rasch, M. Verternstein, P. H. Worley, Z.-L. Yang, and M. Zhang, The Community Climate System Model version 4, *J Climate*, *24*, 4973–4991, 2011.

Giorgetta, M. A., J. Jungclaus, C. H. Reick, S. Legutke, J. Bader, M. Böttinger, V. Brovkin, T. Crueger, M. Esch, K. Fieg, K. Glushak, V. Gayler, H. Haak, H.-D. Hollweg, T. Ilyina, S. Kinne, L. Kornblueh, D. Matei, T. Mauritsen, U. Mikolajewicz, W. Mueller, D. Notz, F. Pithan, T. Raddatz, S. Rast, R. Redler, E. Roeckner, H. Scmidt, R. Schnur, J. Segschneider, K. D. Six, M. Stockhause, C. Timmreck, J. Wegner, H. Widmann, K.-H. Wieners, M. Claussen, J. Marotzke, and B. Stevens, Climate and carbon cycle changes from 1850 to 2100 in MPI-ESM simulations for the Coupled Model Intercomparison Project phase 5, *J Adv Model Earth Syst*, *5*, 572–597, 2013.

Gruber, G., and J. N. Galloway, An Earth-system perspective of the global nitrogen cycle., *Nature*, *451*, 293–296, 2008.

Haidvogel, D., H. Arrango, W. Budgell, B. Cornuelle, E. Curchitser, E. Di Lorenzo, K. Fennel, W. R. Geyer, A. J. Hermann, L. Lanerolle, J. Levin, J. C. McWilliams, A. J. Miller, A. M. Moore, T. M. Powell, A. F. Schepetkin, C. R. Sherwood, R. P. Signell, J. C. Warner, and J. Wilkin, Ocean forecasting in terrain-following coordinates: formulation

and skill assessment of the Regional Ocean Modelling System, *J Comput Phys*, *227*, 3595–3624, 2008.

Hetland, R. D., Relating river plume structure to vertical mixing, *J Phys Ocean*, *35*, 1667–1687, 2005.

Hill, A. E., Buoyancy effects in coastal and shelf seas, in *The Sea*, edited by K. H. Brink and A. R. Robinson, vol. 10, pp. 21–62, John Wiley & Sons, 1998.

Horner-Devine, A., The bulge circulation in the Columbia River plume, *Cont Shelf Res*, *29*, 234–251, 2007.

Horner-Devine, A., R. D. Hetland, and D. G. MacDonald, Mixing and transport in coastal river plumes, *Annu Rev Fluid Mech*, *47*, 569–594, 2015.

Ilyina, T., K. D. Six, J. Segschneider, E. Maier-Reimer, H. Li, and I. Núñez-Riboni, Global ocean biogeochemistry model HAMOCC: Model architecture and performance as component of the MPI-Earth system model in different CMIP5 experimental realizations, *J Adv Model Earth Syst*, *5*, 287–315, 2013.

Isobe, A., Ballooning of river-plume bulge and its stabilization by tidal currents, *J Phys Ocean*, *35*, 2337–2351, 2005.

Jurisa, J. T., and R. J. Chant, Impact of offshore winds on a buoyant river plume system, *J Phys Ocean*, *43*, 2571–2587, 2013.

Kara, A. B., A. J. Wallcraft, E. J. Metzger, H. E. Hurlburt, and C. W. Fairall, Wind stress drag coefficient over the global ocean, *J Climate*, *20*, 5856–5864, 2007.

Kourafalou, V. H., L.-Y. Oey, J. D. Wang, and T. N. Lee, The fate of river discharge on the continental shelf 1. Modeling the river plume and the inner shelf coastal current, *J Geophys Res*, *101*, 3415–3434, 1996.

Laruelle, G. G., V. Robeix, A. Sferratore, B. Brodherr, D. Ciuffa, D. J. Conley, H. H. Dürr, J. Garnier, C. Lancelot, Q. Le Thi Phuong, J.-D. Meunier, M. Meybeck, P. Michalopoulos, B. Moriceau, S. Ni Longphuirt, S. Loucaides, L. Papush, M. Presti, O. Ragueneau, P. Regnier, L. Saccone, C. P. Slomp, C. Spiteri, and P. Van Cappellen, Anthropogenic perturbations of the silicon cycle at the global scale: Key role of the land-ocean transition, *Glob Biogeochem Cycle*, *23*, GB4031, 2009.

Lehrter, J. C., D. S. Ko, M. C. Murrell, J. D. Hagy, B. A. Schaeffer, R. M. Greene, R. W. Gould, and B. Penta, Nutrient distributions, transports, and budgets on the inner margin of a river-dominated continental shelf, *J Geophys Res*, *118*, 1–17, 2013.

Ludwig, W., J.-L. Probst, and S. Kempe, Predicting the oceanic input of organic carbon by continental erosion, *Glob Biogeochem Cycle*, *10*, 23–41, 1996.

Mayorga, E., S. P. Seitzinger, J. A. H. E. Dumont, A. H. W. Beusen, A. F. Bouwman, B. M. Fekete, C. Kroeze, and G. Van Drecht, Global nutrient export from WaterSheds 2 (NEWS 2): Model development and implementation, *Environ Model Softw*, *25*, 837–853, 2010.

McClimans, T., Estuarine fronts and river plumes, in *Physical Processes in Estuaries*, edited by J. Dronkers and W. van Leusen, pp. 55–69, Springer-Verlag, 1986.

McCreary, J. P., S. Zhang, and S. R. Shetye, Coastal circulations driven by river outflow in a variable-density 1 1/2-layer model, *J Geophys Res*, *102*, 15,535–15,554, 1997.

Moore, J. K., K. Lindsay, S. C. Doney, M. C. Long, and K. Misumi, Marine ecosystem dynamics and biogeochemical cycling in the Community Earth System Model [CESM1(BGC)]: Comparison of the 1990s with the 2090s under the RCP4.5 and RCP8.5 scenarios, *J Climate*, *26*, 9291–9312, 2013.

Münchow, A., and R. W. Garvine, Dynamical properties of a buoyancy-driven coastal current, *J Geophys Res*, *98*, 20,063–20,077, 1993.

Nixon, S. W., J. W. Ammerman, L. P. Atkinson, V. M. Bernounsky, G. Billen, W. C. Boicout, W. R. Boynton, T. M. Church, D. M. Ditoro, R. Elmgren, J. H. Garber, A. E. Giblin, R. A. Jahnke, N. J. P. Owens, M. E. Q. Pilson, and S. P. Seitzinger, The fate of nitrogen and phosphorus at the land-sea margin of the North Atlantic Ocean, *Biogeochemisty*, *35*, 141–180, 1996.

O'Donnell, J., The formation and fate of a river plume: A numerical model, *J Phys Ocean*, *20*, 551–569, 1990.

Oey, L.-Y., and G. L. Mellor, Subtidal variability of estuarine outflow, plume, and coastal current: A model study, *J Phys Ocean*, *23*, 164–171, 1992.

Oldham, C. E., D. E. Farrow, and S. Peiffer, A generalized Damköhler number for classifying material processing in hydrological systems, *Hydrol Earth Syst Sci*, *17*, 1133–1148, 2013.

Palmer, J. R., and I. J. Totterdell, Production and export in a global ocean ecosystem model, *Deep-Sea Res*, *48*, 1169–1198, 2001.

Rabalais, N. N., R. E. Turner, Q. Dortch, D. Justic, V. J. Bierman, Jr., and W. J. Wiseman, Jr., Nutrient-enhanced productivity in the northern Gulf of Mexico: past, present, and future, *Hydrobiologia*, pp. 39–63, 2002.

Rabouille, C., F. T. Mackenzie, and L. M. Ver, Influence of the human perturbation on carbon, nitrogen, and oxygen biogeochemical cycles in the global coastal ocean, *Geochim Cosmochim Acta*, *65*, 3615–3641, 2001.

Schiller, R. V., and V. H. Kourafalou, Modelling river plume dynamics with the HYbrid Coordinate Ocean Model, *Ocean Model*, *33*, 101–117, 2010.

Seitzinger, S., and A. E. Giblin, Estimating denitrification in North Atlantic continental shelf systems, *Biogeochemisty*, *35*, 235–260, 1996.

Seitzinger, S., J. A. Harrison, J. K. Böhlke, A. F. Bouwman, R. Lowrance, B. Peterson, C. Tobias, and G. Van Drecht, Denitrification across landscapes and waterscapes: A synthesis, *Ecol Appl*, *16*, 2064–2090, 2006.

Seitzinger, S. P., A. Harrison, E. Dumont, A. H. W. Beusen, and A. F. Bouwman, Sources and delivery of carbon, nitrogen, and phosphorus to the coastal zone: An overview of Global Nutrient Export from WaterSheds (NEWS) models and their application, *Glob Biogeochem Cycle*, *19*, GB4S01, 2005.

Seitzinger, S. P., E. Mayorga, A. F. Bouwman, C. Kroeze, A. H. W. Beusen, G. Billen, G. Van Drecht, E. Dumont, B. M. Fekete, J. Garnier, and J. A. Harrison, Global river nutrient export: a scenario analysis of past and future trends, *Glob Biogeochem Cycle*, *24*, 1–16, 2010.

Sharples, J., J. J. Middelburg, K. Fennel, and T. D. Jickells, Physical controls on riverine delivery of nutrients and carbon to the open ocean, *Unpublished Manuscript*, in revision.

Sheng, J., Dynamics of a buoyancy-driven coastal jet: the Gaspé Current, *J Phys Ocean*, *31*, 3146–3162, 2001.

Simpson, J. H., W. G. Bos, F. Schrimer, A. J. Souza, T. P. Rippeth, S. E. Jones, and D. Hydes, Periodic stratification in the Rhine ROFI in the North Sea, *Oceanol Acta*, *16*, 23–32, 1993.

Taylor, K. E., R. J. Stouffer, and G. A. Meehl, An overview of CMIP5 and the experiment design, *B Am Meteorol Soc*, 2012.

Thandrup, B., New pathways and processes in the global nitrogen cycle, *Annu Rev Ecol Evol Syst*, *43*, 407–428, 2012.

Tjiputra, J. F., C. Roeland, M. Bentsen, D. M. Lawrence, T. Lorentzen, J. Schwinger, Ø. Seland, and C. Heinze, Evaluation of the carbon cycle components in the Norwegian Earth System Model (NorESM), *Geosci Model Dev*, *6*, 301–325, 2013.

Vichi, M., S. Masina, and A. Navarra, A generalized model of pelagic biogeochemistry for the global ocean ecosystem. Part II: Numerical simulations, *J Marine Syst*, *64*, 110–134, 2006.

Vichi, M., E. Manzini, P. G. Fogli, A. Alessandri, L. Pantara, E. Scoccimarro, S. Masina, and A. Navarra, Global and regional ocean carbon uptake and climate chang: sensitivity to a substantial mitigation scenario, *Clim Dynam*, *37*, 1929–1947, 2011.

Volodin, E. M., N. A. Dianskii, and A. V. Gusev, Simulating present-day climate with the INMCM4.0 coupled model of the atmospheric and oceanic general circulations, *Izv Atmos Ocean Phy+*, *46*, 448–466, 2010.

Watanabe, S., T. Hajima, K. Sudo, T. Nagashima, T. Takemura, H. Okajima, T. Nozawa, H. Kawase, M. Abe, T. Yokohata, T. Ise, H. Sato, E. Kato, K. Takata, S. Emori, and M. Kawamiya, MIROC-ESM 2010: model description and basic results of CMIP5-20c3m experiments, *Geosci Model Dev*, *4*, 845–872, 2011.

Whitney, M. M., A study on river discharge and salinity variability in the Middle Atlantic Bight and Long Island Sound, *Cont Shelf Res*, *30*, 305–318, 2010.

Wiseman, W. J., N. N. Rabalais, R. E. Turner, S. P. Dinnel, and A. MacNaughton, Seasonal and interannual variability within the Louisiana coastal current: stratification and hypoxia, *J Marine Syst*, *12*, 237–248, 1997.

Wright, D. G., On the alongshelf evolution of an idealized density front, *J Phys Ocean*, *19*, 532–541, 1989.

Xue, Z., R. He, K. Fennel, W.-J. Cai, S. Lohrenz, and C. Hopkinson, Modeling ocean circulation and biogeochemical variability in the Gulf of Mexico, *Biogeosciences*, *10*, 7219–7234, 2013.

Yankovsky, A. E., and D. C. Chapman, A simple theory for the fate of buoyant coastal discharges, *J Phys Ocean*, *27*, 1386–1401, 1997.

Zhang, X., R. D. Hetland, M. Marta-Almeida, and S. F. DiMarco, A numerical investigation of the Mississippi and Atchafalaya freshwater transport, filling and flushing times on the Texas-Louisiana shelf, *J Geophys Res-Oceans*, *117*, C11009, 2012.

APPENDIX A

SUPPLEMENTARY FIGURES FOR CHAPTER 3

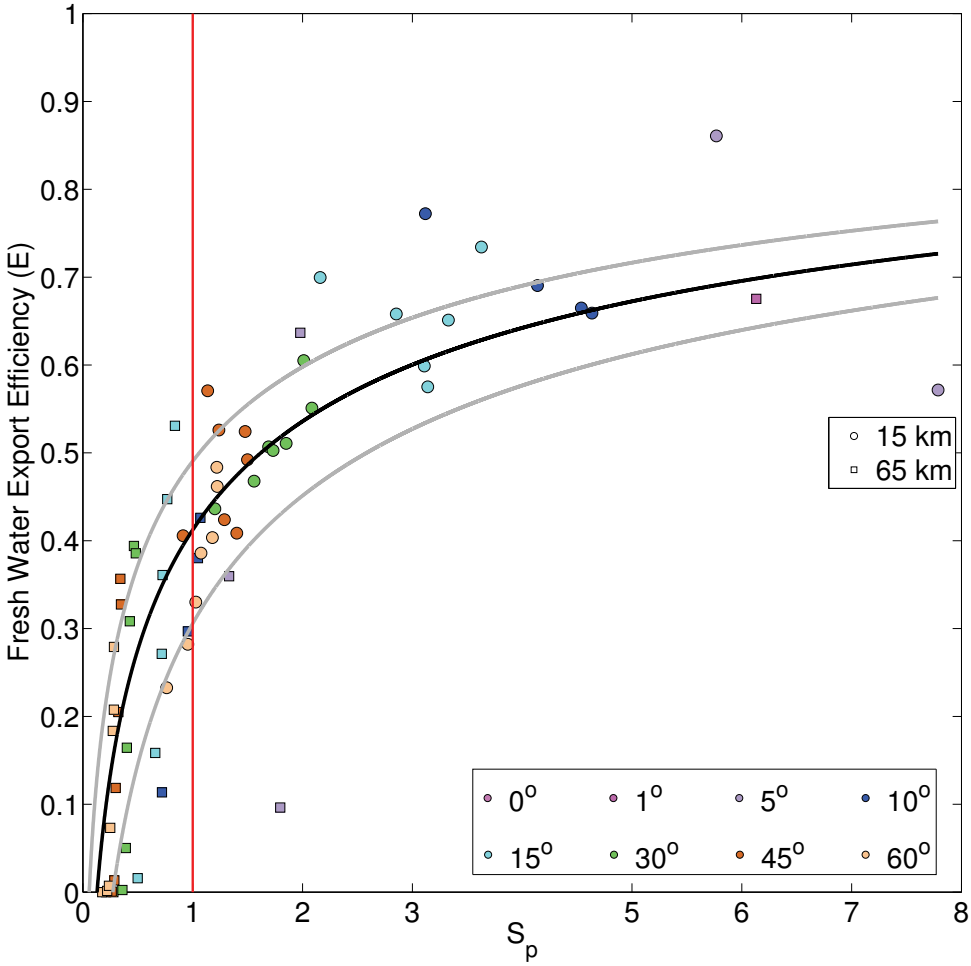

Figure A.1: Freshwater export efficiency beyond 15 km and 65 km for the tidally forced runs as a function of the S_P number. An asymptotic regression was applied following Equation 3.1 with $a = 1.4 \pm 0.4$ and $b = 0.4 \pm 0.1$. The fit is excellent, with an r^2 value of 0.91 and a p-value of 0.

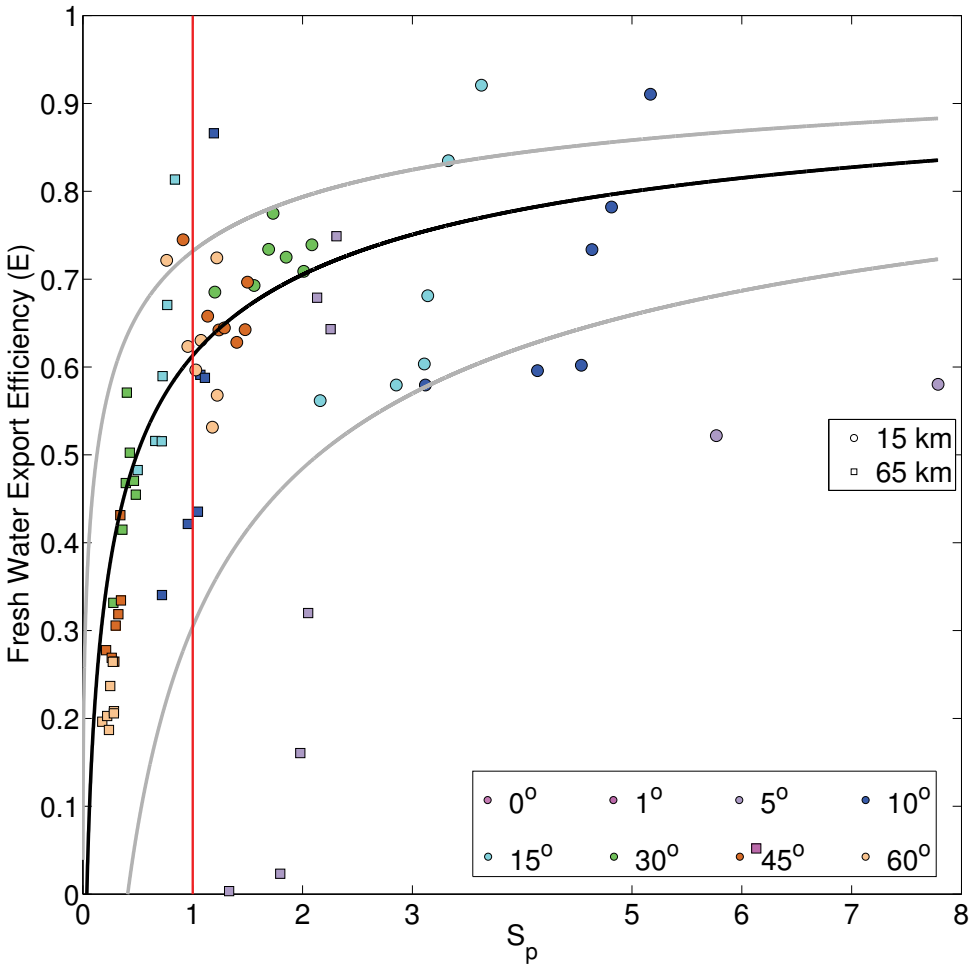

Figure A.2: Freshwater export efficiency beyond 15 km and 65 km for the alongshore wind runs as a function of the S_P number. An asymptotic regression was applied following Equation 3.1 with $a = 1.5 \pm 0.7$ and $b = 1.0 \pm 0.4$. The fit is excellent, with an r^2 value of 0.77 and a p-value of 0.

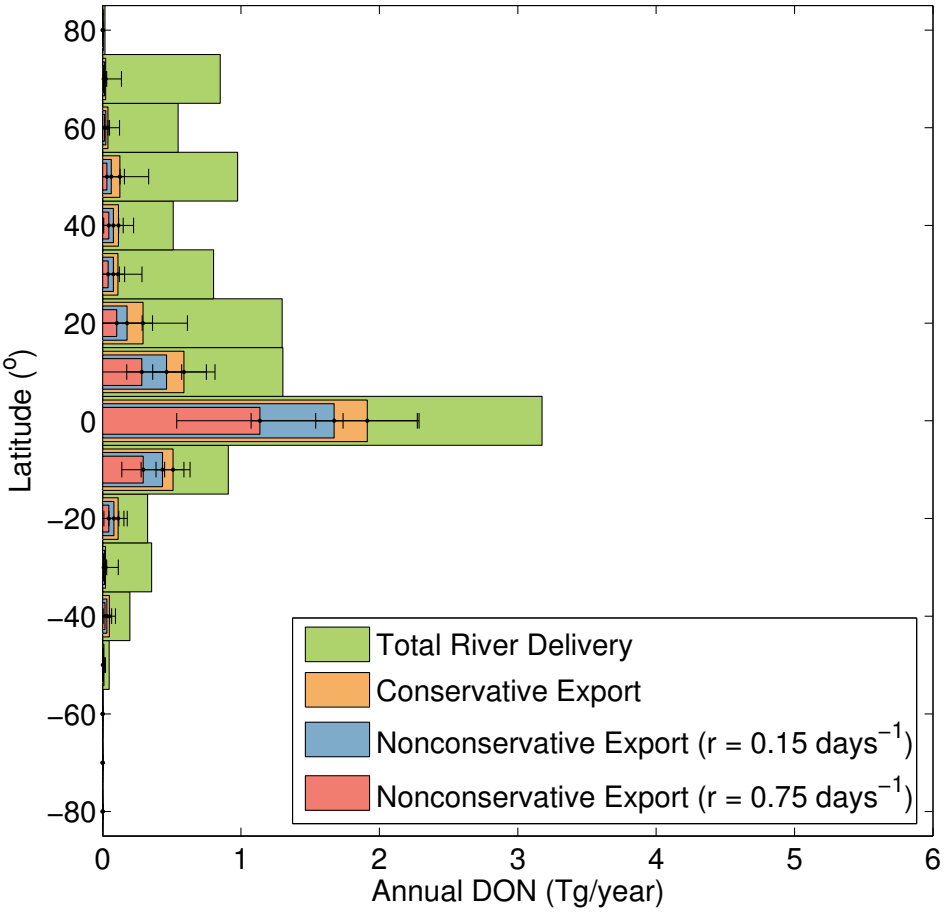

Figure A.3: DON delivery and export in 10° latitude bands.

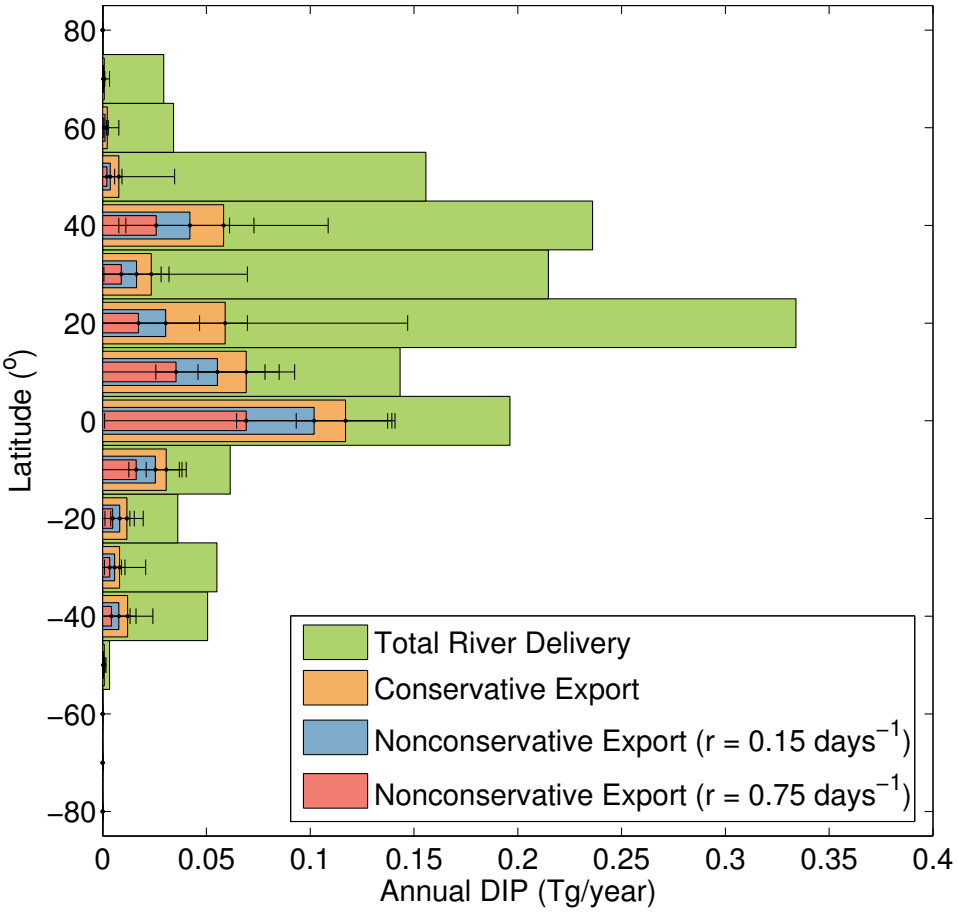

Figure A.4: DIP delivery and export in 10° latitude bands.

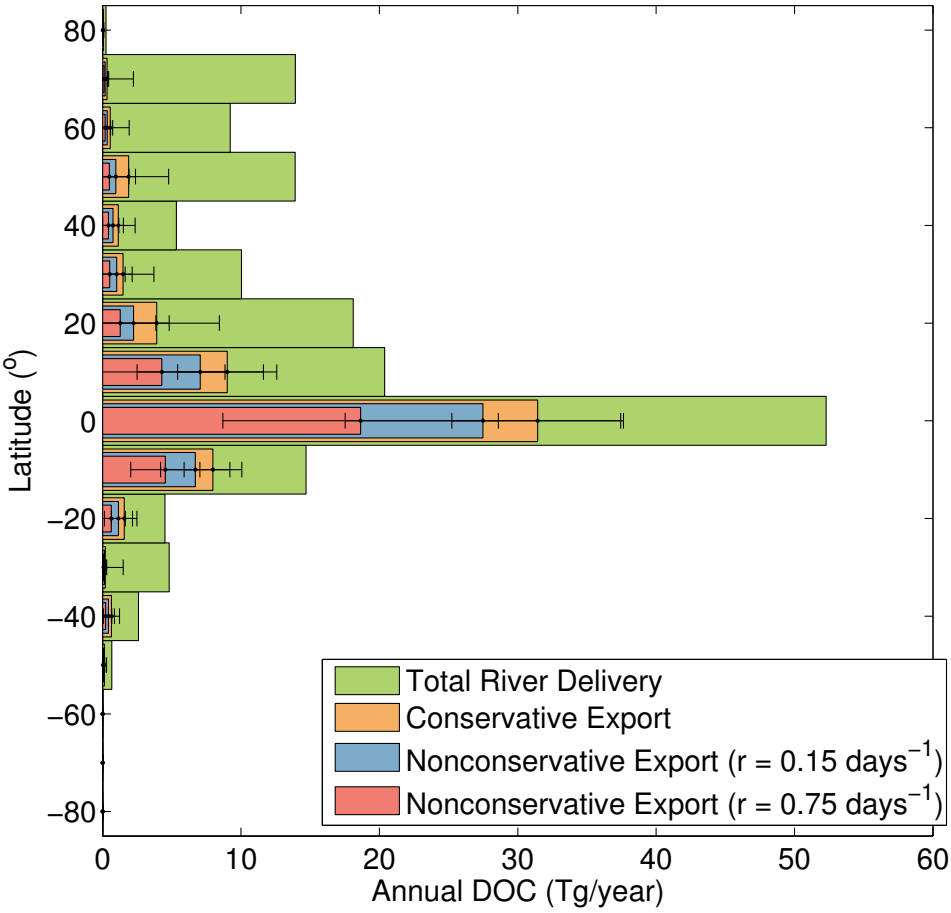

Figure A.5: DOP delivery and export in 10° latitude bands.

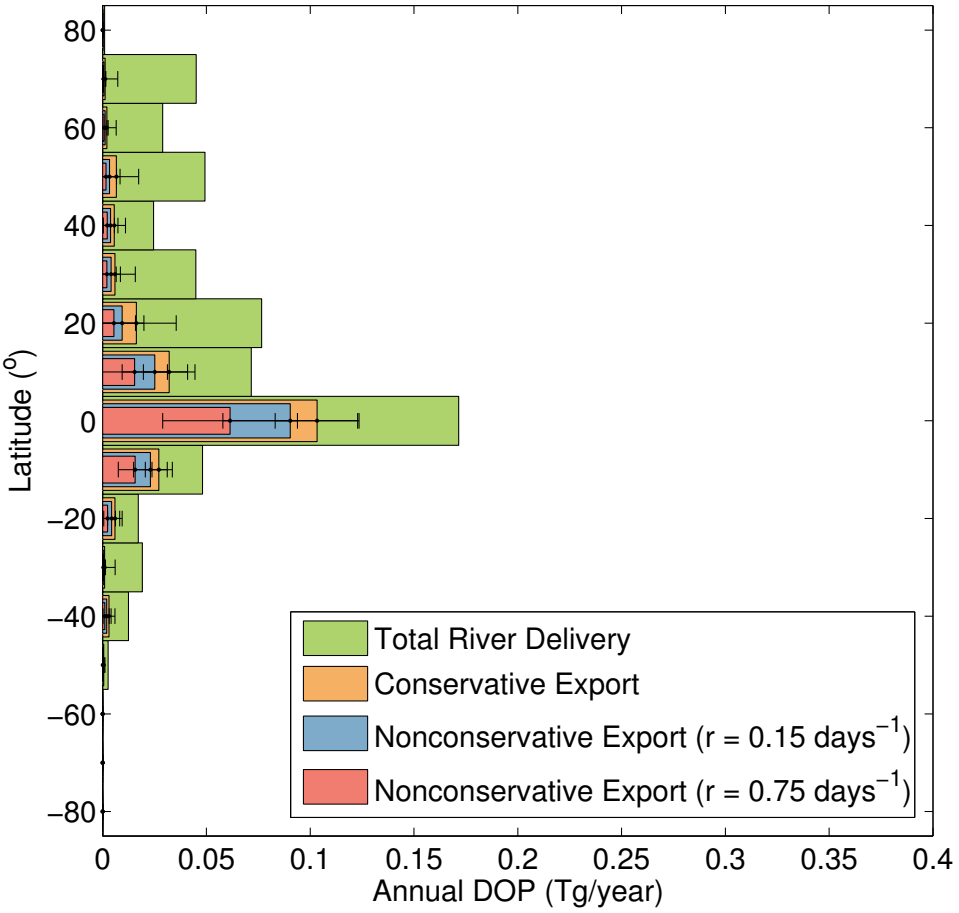

Figure A.6: DOC delivery and export in 10° latitude bands.

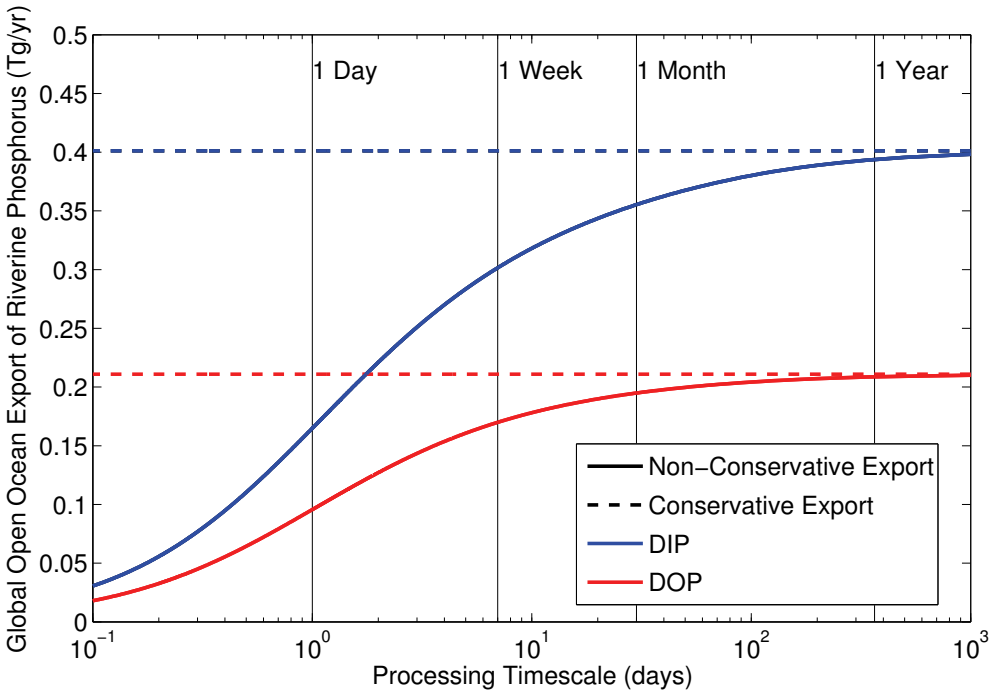

Figure A.7: Global export of DIP and DOP for different shelf processing timescales. The dashed line represents the conservative export.

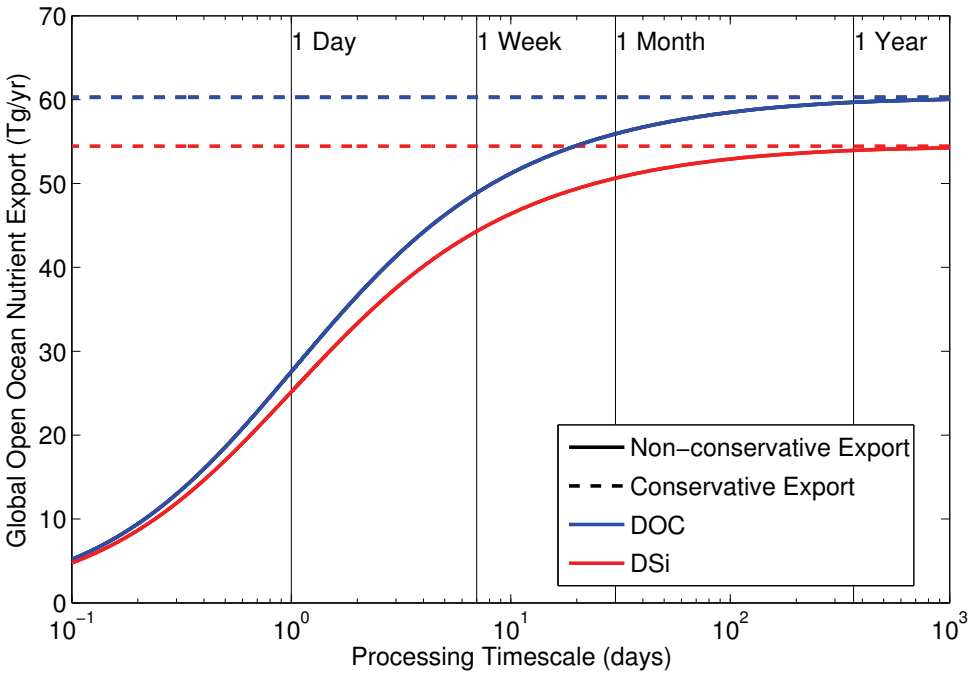

Figure A.8: Global export of DOC and DSi for different shelf processing timescales. The dashed line represents the conservative export.

APPENDIX B

TABLES OF GLOBAL RIVERINE EXPORT OF FRESH WATER AND NUTRIENTS

	Fresh Water ($m^3\,s^{-1}$)	
	Input	Export
Total	1183200.2	15.1–52.9%
80° N	2276.1	5.2–41.6%
70° N	90914.8	0.6–16.8%
60° N	60620.6	1.0–23.2%
50° N	92491.4	1.5–36.2%
40° N	39569.7	3.9–45.0%
30° N	81800.2	0.5–38.0%
20° N	126908.3	4.7–46.9%
10° N	141355.6	13.4–62.1%
0°	358581.9	31.9–72.0%
10° S	97273.6	33.9–69.4%
20° S	33275.6	4.0–54.6%
30° S	31913.1	0.7–31.2%
40° S	20792.7	2.9–48.0%
50° S	5275.2	0.2–44.4%
60° S	151.3	0.0–37.3%

Table B.1: Global freshwater export estimates in 10° latitude bands.

	DIN ($\mathrm{Mg\,y^{-1}}$)			
	Input	Export		
		Cons.	Non-Cons.	
			$r = 0.15\ \mathrm{d^{-1}}$	$r = 0.75\ \mathrm{d^{-1}}$
Total	21910846.8	7.3–44.3%	5.5–28.9%	2.8–24.9%
80° N	10815.3	4.1–35.3%	3.1–18.9%	1.5–16.2%
70° N	501629.0	1.2–16.5%	0.9–5.7%	0.5–4.4%
60° N	795456.9	0.7–21.6%	0.5–8.6%	0.2–6.3%
50° N	2043064.2	1.2–28.7%	0.9–10.2%	0.4–6.6%
40° N	1885990.8	5.4–44.5%	4.1–28.8%	2.1–23.3%
30° N	3761341.7	0.5–31.6%	0.4–13.8%	0.2–12.4%
20° N	5885572.4	2.6–43.1%	2.0–19.5%	1.0–12.7%
10° N	1968352.6	17.2–62.7%	13.0–56.5%	6.6–51.3%
0°	2316725.4	28.9–70.5%	21.9–69.8%	11.1–68.8%
10° S	858999.1	29.1–68.8%	22.0–65.0%	11.2–62.7%
20° S	570434.1	3.9–55.0%	2.9–47.7%	1.4–42.8%
30° S	728307.4	1.3–32.9%	0.9–9.6%	0.5–7.6%
40° S	534306.3	1.9–48.4%	1.4–33.0%	0.7–26.5%
50° S	49167.3	0.1–45.2%	0.0–27.4%	0.0–16.8%
60° S	684.3	0.0–38.5%	0.0–12.4%	0.0–4.5%

Table B.2: Global DIN export estimates in 10° latitude bands.

	DON ($Mg\ y^{-1}$)			
	Input	Export		
		Cons.	Non-Cons.	
			$r = 0.15\ d^{-1}$	$r = 0.75\ d^{-1}$
Total	11310561.8	14.5–51.8%	11.0–42.3%	5.6–39.2%
80° N	17364.6	4.1–38.1%	3.1–22.0%	1.5–18.2%
70° N	850086.3	0.6–16.0%	0.4–3.5%	0.2–2.5%
60° N	546412.0	1.0–22.4%	0.7–9.1%	0.4–6.9%
50° N	975885.0	1.4–34.1%	1.0–16.2%	0.5–10.5%
40° N	509869.7	4.9–44.0%	3.7–29.3%	1.9–23.9%
30° N	802020.9	0.8–35.5%	0.6–19.9%	0.3–18.1%
20° N	1297320.9	5.2–47.2%	3.9–27.8%	2.0–20.7%
10° N	1303154.4	13.9–62.3%	10.5–57.6%	5.3–53.4%
0°	3174979.7	31.8–72.0%	24.1–71.6%	12.2–71.0%
10° S	908475.2	33.7–69.6%	25.6–64.6%	13.0–62.1%
20° S	324831.5	4.1–54.8%	3.1–47.4%	1.5–42.7%
30° S	354202.1	1.2–32.0%	0.9–8.3%	0.5–6.6%
40° S	196723.6	2.7–47.3%	2.0–33.0%	1.0–26.7%
50° S	47851.8	0.2–44.0%	0.1–25.0%	0.1–15.8%
60° S	1384.1	0.0–37.2%	0.0–10.5%	0.0–3.9%

Table B.3: Global DON export estimates in 10° latitude bands.

	DIP ($Mg\,y^{-1}$)			
	Input	Export		
		Cons.	Non-Cons.	
			$r = 0.15\ d^{-1}$	$r = 0.75\ d^{-1}$
Total	1550802.1	9.1–45.9%	6.9–31.8%	3.5–27.9%
80° N	236.7	3.4–38.7%	2.6–22.7%	1.3–18.1%
70° N	29434.3	0.6–11.5%	0.4–3.5%	0.2–2.6%
60° N	34171.1	0.7–22.9%	0.5–8.0%	0.2–5.4%
50° N	155752.8	1.0–22.3%	0.8–6.0%	0.4–3.7%
40° N	236037.6	8.0–46.0%	6.1–30.9%	3.1–25.9%
30° N	214788.6	1.6–32.5%	1.2–14.9%	0.6–13.1%
20° N	334050.3	3.6–44.0%	2.7–20.9%	1.4–14.0%
10° N	143305.2	20.2–64.6%	15.3–59.4%	7.7–54.6%
0°	196240.2	31.0–71.8%	23.4–71.0%	11.8–70.0%
10° S	61477.5	18.3–65.5%	13.9–62.2%	7.1–60.2%
20° S	36238.1	5.0–54.0%	3.7–42.1%	1.8–36.2%
30° S	55058.6	2.5–37.6%	1.9–19.5%	0.9–16.5%
40° S	50583.5	2.0–47.9%	1.4–31.8%	0.7–26.1%
50° S	3367.2	0.1–48.4%	0.1–33.7%	0.0–23.3%
60° S	60.4	0.0–37.3%	0.0–10.2%	0.0–3.7%

Table B.4: Global DIP export estimates in 10° latitude bands.

	DOP (Mg y^{-1})			
	Input	Export		
		Cons.	Non-Cons.	
			$r = 0.15$ d^{-1}	$r = 0.75$ d^{-1}
Total	613303.7	14.4–51.9%	10.9–42.1%	5.5–39.0%
80° N	930.7	4.1–38.1%	3.1–22.0%	1.5–18.2%
70° N	45106.2	0.6–16.2%	0.5–3.5%	0.2–2.5%
60° N	28965.9	1.0–22.6%	0.7–9.1%	0.4–6.9%
50° N	49361.9	1.4–35.2%	1.1–17.0%	0.5–11.1%
40° N	24561.9	4.9–44.8%	3.7–30.1%	1.9–24.5%
30° N	44921.3	0.6–35.0%	0.4–19.1%	0.2–17.4%
20° N	76596.9	4.4–46.3%	3.3–26.0%	1.7–19.0%
10° N	71602.0	13.7–62.2%	10.4–57.2%	5.3–52.9%
0°	171537.0	31.8–72.0%	24.1–71.6%	12.2–71.0%
10° S	48134.5	34.1–69.8%	25.9–64.8%	13.2–62.2%
20° S	17213.4	4.0–54.9%	3.0–47.7%	1.5–43.1%
30° S	19158.7	0.9–31.4%	0.6–7.2%	0.3–5.5%
40° S	12475.9	2.6–47.7%	2.0–33.1%	1.0–26.8%
50° S	2663.2	0.2–44.2%	0.1–25.5%	0.1–16.3%
60° S	74.2	0.0–37.2%	0.0–10.5%	0.0–3.9%

Table B.5: Global DOP export estimates in 10° latitude bands.

	DOC ($Mg\ y^{-1}$)			
	Input	Export		
		Cons.	Non-Cons.	
			$r = 0.15\ d^{-1}$	$r = 0.75\ d^{-1}$
Total	170751318.2	14.9–52.3%	11.2–43.2%	5.7–40.2%
80° N	242192.2	4.1–38.1%	3.1–22.0%	1.5–18.1%
70° N	13930765.6	0.5–16.0%	0.4–3.1%	0.2–2.2%
60° N	9219987.0	0.9–20.9%	0.6–7.9%	0.3–6.0%
50° N	13909673.9	1.5–34.3%	1.1–17.1%	0.6–11.2%
40° N	5328928.0	3.7–44.1%	2.8–28.2%	1.4–22.6%
30° N	10038035.7	0.6–36.9%	0.4–21.3%	0.2–19.4%
20° N	18108498.4	4.3–46.6%	3.2–26.6%	1.6–19.1%
10° N	20382569.4	12.1–61.7%	9.2–57.0%	4.6–53.0%
0°	52289992.6	31.5–72.0%	23.8–71.6%	12.0–71.0%
10° S	14697031.8	32.4–68.4%	24.6–62.6%	12.5–59.3%
20° S	4510130.7	3.8–54.9%	2.9–47.9%	1.4–43.3%
30° S	4816368.8	0.6–31.0%	0.5–6.2%	0.2–4.6%
40° S	2595088.3	2.8–47.4%	2.1–33.2%	1.0–26.8%
50° S	662858.1	0.2–43.9%	0.1–24.8%	0.1–15.7%
60° S	19197.7	0.0–37.2%	0.0–10.5%	0.0–3.9%

Table B.6: Global DOC export estimates in 10° latitude bands.

	DSi ($Mg\ y^{-1}$)			
	Input	Export		
		Cons.	Non-Cons.	
			$r = 0.15\ d^{-1}$	$r = 0.75\ d^{-1}$
Total	137822456.9	18.2–56.4%	13.8–47.8%	7.0–44.3%
80° N	407084.9	2.5–40.7%	1.8–26.0%	0.9–21.2%
70° N	7261639.3	1.2–20.2%	0.9–7.2%	0.5–5.3%
60° N	6538770.7	1.3–28.1%	1.0–12.6%	0.5–9.5%
50° N	9081869.1	1.8–37.1%	1.3–20.6%	0.7–14.0%
40° N	5752351.6	4.5–48.3%	3.4–34.3%	1.7–28.3%
30° N	6344360.4	1.2–40.3%	0.9–24.1%	0.5–21.5%
20° N	15258521.6	7.1–48.5%	5.4–31.0%	2.7–24.4%
10° N	17522594.7	18.2–63.1%	13.8–57.3%	7.0–52.2%
0°	45386241.6	35.8–73.3%	27.1–72.8%	13.8–72.1%
10° S	12770788.3	27.3–65.6%	20.7–58.5%	10.6–54.7%
20° S	3605560.9	6.1–54.6%	4.5–46.3%	2.3–42.3%
30° S	2967564.8	1.6–36.9%	1.2–14.7%	0.6–12.2%
40° S	4109459.7	2.4–48.8%	1.8–34.4%	0.9–27.8%
50° S	770772.2	0.1–44.6%	0.1–24.0%	0.0–14.4%
60° S	44877.1	0.0–36.5%	0.0–9.9%	0.0–3.8%

Table B.7: Global DSi export estimates in 10° latitude bands.

APPENDIX C

CALCULATION STEPS FOR ESTIMATING EXPORT

The following is how freshwater and nutrient export is calculated for a real river, using the following properties for the example: ϕ = 45° N
Q = 10 000 m^3 s^{-1}
L^{Nut}_{River} = 50 000 Mg y^{-1}
D_S = 50.0 km

First, $R^{'}_o$ is calculated according to Equations 3.3 and 3.4:

$$\begin{aligned} R^{'}_o &= \sqrt{\frac{g}{f^2 \rho_o}\left(\Delta\rho h - \frac{\Delta\rho h^2}{H}\right)} \\ &= 10 \text{ km} \end{aligned} \tag{C.1}$$

Next, the S_P number is calculated from Equation 2.1:

$$\begin{aligned} S_P &= \frac{2R^{'}_o}{D_S} \\ &= 0.4 \end{aligned} \tag{C.2}$$

The freshwater export efficiency is then determined using Equation 3.1.

$$\begin{aligned} E^{FW}_X &= 1 - \frac{1}{a\sqrt{S_P} + b} \\ &= 30\% \end{aligned} \tag{C.3}$$

For a removal rate of 0.1 d^{-1}, the corresponding non-conservative export efficiency

is calculated from Equation 3.7, with the export timescale (5.75 d) estimated from the equation in Figure 3.18.

$$\begin{aligned} E_{X\overline{C}}^{Nut} &= \frac{1}{1 + rT_E} E_X^{FW} \\ &= 20\% \end{aligned} \tag{C.4}$$

The absolute export values are calculated by multiplying the efficiencies by the riverine loads.

$$\begin{aligned} T_X^{FW} &= E_X^{FW} Q \\ &= 3\,000 \text{ m}^3 \text{ s}^{-1} \end{aligned} \tag{C.5}$$

$$\begin{aligned} T_{X\overline{C}}^{Nut} &= E_{X\overline{C}}^{Nut} L_{River}^{Nut} \\ &= 10\,000 \text{ Mg y}^{-1} \end{aligned}$$